Euchromatic histone methyltransferases regulate peripheral heterochromatin tethering via histone and non-histone protein methylations

Alhad Ashok Ketkar[1ξ], Radhika Arasala Rao[1,3ξ], Neelam Kedia[1], Febina Ravindran[1], Vairavan Lakshmanan[2,3], Pankaj Kumar[1], Abhishek Mohanty[1], Shilpa Dilip Kumar[2], Sufi O Raja[2], Akash Gulyani[2], ChandraPrakash Chaturvedi[5], Marjorie Brand[4], Dasaradhi Palakodeti[2], Shravanti Rampalli[1*]

[1]Centre For Inflammation and Tissue Homeostasis, Institute for Stem Cell Biology and Regenerative Medicine (inStem), GKVK Campus, Bellary Road, Bangalore-560065, Karnataka, India. [2]Technologies for the Advancement of Science, Institute for Stem Cell Biology and Regenerative Medicine (inStem), GKVK Campus, Bellary Road, Bangalore-560065, Karnataka, India. [3]Sastra University, Tirumalaisamudram, Thanjavur-613 401, TamilNadu, India. [4]Sprott Centre for Stem Cell Research, Ottawa Hospital Research Institute, Mailbox 511, 501 Smyth Road, Ottawa, Ontario, K1H 8L6, Canada, [5]Department of Hematology Sanjay Gandhi Postgraduate Institute of Medical Sciences, Rae Bareli Road, Lucknow 226014, Uttar Pradesh, India.

*** Correspondence should be addressed to:**

Dr. Shravanti Rampalli
Assistant Investigator
Wellcome Trust/DBT Alliance Intermediate Fellow
Institute for Stem Cell Biology and Regenerative Medicine (inStem)
GKVK PO, Bellary Road, Bangalore 560065
Phone: 080-2366 6716
Email: shravantird@instem.res.in

ξ these authors contributed equally.

Running Title: Peripheral Heterochromatin organization during aging

Abstract

Euchromatic histone methyltransferases (EHMTs) methylate histone and non-histone proteins. Here we uncover a novel role for Euchromatic histone methyltransferases in regulating heterochromatin anchorage to the nuclear periphery (NP) via non-histone (LMNB1) methylations. In search for mechanism, we identified EHMTs methylate LMNB1 that associates with the H3K9me2 marked peripheral heterochromatin. Loss of LMNB1 methylation or EHMTs abrogates the heterochromatin anchorage from the nuclear periphery. We further demonstrate that the loss of EHMTs induced many hallmarks of aging including global reduction of H3K27methyl marks along with altered nuclear-morphology. Keeping consistent with this, we observed gradual depletion of EHMTs, which correlated with loss of methylated LaminB1 and peripheral heterochromatin in aging human fibroblasts. Restoration of EHMT expression reverts peripheral heterochromatin defect in aged cells. Collectively our studies elucidated a new mechanism by which EHMTs regulate heterochromatin domain organization and explains its impact on fundamental changes associated with the intrinsic aging process.

Keywords: Aging/ Euchromatic histone methyltransferases / Heterochromatin / LaminB1/ Nuclear periphery

Introduction

The Euchromatic histone lysine methyltransferases G9a, encoded by EHMT2, and GLP, encoded by EHMT1, are present as heteromeric complex and negatively regulate gene transcription (KMT1/Suv39 methyltransferase family). The SET domain of EHMT catalyzes mono and dimethylation of lysine residues at histone3 (H3) in vitro and in vivo (Herz et al., 2013; Peters et al., 2003; Rice et al., 2003; Tachibana et al., 2002; Tachibana et al., 2005). H3K9me2 deposited by EHMT1/2 complex demarcates heterochromatin, particularly non-genic regions and is prevalent in gene deserts, pericentromeric and subtelomeric regions, with little being observed at individual active or silent genes. Non-coding and gene containing DNA present at the NP are also marked by the presence of H3K9me2 which spans several megabases in size (Guelen *et al.*, 2008; Black and Whetstine, 2011). Specifically, these domains are strongly correlated with binding of LaminB1 (LMNB1) and are depleted of H3K4me3 and RNA Polymerase II activity (Black and Whetstine, 2011). These data suggest that H3K9me2 domains are critical determinants of higher-order chromosome structure in association with the nuclear lamina (NL).

In mammalian cells the NL acts as a hub for multiple cellular functions including chromatin organization (Goldberg, Nili and Cojocaru, 1999; Goldman *et al.*, 2002; Dixon *et al.*, 2012; Shevelyov and Nurminsky, 2012). NL is composed of A and B type lamins along with inner nuclear membrane (INM) proteins (Foisner, 2001), and together mediator proteins such as BAF and HP1, facilitate attachment of chromatin to NL (Burke and Stewart, 2013; Montes de Oca, Andreassen and Wilson, 2014).

Additionally, these interactions have been proposed to form specific chromatin organization that opposes transcriptional activity (Coutinho *et al.*, 2009). Association between LMNB receptor and LMNA/C was shown as a key means of peripheral heterochromatin attachment in wide variety of mammalian tissue (Solovei *et al.*, 2013). Any perturbation in such organization leads to complete loss of peripheral heterochromatin and developmental abnormalities (Mozzetta *et al.*, 2015).

Recent studies demonstrated that the Lamina associated domains (LADs) enriched in H3K9 methyl (me2/me3) marks contact NL via association with LMNB1 (Guelen *et al.*, 2008; Bian *et al.*, 2013; Kind *et al.*, 2013; Harr *et al.*, 2015). These interactions are highly stochastic in nature and are dependent on H3K9me2 activity governed by G9a/EHMT2. Accordingly G9a/EHMT2 promote LAD formation and its loss leads to the opposite effect (Kind *et al.*, 2013). Similar to humans, H3K9 methylation is important for heterochromatin positioning in *C. elegans* (Towbin *et al.*, 2012), as depletion of H3K9 methyltransferases Met2 and Set-25 (mammalian SETDB1 and G9a /EHMT2 homologue) leads to detachment of large gene-array from peripheral heterochromatin. Altogether, loss of lamins and INMs or H3K9me2 activity leads to peripheral heterochromatin defects, however the link between the common consequences remain unknown. In the current study we establish EHMT proteins as a common module that govern heterochromatin tethering via histone dependent (H3K9me2) and independent mechanisms (by directly regulating LMNB1 methylation).

Results

Euchromatic histone methyltransferases (EHMTs) associates with LMNB1

To identify the novel non-histone interactors of EHMT proteins, we performed mass-spectrometry analysis using HEK-293 extracts. Endogenous EHMT1 was immunoprecipitated and the bands that were uniquely present in IP-EHMT1 compared to IP-Control, were subjected to LC/MS analysis. We found NL protein LMNB1 and histone proteins as interactors of EHMT1 (Figure 1A). Mass spectrometry data was validated by sequential immunoprecipitation (IP) reactions using antibodies that recognize endogenous EHMT1, EHMT2 and LMNB1 proteins (Figure 1B). To determine if this complex was cell type specific, we performed IPs using nuclear extracts from human dermal fibroblasts (HDFs) (Fetal derived, unless mentioned otherwise). Western blot analysis identified association between all three proteins, suggesting this interaction is not cell type specific (Supplementary Figure 1A). We also detected HP1 in association with EHMT and LMNB1 (Supplementary Figure 1A). This result is in agreement with previously published reports where in HP1 was shown to interact with nuclear lamins and EHMT complex independently. The absence of Ash2l (a member of H3K4 methyltransferase complex) in the IP-EHMT1 or IP-LMNB1 confirmed the specificity of IP reaction (Supplementary Figure 1A). To map LMNB1 interacting domain of EHMT1, we cloned the Ankyrin and SET domains in pEGFPC1 vector. IP using a GFP antibody revealed that the SET domain of EHMT1 interacted with LMNB1 (Supplementary Figure 1B). Similar results were obtained when His-EHMT1-SET domain bound Ni-NTA beads were incubated with recombinant GST-LMNB1 protein (Supplementary Figure 1C and Figure 1C). These results confirmed that the EHMT1/2 directly associates with LMNB1 via SET domain.

Both EHMT and LMNB1 are known to interact with chromatin independently or via mediator proteins (Shinkai and Tachibana, 2011; Camps, Erdos and Ried, 2015; Mozzetta *et al.*, 2015). To identify EHMT1-LMNB1 co-bound regions in the genome, we performed ChIP Seq analysis. Individually, EHMT1 and LMNB1 occupied 36807 and 32688 number of peaks respectively and 8584 peaks were co-bound by EHMT1 and LMNB1 (Figure 1D). A majority of EHMT1 and LMNB1 reads were distributed on non-TSS regions such as introns and gene poor regions (represented as "others") (Figure 1E,F), whereas only 1.5% of reads were found on the upstream region of genes (Figure 1F). Functional category analysis of the genes occupied by EHMT1, LMNB1 or EHMT1-LMNB1 revealed enrichment of genes regulating transcription, signal transduction and cell adhesion (Supplementary Figure 1D-F).

H3K9me2 deposited by EHMT1/2 complex demarcates heterochromatin, particularly non-genic regions and is prevalent in gene deserts, pericentromeric and subtelomeric regions, with little being observed at individual active or silent genes. Thus we focused our analysis to explore ChIP-Seq reads obtained from EHMT1 and LMNB1 that were present on "other" regions. Detailed analysis of read densities performed on individual chromosomes identified a striking correlation between EHMT1 and LMNB1 localization onto subtelomeric, telomeric and around centromeric regions (indicated as a red line on the chromosome) that are preferentially maintained in the silent state (Figure 1G,H and Supplementary Figure 1G). These data suggested that EHMT1-LMNB1 associate on gene poor areas that are the critical determinants of higher-order chromosome structure at the nuclear periphery (NP).

EHMTs methylate LMNB1

Next we tested if LMNB1 is a substrate for methylation by the EHMT enzymes. Towards this we cloned and purified LMNB1 containing the rod domain and tail

domains (LMNB1-CT), which was sufficient to interact with EHMT1-SET domain (Supplementary Figure 2A & data not shown). Using an in vitro fluorometric methyltransferase assay we demonstrate an increase in fluorescence upon incubation of EHMT1-SET domain with LMNB1-CT in presence of S-adenosyl methionine (SAM), while no SAM reaction was used as a negative control and H3 peptide served as a positive control in this assay (Supplementary Figure 2B). To confirm that EHMT proteins indeed methylate LMNB1, we used lysine methyl specific (Methyl-K) antibody to probe for methylated LMNB1. Towards this we performed in vitro methyltransferase assay using different concentrations of LMNB1 and incubated with equimolar ratio of EHMT1/2-SET domain in presence or absence of SAM. When products of these reactions were immunoblotted using Methyl-K antibody, specific methylation signal was observed upon incubation of LMNB1 with EHMT1/2-SET in presence of SAM. These results confirm EHMT1 and EHMT2 methylates LMNB1 in vitro.

Further, to examine if LMNB1 is methylated in vivo, we performed anti-Methyl-K or anti-LMNB1 IPs using HEK-293 nuclear lysate. Products of IPs were split into two halves and probed with either anti-LMNB1 or anti-Methyl-K specific antibodies. Several lysine residues are methylated on the H3 tail, detecting the histone signal in IP-Methyl-K confirming the specificity of IP reaction and served as a positive control (Figure 2C). The presence of LMNB1 band in the same Methyl-K IP samples indicated the presence of endogenous methylated LMNB1 (Figure 2C). In vice versa IP reaction in which LMNB1 was IPed and probed with Methyl-K antibody, identification of Methyl-K signal in the IP-LMNB1 confirmed LMNB1 methylation in vivo (Figure 2D).

EHMT2 methylates lysine on dipeptide Arg-Lys (RK) sequence of non-histone proteins (Rathert *et al.,* 2008). We synthesized peptides for such motifs that were present on the c-terminus region of LMNB1 and identified lysine residue at amino acid 417 as the methylation site targeted by EHMT1 and EHMT2 (Figure 2E). Mutation of lysine (K) to alanine (A) abolished methylation of LMNB1 peptide (Figure 2E). To investigate the function of methylated LMNB1 in vivo, we mutated the 417K residue to alanine (K417A) in the wild type (Wt.) LMNB1-mWasabi construct. As opposed to Wt.LMNB1, which was localized at the NP, K417A-LMNB1 was accumulated in the nucleoplasm (Figure 2F and Supplementary Figure 2C). We also observed aggregates of mutant-LMNB1 transported into the cytoplasm, which was accompanied by grossly abnormal nuclear morphology (Figure 2F). Co-staining with LMNB1 antibody showed localization of endogenous LMNB1 and overexpressed Wt.LMNB1 at the NP in Wt.LMNB1 expressing cells. However, in mutant-LMNB1 expressing HDFs, endogenous LMNB1 was localized in K417A-LMNB1 aggregates indicating dominant negative function of the mutant protein. Further mislocalization of LMNA/C in the aggregates of mutant-LMNB1 (Supplementary Figure 2D) indicated LMNB1 methylation is critical for maintaining NL meshwork composition at the periphery. Our data from methylation deficient mutant-LMNB1 showed its mislocalization in the nucleoplasm and the cytoplasm, which lead us to speculate that the methylation modification prevents degradation of LMNB1 and confers protein stability.

EHMTs regulate LMNB1 levels

To test the consequence of the loss of EHMTs on LMNB1 levels we depleted EHMTs in HDFs using shRNAs. Immunoblotting results showed 70% depletion of EHMT1 and 80% depletion of EHMT2 using respective shRNAs (Supplementary Figure 3 A-

C). Reduced expression of EHMT2 in shEHMT1 cells and vice-versa indicated reciprocal stabilization of these proteins within the heteromeric complex (Supplementary Figure 3 A-C). Further reduced levels of LMNB1 protein in shEHMT1 and shEHMT2 cells (Figure 3A) confirm the regulation of LMNB1 by EHMTs. Immunostaining analysis of EHMT proteins counter-stained with LMNB1 and DAPI demonstrated significant distortion of nuclear morphology and loss of LMNB1 (Figure 3B-C and Supplementary Figure 3D).

Recent studies demonstrate that the B-type lamins are long-lived proteins (Razafsky *et al.*, 2016). Therefore loss of such proteins would occur when there is transcriptional inhibition coupled with degradation of existing protein. Thus, we tested if EHMT proteins regulated LMNB1 expression transcriptionally. Our data demonstrate approximately 60% loss of LMNB1 transcript upon depletion of EHMT proteins (Fig. 3d) indicating its role in transcriptional regulation of LMNB1. Overall our results demonstrate that EHMT1 and 2 regulate LMNB1 expression transcriptionally and directly via post-translational modification.

EHMT proteins regulate peripheral heterochromatin anchorage via histone dependent and independent interactions

H3K9 methylation and LMNB1 are the critical determinants for formation of the LADs at the NP (Guelen *et al.*, 2008; Bian *et al.*, 2013; Kind *et al.*, 2013; Harr *et al.*, 2015). To test the requirement of EHMT mediated H3K9 dimethylation in tethering peripheral heterochromatin, we depleted EHMTs in fibroblasts and monitored the co-localization of H3K9me2 with LMNB1 by confocal microscopy. Global H3K9me2 was decreased by 50% in shEHMT1 cells (Supplementary Figure 4A,B). On the contrary, EHMT2 depletion reduced H3K9me2 methylation by 80% (Supplementary Fig. 4A,B). Substantial reduction of H3K9me2 activity in shEHMT2 HDFs confirmed

EHMT2 as the predominant HMTase among EHMT proteins. Visualization of H3K9me2 pattern demonstrated its predominant localization to the NP in shCnt and shEHMT1 HDFs (Supplementary Figure 4C-E and Figure 4A). In shEHMT2 cells, there was a significant loss of enrichment of H3K9me2 at the NP (Supplementary Figure 4C-E and Figure 4A).

Next we performed EM to investigate the status of heterochromatin in EHMT depleted cells. shCnt transduced HDFs exhibited a layer of electron dense peripheral heterochromatin just beneath the nuclear envelope (NE) (Figure 4B). Knockdown of EHMT2 led to partial disruption of heterochromatin from the periphery to the interior of the nucleus (Figure 4D). This result was correlated with redistribution of H3K9me2 marks towards the interior of the nucleus. In shEHMT1 HDFs, we noticed complete detachment of peripheral heterochromatin and a distorted NE (Figure 4C). We also detected floating islands of heterochromatin in the nuclei. Interestingly, the severity of heterochromatin detachment and compromised NE integrity were unique to shEHMT1 knockdown wherein H3K9me2 activity was modestly affected.

We also looked at the effects of overall heterochromatin positioning and nuclear distortion upon inhibition of H3K9me2 activity using small molecule inhibitor BIX-01294. HDFs treated with BIX-01294 showed 40% less H3K9me2 staining compared to controls (Supplementary Figure 4F,G). Unlike EHMT depleted cells, we did not notice any significant changes in the nuclear morphology of BIX treated cells (Supplementary Figure 4F). EM imaging indicated significant but modest but significant changes in heterochromatin anchorage (Supplementary Figure 4I).

To obtain a clearer picture of role of LMNB1 methylation, HDFs were transfected with either the Wt.LMNB1 or K417A-LMNB1 construct. Immunostaining for H3K9me2 followed by confocal microscopy revealed co-localization of H3K9me2

with LMNB1 at the NP in Wt.LMNB1 overexpressing cells (Figure 4E upper panel). In mutant-LMNB1 expressing cells peripheral distribution of H3K9me2 was severely compromised and we noticed segregation of LMNB1 and H3K9me2 aggregates in the nucleoplasm (Figure 4E lower panel). Visualization by EM revealed that the nuclei of mutant-LMNB1 expressing cells were completely devoid of peripheral heterochromatin (Figure 4F,G). Additionally we also observed ruptured nuclear-envelope in K417A transfected cells (Figure 4G). Overall these results demonstrate the significance of LMNB1 methylation in maintaining nuclear integrity and heterochromatin tethering to the NP.

To investigate the additional changes that could influence heterochromatin organization in EHMT depleted cells we profiled gene expression changes in shEHMT1 and shEHMT2 HDFs. RNA-Seq analysis identified overlapping and unique genes that were regulated by EHMT1 or EHMT2 (Supplementary Figure 5A, Supplementary Table 1&2). Gene Set Enrichment Analysis (GSEA) (adjusted value <0.05) demonstrated that the pathways such as cell-cycle, homeostasis and axon guidance etc. were regulated by both EHMT1 and EHMT2 (Supplementary Table 3). Interestingly, significantly high numbers of pathways were distinctly regulated by EHMT1 and EHMT2. For example, EHMT1 regulated vesicle biogenesis, GPCR signaling, calcium signaling and metabolic pathways for carbohydrates and lipids (Supplementary Table 3). On the contrary EHMT2 exclusively regulated pathways involved in RNA metabolism, translation and autophagy (Supplementary Table 3). Varying degree of peripheral heterochromatin detachment in shEHMT1 and shEHMT2 HDFs led us to investigate the number of chromatin modifiers that were altered upon EHMT depletion. While there were overlapping chromatin modifiers (including HDACs, EZH1, EZH2 specific isoform, DOT1L) that changed in response

to EHMT depletion, EHMT1 loss reduced expression of repressive PRC1 components (PCGF5, CBX6), NCOR2, HMGs, CBX and Tet proteins. On the contrary EHMT2 reduction predominantly influenced expression of KDMs, SIRT6 and SETD1 proteins (Supplementary Figure 5B, Supplementary Table 4). Functional validation of the loss of PRC members was performed by H3K27me3 immunostaining. Reduced H3K27me3 staining in shEHMT1 and shEHMT2, indicates that knockdown of EHMTs affect PRC protein expression (Figure 4H,I, upper panel). Interestingly, we detected the loss of HP1 only in shEHMT1 cells but not in shEHMT2 HDFs (Figure 4I, lower panel). Above data indicated that EHMT proteins target identical as well as distinct chromatin modifiers. Overall our results revealed the commonalities and differences upon individual knockdown between two structurally similar proteins that contribute to phenotype of peripheral heterochromatin detachment.

Sequential loss of EHMT proteins leads to diminished peripheral heterochromatin during physiological aging

Alterations in nuclear shape, reduction in repressive H3K27 methyl marks and loss of peripheral heterochromatin as a consequence of loss of` the EHMT proteins impinges on known molecular hallmarks of cellular aging (López-Otín *et al.*, 2017). These observations prompted us to survey if age related genes were affected in response to EHMT depletion. Comparison of RNA-Seq profile obtained from shEHMT1 and shEHMT2 HDFs to the aging gene database, identified approximately 30% of aging specific genes (Total 108 of 307 genes listed in aging database) were altered in response to depletion of EHMT (Supplementary Figure 6A and Supplementary Table 5). For example upregulation of CDKN2B and downregulation of FOXM1 is linked to senescence and aging. Also attenuation of FGFR1 receptor for FGF signaling develops in diabetes with age. All three genes (FGFR1, CDKN2B and FOXM1)

showed differential expression, which were validated by quantitative RT-PCR analysis (Supplementary Figure 6B,C).

To test if EHMTs and H3K9me2 are indeed involved in regulating the aging process, we monitored the expression of EHMT1 and EHMT2 in HDFs derived from individuals of different age groups that were controlled for gender and ethnicity. Histone methyl marks H3K27me3 and H3K9me3 are known to diminish in aged and progeria cells. Reduction of H3K27me3, H3K9me3 methyl marks coupled with downregulation of HP1 in 58Y individual in comparison with HDFs derived from fetal and 18Y old individuals, confirmed the previous findings (Supplementary Figure 6D,E). Further investigation into levels of EHMT proteins revealed a decline of EHMT1 and EHMT2 in an age dependent manner. Compared to fetal cells, 31Y old HDFs had a statistically significant (40%) decrease in EHMT2 and preceded the loss of EHMT1 (Figure 5B). We observed a 50% decline of both the EHMT's in age bin of 40Y (38 and 40Y) with the drastic reduction of protein levels at 58Y of age (Figure 5A-C and Supplementary Figure 6F). An investigation of the status of H3K9me2 methylation demonstrated its consecutive decline with altered sub-nuclear localization in aging fibroblasts (Figure 5D,E). The levels of H3K9me2 were reduced from fetal to adult bin (18, 19 and 31Y) with considerable reduction in the 40Y age bin and drastically low amounts in the aged state (Figure 5D-E and Supplementary Figure 6G). An equally important observation was that the preferential localization of H3K9me2 was noticed at the NP in fetal HDFs, while these marks were distributed in the nucleoplasm in 18Y and 58Y HDFs (Figure 5D and supplementary Figure 7A-D). This data correlated with results obtained in Figure 4A and Supplementary Figure 4C where in reduction of EHMT2 in fetal-HDFs resulted in re-localization of H3K9me2 methyl marks to the nucleoplasm.

Anchoring of heterochromatin to the NP was compromised in EHMT1/2 knockdown cells. To test if the consequent loss of EHMTs and altered distribution of H3K9me2 impacts heterochromatin organization in aging cells, we performed electron microscopy (EM). Compared to fetal cells, in 18Y HDFs, we observed redistribution of peripheral heterochromatin, which correlated, with redistribution of H3K9me2 marks (Figure 5F and Figure 4D). A significant amount of heterochromatin was still retained at the periphery of 31Y age group HDFs where there was substantial loss of EHMT2 (Supplementary Figure 6F). Further there was gradual loss of peripheral heterochromatin in 40Y old cells with complete depletion observed in 58Y aged nuclei (Figure 5F). Interestingly complete loss of peripheral heterochromatin organization was correlated with loss of EHMT1 in aging cells (Figure 5A and Supplementary Figure 6F).

Since both EHMTs were downregulated during aging we decided to explore regulation of EHMT1 and EHMT2 proteins. Towards this we performed qRT-PCR experiments. The EHMT1 transcript was downregulated by 10% from fetal to 18Y HDFs and was further downregulated by 90% from 18Y to 58Y stage (Figure 5G). This data clearly indicated that EHMT1 expression is controlled transcriptionally during aging. On the contrary only 30% EHMT2 was regulated transcriptionally (20% downregulation from fetal to adult state, with further decline by 30% from adult to aged cells) (Figure 5G). Since a small amount of EHMT2 was regulated transcriptionally; there seemed a strong possibility of post-translation regulation during aging. Hence, to investigate if EHMT2 protein levels are regulated via ubiquitin proteasome pathway, we treated 18Y and 58Y old HDFs with the proteasome inhibitor MG-132. In 18Y old cells, EHMT2 protein levels were increased to 2-fold upon MG-132 treatment, whereas no such increase was noticed in

EHMT1 levels. Interestingly, EHMT2 levels could not be rescued in 58Y HDFs (Figure 5H), indicating that the blockade of UPS activity can restore the EHMT2 degradation only in early age group and such mechanisms do not operate in aged cells where in EHMT2 is already drastically low. Taken together our data on the loss of EHMT1 either as a consequence of physiological aging or by forced depletion in fetal HDFs establishes the direct link of EHMTs to heterochromatin organization at the NP.

Low levels of LMNB1 have been observed in senescent cells and fibroblasts derived from Progeria patients (Dreesen *et al.*, 2013). In this study, expression analysis of nuclear lamins in intrinsically aged cells showed reduction of LMNB1 starting in the 31Y age group with significant loss at 58Y (Figure 5J). On the contrary, LMNB2 was reduced in aged cells without significant changes seen in LMNA/C (Figure 5J) levels. Diminishing levels of LMNB1 were correlated with reduction in EHMT2 protein with drastic loss upon depletion of EHMT1 protein in 58Y cells (Supplementary Figure 6F). This is consistent with the data in Fig 3 where we found that EHMT proteins directly regulate levels of the LMNB1 protein.

Next we questioned if diminishing perinuclear heterochromatin organization in aging nuclei is a result of the loss of EHMT1, EHMT2 and LMNB1 interaction. Towards this we performed IP experiments using Fetal, 18Y and 58Y nuclear extracts. Our results revealed association between EHMT2 and LMNB1 occurred only in fetal cells. On the contrary EHMT1 associated with LMNB1 in all the age groups and the interaction was reduced gradually in age dependent manner (Supplementary Figure 7E,F). The complete absence of perinuclear heterochromatin in 58Y-aged nuclei corresponded to over 80% reduction in the interaction between EHMT1 and LMNB1. These data indicated that EHMT1 and LMNB1 association is critical to maintain

peripheral heterochromatin in aging fibroblasts.

Further we tested the status of LMNB1 methylation during the physiological aging. Immunoprecipitation of LMNB1 from Fetal, 31Y and 58Y old fibroblasts followed by immunoblotting with the Methyl-K antibody showed reduced intensity of methylated LMNB1 signal from Fetal to 31Y with virtually no band in 58Y-aged cells (Figure 5K). Taken together our results indicate that the loss of peripheral heterochromatin in EHMT depleted cells or aged cells occurs due to loss of H3K9 activity coupled with the loss of LMNB1, which are critical determinants of peripheral heterochromatin anchorage.

Overexpression of EHMT proteins rescues peripheral heterochromatin defect in aged cells

To test if depletion of EHMT proteins are indeed responsible for loss of peripheral heterochromatin in aged cells we transfected full length V5 tagged EHMT1 or Flag-EHMT2 (set domain) plasmids in 58Y HDFs. Immunostaining using V5 or Flag antibodies confirmed the over expression of EHMT1 and EHMT2 proteins (Figure 6A). The increase in EHMT1 levels enhanced the expression of LMNB1. Flag-SET of EHMT2 however was no sufficient to enhance LMNB1 expression (Figure 6A middle and lower panel and Supplementary Figure 8 A,B).

We further examined H3K9me2 localization and organization of heterochromatin in EHMT1 and EHMT2 overexpressing cells. In both the cases H3K9me2 was co-localized with LMNB1 at the NP (Figure 6B). Consistent with this, EM imaging revealed peripherally organized heterochromatin upon EHMT1 and EHMT2 overexpression, which was completely absent in untransfected aged cells (Figure 6C-E). These results convincingly demonstrate that loss of EHMT proteins contributes to

the loss of peripheral heterochromatin organization during aging and this defect can be reverted upon re-expression of EHMT proteins.

To investigate the contribution of LMNB1 methylation in reversing peripheral heterochromatin tethering in aged cells we co-expressed wild type or mutant-LMNB1 with V5-EHMT1 or Flag-EHMT2. As expected Wt.LMNB1 localized with H3K9me2 at the NP in EHMT1 overexpressing cells (Supplementary Figure 8C, upper panel). Instead, H3K9me2 showed aggregated staining in the nucleoplasm and did not localize with mutant-LMNB1 (Supplementary Figure 8D,E) convincingly demonstrating the methylated LMNB1 organizes heterochromatin to the NP.

Proliferation rate of HDFs correlate with EHMT expression

The reduction in LMNB1 expression results in reduced proliferation and induction of premature senescence (Shimi *et al.*, 2011; Freund *et al.*, 2012). Therefore we tested if EHMT mediated reduction of LMNB1 expression leads to altered proliferation. Interestingly, monitoring EHMT1 & 2 shRNA transduced cultures (HDFs P#5) showed significant reduction in cell number (Figure 7A,B). Cell-cycle analysis revealed a small fraction of EHMT2 transduced cells (8.4%), were in SubG1 phase compared to shCnt and shEHMT1 HDFs (Supplementary Figure 9A-C and Figure 7C). This indicated a small but significant apoptosis in shEHMT2 cultures. Transcriptome data revealed that the genes involved in apoptosis were upregulated upon knockdown of EHMT2 supporting the apoptosis in shEHMT2 cultures (Supplementary Table 3). Other than that there were no striking differences in the cell-cycle profile of shCnt, shEHMT1 and shEHMT2 cultures. Enhanced expression of CDKN2B, TGFBR2 in shEHMT1 and DAFK1, TNFSF10 in shEHMT2 HDFs verified proliferation and apoptosis phenotype noticed in shEHMT HDFs (Supplementary Table 1 and 3). shRNA mediated loss of EHMT proteins also induced

senescence programme. We observed higher number (40%) of senescent cells in shEHMT1 in comparison to shEHMT2 (4%) (Figure 7 D,E).

Next we examined the correlation of EHMT expression with proliferation and senescence during physiological aging. Cell-cycle analysis of 58Y old HDFs showed a greater percentage of cells in G0/G1 phase with reduced proliferation capacity (Supplementary Figure 9D). β-gal staining in HDFs indicated insignificant changes in the number of senescent cells in 58Y HDFs (Supplementary Figure 9E). The telomerase enzyme prevents the replicative senescence in primary fibroblast cells (Bodnar *et al.*, 1998; Choi *et al.*, 2001). Examining the levels of telomerase activity in shEHMT and aged cells identified a correlation between the loss of EHMT proteins with reduced telomerase activity (Figure 7F,G). While this data accounted for proliferation defects, it did not explain the difference seen in senescence phenotype in shEHMT vs. aged cells. Nonetheless, these results demonstrated that the depletion of EHMT1 and EHMT2 was correlated with reduced proliferation.

Age related molecular defects contributed by EHMT proteins are magnified upon stress

Aging is known to compromise the intrinsic and extrinsic stress response (Kourtis and Tavernarakis, 2011). Thus, to understand the complex molecular interaction associated with EHMT mediated loss of peripheral heterochromatin, in a stress response, we deliberately provided culture induced stress to HDFs of various age groups. Cell proliferation assays in early-passage (P#5) HDFs did not detect any proliferation differences between 18 and 31Y age groups, while 58Y grew albeit slower (Figure 8A). On the contrary, late-passage (P#20) of 31Y cells showed minor but significant changes compared to 18Y late-passage HDFs (P#20) (Figure 8A). Interestingly 58Y late-passage HDFs grew much slower and could not be cultured

beyond P#18 (Figure 8A). These results demonstrated that the differences in growth rate of HDFs from aged cells with reduced EHMT1 were magnified upon exposure to stress. This also indicates that complete loss of EHMT proteins renders cells more sensitive towards a stress response. Assessment of nuclear distortion in low and high passage cells also exhibited similar outcome as defects in cell proliferation. Number of distorted nuclei was comparable in p#5 18Y and 31Y aged cells, with significant increase in 58Y old HDFs (Figure 8B,C). However these effects were over-represented in high passage cells from each age group (Figure 8B,C). Finally, assessing the levels of p16, a key regulator of senescence in early-passage HDFs showed age dependent increase in protein levels, which were further, elevated in high passage cells (Figure 8D,E). Overall our results suggest that the loss of EHMT1 is sufficient to initiate multiple molecular changes associated with aging. Cumulative deterioration of such processes in combination with stress further elicits senescence response, which is one of the hallmarks of aging.

Discussion

The NL is a meshwork of lamins that constitutes the nucleoskeleton required for nuclear structure and function (Goldberg, Nili and Cojocaru, 1999; Goldman *et al.*, 2002; Dechat *et al.*, 2008; Shevelyov and Nurminsky, 2012). The NL undergoes extensive posttranslational modifications (PTM) that are crucial for their localization to regulate a variety of biological processes (Snider and Omary, 2014). While uncovering the mechanism by which EHMTs organize heterochromatin, we have identified lysine methylation as a novel PTM of LMNB1 that is critical for its retention at the NP and maintaining the NL stability. High resolution imaging of endogenous LMNA and LMNB1 demonstrated that individual homopolymers exists in close contact with each other (Shimi *et al.*, 2011). Our results showing concentration of LMNA in the aggregates of mutant-LMNB1 indicates the potential crosstalk between two proteins via PTMs thereby opening new avenues to explore the role of methylated LMNB1 towards the assembly of NL and its integrity. LMNA is extensively studied with several known binding partners and disease causing mutations (Simon and Wilson, 2013). In this regard our study offers a new perspective on the less studied LMNB1 in the context of normal physiology and perhaps in laminopathies/disease.

Methylation of lysine residues facilitates a variety of functions including protein stability (Trojer and Reinberg, 2008; Egorova, Olenkina and Olenina, 2010; Zhang, Wen and Shi, 2012; Lanouette *et al.*, 2014). Altogether our data demonstrated EHMT1 and EHMT2 as upstream regulators of LMNB1 that influences its protein levels via posttranslational modification. While EHMT2 is known to methylate variety of non-histone proteins (Rathert *et al.*, 2008), our study for the first time demonstrates the competency of EHMT1 enzyme in methylating non-histone protein

and utilizing it as a mechanism to glue heterochromatin to the NP during aging. Structurally similar EHMT1/2 proteins form heteromeric complex mammalian cells (Shinkai and Tachibana, 2011) and are known to fulfill both overlapping and unique physiological roles in developing and adult animals (Kramer, 2015). In the quest to understand the individual contributions of EHMT proteins in specifying the peripheral heterochromatin we identified that both the EHMTs regulate LMNB1, however, unique molecular changes seen upon EHMT1 loss such as disruption of NE integrity coupled with loss of architectural proteins like HP1 and HMG that influence heterochromatin organization upon EHMT1 loss needs further investigations. Nonetheless, our studies provide a broader role for EHMTs by which it regulates the spatial distribution of the genome within the nucleus.

There are a number of studies demonstrating redistribution or loss of chromatin modifiers and their implications in aging (Oberdoerffer *et al.*, 2008; Pegoraro *et al.*, 2009). These studies mainly focused on the consequence of global loss of chromatin structure but none addressed the mechanisms underlying the alteration of genome architecture. Our study not only demonstrates the correlation between the expression of EHMTs with peripheral heterochromatin organization during aging, but also provides a mechanism by which EHMT regulates higher-order chromatin structure via stabilization of the NL and architectural proteins. These results are supported by previous observations wherein defects in the sophisticated assembly of nuclear lamins along with architectural proteins results in disease or aging (Fan *et al.*, 2005; Scaffidi and Misteli, 2006; Hock *et al.*, 2007; Murga *et al.*, 2007; Pegoraro *et al.*, 2009). Reorganization of heterochromatin at the NP by restoration of EHMT1 or EHMT2 in aged cells further reinforces the fact that EHMT proteins are key determinants of higher-order chromatin organization.

Aging associated defects in chromatin organization exhibits variety of functional consequences such as misregulation of gene expression via alteration of epigenome, activation of repeat elements and susceptibility to DNA damage (Gaubatz and Cutler, 1990; Shumaker *et al.*, 2006). In addition, loss of lamins leads to altered mechano-signalling (Osmanagic-Myers, Dechat and Foisner, 2015). Together, these processes make aged cells stressed and also influence the stress response contributing towards reduced proliferation and enhanced senescence. While our studies revealed a direct correlation between loss of peripheral heterochromatin and reduced proliferation in shEHMT and 58Y cells, we did not find a senescent phenotype in aged HDFs. We propose that the senescence seen in shEHMT1 cells could be because of the sledgehammer approach where loss of EHMT1 and peripheral heterochromatin occurs in acute manner. On the contrary, during aging, levels of EHMT proteins and peripheral heterochromatin decline gradually thereby allowing cell to co-opt mechanisms to evade the senescence response. Unlike the differences seen in the senescence phenotype, alteration of the epigenome is a common feature observed in shEHMT or aged HDFs. Together these results strengthen our conclusion that the loss of EHMTs confers age-associated defects and makes HDFs sensitive to stress. This interpretation is further supported by experiments where in culture induced stress magnified the effects of nuclear distortion and accelerated senescence in EHMT depleted high passage HDFs. Thus, we conclude that the steady loss of EHMT proteins drive normal aging. It remains a mystery as to how EHMT proteins are regulated. For now we propose that EHMT2 degradation leads to gradual destabilization of EHMT1 in response to aging via currently unknown mechanisms.

Materials and Methods

Antibodies & Inhibitors:

The following antibodies were used in the current study: EHMT1 (A301-642A, Bethyl Laboratories, Rabbit polyclonal), EHMT1 (NBP1-77400, Novus Biologicals, Rabbit polyclonal), EHMT2 (NBP2-13948, Novus Biologicals, Rabbit polyclonal), EHMT2 (07-551; Millipore, Rabbit polyclonal), H3K9me2 (ab1220, Abcam, Mouse monoclonal), LMNB1 (ab16048, Abcam, Rabbit polyclonal), LMNB2 (ab8983, Abcam, Mouse Monoclonal), LMNA/C (sc-20681, Santacruz, Rabbit polyclonal), HP1-β (ab101425, Abcam, Mouse monoclonal), H3K9me3 (ab8898, Abcam, Rabbit polyclonal), H3K27me3 (07-449, Millipore, Rabbit polyclonal), H3 (ab1791, Abcam, Rabbit polyclonal), p16 (ab54210, Abcam, Mouse monoclonal), GAPDH (G9545, Sigma, Rabbit polyclonal), Anti-Methyl (-N) Lysine antibody (ICP0501, Immunechem, Rabbit polyclonal), Anti-6XHis-tag antibody (ab9108, Abcam, Rabbit polyclonal), Anti GST (ab9085, Abcam, Rabbit polyclonal), Anti-GFP (ab290, Abcam, Rabbit polyclonal), Ash2L (ab176334, Abcam, Rabbit monoclonal), Normal Rabbit IgG (12-370, Millipore), Normal Mouse IgG (12-371, Millipore). Secondary antibodies Alexa Fluor 488 Goat anti-mouse (A-11001), Alexa Fluor 488 Goat anti-rabbit (A-11008) and Alexa Fluor 568 Goat anti-rabbit (A-11011) were purchased from Thermo Fisher Scientific while secondary antibodies Goat anti-mouse HRP (172-1011) and Goat anti-rabbit HRP (170-8241) were from Bio-Rad. MG132 (C2211) and BIX 01294 (B9311) inhibitors were purchased from Sigma-Aldrich.

Cell lines:

Fetal (2300), 18Y (2320) old human dermal fibroblasts (HDFs) were purchased from ScienCell, 38Y old HDFs (CC-2511) from Lonza while 19Y (C-013-5C), 31Y (C-

013-5C), 40Y (C-013-5C) and 58Y (A11634) old HDFs were purchased from Thermo Fisher Scientific.

shRNA constructs and Virus preparation:

EHMT1 shRNA- V3LHS_36054, was purchased from Sigma. The vector was co-transfected with psPAX2, pMDG2 in 293-LX packaging cell line using lipofectamine LTX (15338500, Thermo Fisher Scientific). Viral supernatants were harvested 48 hr. post transfection and concentrated using Amicon Ultra-15 centrifugal filter units (UFC910024, Millipore). Retroviral pSMP-Ehmt1_4 (plasmid # 36338, Addgene), pSMP-EHMT2_4 (Plasmid # 36334, Addgene), pSMP-EHMT2_1 (Plasmid # 36395, Addgene) vectors were purchased from addgene. These vectors were transfected in AmphoPack-293 cell line (631505, Clontech). Viral supernatants were harvested 48 h post transfection. Viral supernatant was used to transduce HDFs. V5-EHMT1 and Flag-EHMT2 constructs were obtained from Dr. Marjorie Brand (OHRI, Ottawa, Canada).

Transfection:

HEK293 cells were maintained in Dulbecco's Modified Eagle Medium (DMEM) (10566-016, Thermo Fisher Scientific) supplemented with 10% fetal bovine serum (FBS) (10082147, Thermo Fisher Scientific), 2mM L-glutamine (25030081, Thermo Fisher Scientific), and 1% nonessential amino acids (NEAA, 11140050, Thermo Fisher Scientific). At 70% confluence, HEK293 cells were transfected with pEGFPC1, pEGFP-ANK or pEGFP-SET plasmids using Lipofectamine 2000 (11668019, Thermo Fisher Scientific). HDFs were maintained in DMEM supplemented with 10% FBS, 2mM L-glutamine and 1%NEAA. For knockdown experiments, cells were transduced with viral particles containing shRNAs against EHMT1 or EHMT2 and incubated for 48 h. Post 48 h transduction, cells were washed

with complete media. Transduced fibroblasts were further cultured for 48h, harvested for protein and RNA extraction. For proteasome degradation pathway inhibition experiments, cells were treated with MG132 for 6h at 10μM concentration. For Bix-01294 experiments, cells were treated at 1μM concentration for 48h. Respective inhibitor treated cells were further processed for western blot, immunostaining &/or electron microscopy.

Over expression of EHMT1 and EHMT2 was carried out by transfecting V5-EHMT1 and Flag-EHMT2 over expression constructs in old HDFs using Neon transfection method (MPK10096, Thermo Fisher Scientific). Untransfected old HDFs served as a control. 5 X 10^5 - 2 X 10^6 cells were collected and the pellet was washed twice with PBS. Cell pellet was then resuspended in Buffer R along with 2-3μg of respective plasmids. Cell suspension was electroporated using Neon pipette and immediately transferred to pre-warmed media. Transfected and control cells were seeded for immunostaining and electron microscopy.

Cell growth curve:

HDFs from different age groups (18Y, 31Y and 58Y) and fetal fibroblasts transduced with shCnt or shEHMT1 and shEHMT2, were independently seeded per well of a 6 well plate, with one well each for different time points. After each time point, cells were harvested and cell count was determined. Cell count was plotted against the time points to determine the growth curve.

SA-β-Galactosidase Assay:

SA-β-Galactosidase staining was performed using the Senescence Cells Histochemical Staining Kit (CS0030, Sigma). In Brief, cells were seeded at a density of 3x10^4 cells per well of a 24 well plate and allowed to attach overnight. Cells were then rinsed with PBS followed by fixing with 1X Fixation buffer provided with the kit

for 8 min at RT. After rinsing thrice with PBS, 0.5ml of the staining mixture was added and incubated at 37°C without CO_2 for 18h. The percentage of β-gal positive cells were quantified from the images taken at 10 randomly selected microscopic fields.

Cloning:

The Ankyrin and SET domains of EHMT1 were amplified from cDNA prepared using the Superscript III cDNA synthesis kit (11752-050, Thermo Fisher Scientific) from HDFs with the help of Ankyrin (737-1004 AA) and SET (1013-1265 AA)domain primers (Supplementary Table 6). The PCR amplified EHMT1-Ankyrin and -SET products were then cloned into pEGFPC1 vector (6084-1, Clontech) to generate the plasmid constructs, pEGFP-ANK and pEGFP-SET. For cloning the C-Term of LMNB1, the cDNA from HDFs was PCR amplified using primers LMNB12F and LMNB1-1R (Supplementary Table 6) and cloned into pET28a+ vector between BamHI and HindIII restriction digestion sites. The identity of all plasmids was confirmed by sequencing.

Site directed mutagenesis was carried out at 417th lysine residue in LMNB1 plasmid construct mWasabi-LaminB1-10 (411th position in mWasabi-LaminB1 plasmid and 417th in Uniprot LMNB1 sequence). mWasabi-LaminB1-10 was obtained from Addgene (plasmid # 56507). Briefly, 200 ng of the LMNB1 plasmid construct was subjected to a standard mutagenic PCR reaction with *Q5* High Fidelity DNA polymerase (M0491, New England Biolabs) and 25 ng of specific primers. The primers used for site-directed mutagenesis are listed in supplementary table 7. The mutagenic PCR reaction parameters were as follows: 98°C for 1 min, 18 cycles (98°C for 15 sec, 70°C for 15 sec, 72°C for 2 min) and 72°C for 5 min. The final reaction volume was 50 µL. The reaction product was digested with 10 U of methylation-

sensitive enzyme *DpnI* at 37°C for 1h. (R0176, New England Biolabs). *E. coli* DH5-α competent cells were transformed with the amplified products. Finally, the plasmids were purified using the Qiagen plasmid DNA purification kit. Sequence for the K417A plasmid is provided in Supplementary Text 2.

qPCR and PCR:

Total RNA was isolated using Trizol reagent (15596018, Thermo Fisher Scientific) as per manufacturer instructions. RNA was subjected to cDNA synthesis using Maxima First strand cDNA synthesis kit (K1641, Thermo Fisher Scientific). Semi-quantitative PCR reactions were performed using 2X PCR Master Mix (K0171, Thermo Fisher Scientific). Products were resolved on 1.2% agarose gels. Quantitative PCRs were performed using Maxima SYBR green qPCR master mix (2X) (K0251, Thermo Fisher Scientific). GAPDH was used as an internal control. Primer sequences are provided in supplementary Table 6.

Preparation of whole cell extracts:

HEK293 cells transfected with pEGFPC1, pEGFP-ANK and pEGFP-SET constructs were centrifuged and cell pellets were washed with ice-cold PBS and lysed in ice-cold RIPA buffer containing protease inhibitor cocktail (PIC) (11697498001, Sigma) per 10^6 cells for 10 min on ice. The cell lysates were cleared by centrifugation and the supernatant was transferred to a fresh tube. Supernatant was used for immunoprecipitation experiments followed by western blotting.

Protein Induction & purification from bacterial cells:

The plasmids containing the human EHMT1-SET domain, EHMT1 (2IGQ) and EHMT2-SET domain, (Addgene plasmid # 25504 and Addgene plasmid # 25503 respectively) were expressed in *Escherichia coli C43 (DE3)* while LMNB1-CT was expressed in *Escherichia coli B834 (DE3)* cultured in LB medium with 50 µg/mL of

kanamycin (Sigma). After induction, cells were harvested and resuspended in lysis buffer containing 25 mM Tris pH 8.0, 0.5 M NaCl, 2 mM L-Dithiothreitol (DTT, M109, Amresco), 5% glycerol, 0.05% Nonidet P-40 Substitute (M158, Amresco); 3 µg/ml of deoxyribonuclease I (DNase I, DN25, Sigma), 50 mM imidazole supplemented with Complete protease inhibitor cocktail and 0.2 mM phenyl methyl sulfonyl fluoride (PMSF, 93482, Sigma). Cells were lysed by sonication using Vibra Cell Sonicator (Sonics & Materials Inc.). The crude extract was cleared and the supernatant was incubated overnight with 2 ml Ni-NTA Agarose resin pre-washed with the lysis buffer described above. The resin was packed into Econo-Column (738-0014, Biorad). The column was washed and 6x His tagged protein was eluted from the resin in protein elution buffer supplemented with 250 mM and 500 mM imidazole. The purity of protein was assessed by SDS–PAGE. The purified protein was concentrated, buffer exchanged and protein dialysis was performed using Amicon Ultra-4 centrifugal concentrators (UFC801008, Millipore,) with a molecular weight cut off of 10 kDa and the final concentration was estimated using the Bradford protein assay (5000006, Bio-Rad). The protein was also subjected to mass spectrometry to assess its purity and molecular weight. In-gel digestion for mass-spectrometry analysis revealed a Mascot Score of 2354.46 for 6X His EHMT1-SET.

Protein-protein interaction assays:

For interaction assays, Ni-NTA beads pre-washed with IP100 buffer (25 mM Tris pH 7.5, 100 mM KCl, 5 mM $MgCl_2$, 10% glycerol, 0.1% NP-40 and 200 µM PMSF) were incubated with 300 to 500 ng of 6X His-EHMT1-SET. The beads were washed twice with IP100 buffer followed by two washes with Flag buffer (20 mM HEPES, 150 mM KCl, 2 mM $MgCl_2$, 0.2 mM EDTA pH 8.0, 15% glycerol, 0.1% NP-40 and 200 µM PMSF) both supplemented with 100 mM imidazole. The beads were then

incubated with LMNB1-GST (H00004001-M01, Novus Biologicals) or GST alone (negative control) followed by washes with IP100 buffer and Flag buffer as mentioned above. The bead bound proteins were eluted and subjected to western blotting with anti-GST and anti-6x His antibodies.

Methyltransferase assay:

Detection by Western blot LMNB1-CT and EHMT1-SET/ EHMT2-SET were incubated along with 50 µM S-adenosyl methionine (SAM) in methyltransferase assay buffer in a 50 µl reaction at RT for 1 hour. 12 µl of 4x-SDS-PAGE loading dye was added to all the tubes to stop the reaction, samples were heated at 95°C for 8 min and resolved by 10% SDS-PAGE. The reaction was split into two, one was used for Western blot to probe with Anti-Methyl-K antibody and the other half was used to stain with Coomassie Blue stain (Coomassie Brilliant Blue R-250, Amresco).

Detection by fluorescence: The Methyltransferase assay was performed as per manufacturers instructions (ADI-907-032, Enzo Life Sciences). Sequences for LMNB1 peptides used for the assay are provided in Supplementary Table 6.

Immunoprecipitation (IP):

For IP experiments, cell or nuclear lysates (400 ug) prepared from HEK293 or HDFs to Dynabeads Protein A (10001D, Thermo Fisher Scientific) that were prebound with 2–3µg of indicated antibody and incubated overnight at 4°C. Beads were then washed and eluted in 2X loading dye. Eluted proteins were subjected to western blotting with indicated antibodies.

Chromatin Immunoprecipitation (ChIP):

ChIP was performed as described previously Brand *et al* 2008 (Brand *et al.*, 2008) with some modifications. In Brief, fetal HDFs were cross-linked with 1% formaldehyde. Cells were lysed in buffer N containing DTT, PMSF and 0.3% NP40.

After isolation of nuclei, comatin fractionation was done using 0.4U of MNase (N5386, Sigma) at 37^{o}C for 10min. Reaction was stopped using MNase stop buffer without proteinase K. Simultaneously, antibodies against EHMT1, LMNB1 and Rabbit IgG were kept for binding with Dynabeads for 2h at RT. After equilibration of beads, chromatin was added for pre-clearing. To antibody bound beads pre-cleared chromatin was added and kept for IP at 4^{0}C overnight.

Next day, beads were washed eluted at 65^{o}C for 5 min each. Eluted product was subjected to reverse cross-linking along with input samples, first with RNAse A at 65^{o}C overnight and then with proteinase K at 42^{o}C for 2h. After reverse cross-linking, DNA purification was performed using phenol-chloroform-isoamyl alcohol extraction method. The amount of DNA was quantitated using Qubit fluorometer.

ChIP-seq library preparation:

ChIP DNA was subjected to library preparation using TruSeq ChIP sample preparation kit from Illumina (IP-202-1012). Briefly, ChIP samples were processed for end repair to generate blunt ends using end repair mix. A single 'A' nucleotide was added to the 3' ends of the blunt fragments to prevent them from ligating to one another during the adapter ligation reaction. In the next step, indexing adapters were ligated to the ends of the DNA fragments. The ligated products were purified on a 2% agarose gel and narrow 250-300bp size range of DNA fragments were selected for ChIP library construction appropriate for cluster generation. In the last step, DNA fragments with adapter molecules on both ends were enriched using PCR. To verify the size and quality of library, QC was done on high sensitivity bioanalyzer chips from Agilent and the concentration was measured using Qubit dsDNA HS assay kit (Q32851, Thermo Fisher Scientific). After passing QC, samples were sequenced 75

paired end (PE) on NextSeq Illumina platform. Genotypic Technology Pvt. LTD. Bengaluru, India, performed the sequencing.

ChIP-seq Analyses:

Alignment of ChIP-seq derived short reads to the human reference genome (UCSC hg19) was done using Bowtie2 short read aligner (Langmead and Salzberg, 2012) with default parameters. Subsequently, aligned ChIP-seq reads from two replicates were merged. Peak calling was done for each sample with their respective control using MACS 1.4 algorithm (Zhang *et al.*, 2008). The following parameters deviated from their default value: - effective genome size = 2.70e+09, bandwidth = 300, model fold = 10, 30, p-value cutoff = 1.00e-03.

In order to identify regions enriched for EHMT1 and LMNB1, we employed a two-step approach, first total peak counts for EHMT1 and LMNB1 was calculated in 1MB window for all the chromosomes. Next, ratio of total peak count over expected peak count (total peaks from a chromosome divided by total 1 MB window for the same chromosome) was calculated for each 1MB window. Raw data has been deposited in NCBI {SRP110335 (PRJNA391761)}.

RNA-seq and data analysis

Fibroblasts from indicated age groups as well as fetal HDFs transduced with shEHMT1, shEHMT2 or shCnt were harvested and RNA was extracted by Trizol method. RNA concentrations were estimated using Qubit fluorometer and quality was assessed using Bioanalyzer. After passing the QC, samples were subjected for library preparation and QC for the same. Samples were sequenced at Genotypic Technology Private Limited, Bengaluru, India.

We obtained ~30-45 million reads million reads from EHMT1 and EHMT2 knockdown samples. From the sequencing reads, adapters were trimmed using

Trimmomatic program (Bolger, Lohse and Usadel, 2014). The reference based transcriptome assembly algorithms TopHat v2.1.0 (Trapnell, Pachter and Salzberg, 2009), Cufflinks v2.2.1 (Trapnell *et al.*, 2012) pipeline were used to assemble the transcripts with hg19 genome/ transcriptome (http://genome.ucsc.edu/) ('Initial sequencing and analysis of the human genome', 2001) as reference annotation to guide RABT assembly. Cuffdiff v2.2.1 (Trapnell *et al.*, 2013) was used to identify differentially expressed genes. The transcripts with adjusted *p* value < 0.05 & fold change > 1.5 were considered to be significantly expressed. We used GSEA (Subramanian *et al.*, 2005) to identify top 100 pathways (FDR qvalue < 0.05).

To shortlist genes involved in epigenetic modifications, Epigenetic Modifiers (http://crdd.osdd.net/raghava/dbem/)(Singh Nanda, Kumar and Raghava, 2016) & Epifactors (http://epifactors.autosome.ru/description) (Medvedeva *et al.*, 2015) database were used. The aging related genes were shortlisted GenAge (http://genomics.senescence.info/genes/allgenes.php) database (Tacutu *et al.*, 2013). Significantly expressed genes from both EHMT1 & EHMT2 knockdown datasets were overlapped with above mentioned databases. We used customized Perl scripts for all the analysis done in this study. All the plots and statistical analysis were done using R studio [63] (R Development Core Team, 2011). Raw data has been deposited in NCBI {SRP110335 (PRJNA391761)}.

Immunostaining:

Briefly, cells were fixed with 4% Paraformaldehyde (PFA, P6148, Sigma) for 10 minutes at room temperature (RT) and permeabilized with 0.5% triton X-100. The blocking was done with 5% BSA for 1h. Antibodies mentioned previously were used at desired dilution and imaging was carried out on FV1000 Confocal Microscope (Olympus).

Transmission Electron Microscopy (TEM):

For TEM sample preparation cells of different age groups or treated with different conditions as mentioned in results sections were trypsinized and the pellet was fixed with 2.5% glutaraldehyde and 2% sucrose at RT for 1h. Next, fixative was removed and pellet was washed with 0.1M phosphate buffer pH7.4. The buffer was replaced with 1% osmium tetraoxide and 1.5% potassium ferrocyanide and kept at 4^{o}C for 75min. Cell pellet was washed with 0.1M phosphate buffer as well as distilled water, subsequently dehydrated with gradient of ethanol followed by two changes of propylene oxide. Cell pellet was embedded gradually in Epoxy812 resin mixture (EMS). Resin embedded pellets were allowed to polymerize at 60^{o}C for 72h. The blocks were trimmed; sections of 60nm size were collected and imaged with the Tecnai G2 Spirit Bio-TWIN Transmission Electron Microscope at National Centre for Biological Sciences (NCBS) EM facility.

Flow cytometry:

Cells were harvested and fixed in ice cold 70% ethanol for 30 min at 4°C. Post fixation, cells were pelleted, washed twice in PBS and resuspended in 0.5ml PBS containing 0.2mg/ml RNase A (EN0531, Thermo Fisher scientific) and incubated for 30 min at 37°C. To this Propidium Iodide (P3566, Thermo Fisher Scientific) at a concentration of 50µg/ml was added and incubated for 10 min at 37°C. The percentage of cells in various phases of cell-cycle was assessed by flow cytometry (BD FACSVerse) and analyzed using the FlowJo software.

Telomerase assay:

Telomerase activity was detected using the PCR-based Telomeric Repeat Amplification Protocol (TRAP) assay kit (Millipore, S7700). Briefly, HDFs were seeded at a density of 1.5×10^5 cells per well in a 12-well plate 1 day before

transduction. Cells were transduced with shEHMT1, shEHMT2 or shCnt. Both the untransduced fibroblasts and the fibroblasts transduced with shEHMT1/shEHMT2 were harvested 48h after transduction. The cell pellet was resuspended in 1X CHAP Buffer provided with the kit and the protocol was followed as per the manufacturer's instructions.

Quantitation for mean fluorescence intensity:

For quantitation of fluorescence intensity in Fig. 4a and Supplementary Fig. 7a-d, MATLAB programming was used. Briefly, centroid of nuclei was determined and 200 line scans from center to periphery of the cells were drawn. Each line was further divided into 200 points. Average intensity distribution was calculated for each nucleus by calculating mean of 200 line scans from center to periphery. Mean fluorescence intensity (MFI) was plotted for center vs. periphery of nuclei. Mean intensity profile with standard deviation for all the measured nuclei. The Script for MATLAB programme is provided in Supplementary Text 3.

Statistics:

The detailed statistical analysis and methods have been described in the figure legends along with the p-values for respective data sets. For statistical analysis, GraphPad Prism version 6 software was used.

Acknowledgments

We thank Drs. Colin Jamora, Arjun Guha and Pavan Kumar P for the helpful suggestions and critical reading of the manuscript. The authors acknowledge the facilities, and the scientific and technical assistance of the electron microscopy facility at National Centre for Biological Sciences (NCBS) -TIFR Bangalore. RNA sequencing was performed at the Genotypic Technology Private Limited, Bangalore, India. Confocal microscopy, Transmission Electron microscopy and Flow cytometry were performed at the Central Imaging and Flow Facility (NCBS/inStem). This work was supported by grant from the Wellcome Trust/DBT India Alliance (to S.R.) and inStem core funding. A.K. is Career Development Fellow (CDF) supported by funds from NCBS. R.R.A is supported by Indian Council of Medical Research (ICMR)-Senior Research Fellowship (SRF). S.R. C.P and D.P. are Wellcome Trust/ DBT India Alliance Intermediate Fellows.

Author contributions

A.K performed experiments on immunostaining, western blotting, electron microscopy, ChIP, PCRs, MG132 and Bix-01294 studies. R.R. performed experiments on lentivirus, retrovirus production, shRNA transduction, overexpression studies, PCRs, immunostaining, TRAP assays, IPs, cell growth and cell-cycle studies. N.K. is responsible for cloning and purification of EHMT1 and LMNB1 truncation proteins and LMNB1 methylation studies. P.K. is responsible for analysis of ChIP Seq data. F.R. performed western blotting, immunostaining, long-term fibroblast passage experiments, cell cycle and cell growth analysis, nuclear distortion and culture induced stress experiments. A.M. cloned mammalian EHMT1 truncations; performed IP and western blot analysis. V.L is responsible for bioinformatics analysis of RNA-Seq data sets. S.D and S.R. wrote program-using MATLAB for the analysis

of immunostaining experiments. A.G provided intellectual inputs. D.P. supervised bioinformatics analysis of RNA and ChIP sequencing and provided intellectual inputs on the manuscript. M.B and C.P provided EHMT1 and EHMT2 overexpression constructs. S.R. conceptualized the project, designed the experiments and wrote the manuscript.

Conflicts of Interest

The authors declare no competing financial interests.

Figure Legends

Figure 1. EHMT1, EHMT2 and LMNB1 are members of the same complex. a. EHMT1 interacting proteins identified by mass spectrometric analysis with details indicating coverage and peptide score. **b.** Sequential IP in HEK293 cells demonstrating EHMT1, EHMT2, LMNB1 are a part of the same complex. **c.** LMNB1 interacts with EHMT1 via SET domain. Recombinant GST or GST-LMNB1 was incubated with Ni-NTA bound His-EHMT1 SET protein. Post washing eluents were loaded for immunoblotting using GST or His antibody. Recombinant pure proteins GST-LMNB1 (lane 1), GST (lane 2), EHMT1-SET (lane 3) were used as controls. **d.** Venn diagram showing unique and overlapping reads obtained from EHMT1 and LMNB1 ChIP-Sequencing. **e.** Composite profile of EHMT1 and LMNB1 read density around the transcription start site (TSS). **f.** Genomic distribution of EHMT1 and LMNB1 peaks. The majority of binding sites obtained were enriched in intronic region or distal regions from a gene. **g-h.** Representative histogram showing normalized ChIP-seq read density (above 1.5 fold over expected) of EHMT1 and LMNB1 in 1MB bin for chromosome 1 & 9.

Figure 2. EHMT1 and EHMT2 methylate LMNB1 at C-terminus. a-b. Western blot probed with anti-Methyl-K antibody. Lanes to the left of ladder are control reactions containing 2 µg LMNB1-CT + 50 µM SAM (lane 1) or 2 µg of EHMT1-SET/EHMT2-SET + 2 µg LMNB1-CT (lane 2) and 2 µg LMNB1-CT only (lane 3). Lanes to the right of ladder are methyltransferase reactions containing 1, 2 and 4 µg of LMNB1-CT and EHMT1-SET/EHMT2-SET along with 50 µM SAM. Lower panel: Coomassie stained gel representing all the reactions mentioned above. **c-d.** Nuclear lysates from HEK-293 were immunoprecipitated with anti-Methyl-K or anti-

LMNB1 antibody followed by western blotting with anti-Pan H3, anti- LMNB1 and anti-Methyl-K antibodies. **e.** Reduced methylation of LMNB1 by EHMT1 and EHMT2 upon single amino acid substitution from lysine (RKR) to alanine (RAR). Mutant LMNB1 peptides were synthesized and subjected to methyltransferase reaction containing EHMT1-SET and EHMT2-SET with SAM as a methyl donor. H3 peptide was used as a positive control for the reaction. **f.** Immunostaining for LMNB1 in fetal HDFs transduced with Wt. LMNB1 and K417A-LMNB1 constructs. (Scale bar: 20µm). Arrows indicate the cells zoomed in the far right image presented.

Figure 3. EHMT1 and EHMT2 knockdown results in reduced LMNB1 levels. a. Western blot analysis for LMNB1 and LMNA/C in fetal HDFs transduced with shEHMT1 and shEHMT2 virus. Untransduced (UT) and control shRNA (shCnt) were used as controls. **b-c.** Fetal HDFs were transduced with shCnt, shEHMT1 and shEHMT2 virus. Post transduction cells were immunostained for EHMT1 or EHMT2 and co-stained for nuclear lamina using LMNB1 antibody. Distortion of nuclear architecture was seen upon loss of EHMT1 and EHMT2 proteins. (Scale bar: 20µm). Arrows indicate the cells zoomed in the far right image presented. **d.** Relative expression of LMNA and LMNB1 in fetal HDFs upon EHMT1 and EHMT2 knockdown compared to UT/shCnt cells.

Figure 4. EHMT1 and EHMT2 lead results in detachment of peripheral heterochromatin. a. MFI for H3K9me2 staining in fetal HDFs transduced with shEHMT1 and shEHMT2. MFI has been represented as center vs. periphery of the nuclei and compared with respect to shCnt cells. $p<0.0001$, Kruskal-Wallis test (Dunn's multiple comparison post hoc test). **b-d.** Fetal HDFs were transduced with shCnt, shEHMT1 and shEHMT2 virus. TEM was performed to visualize the heterochromatin in EHMT1 and EHMT2 knockdown cells. Peripheral

heterochromatin was intact at the nuclear periphery beneath the NL in control cells while this distribution was drastically altered upon knockdown of EHMT1 and EHMT2. (Scale bar: 1µm). Arrows indicate the heterochromatin staining. **e.** Immunostaining for H3K9me2 in fetal HDFs expressing Wt. LMNB1 or K417A-LMNB1 mutant plasmids. (Scale bar: 20µm). Arrows indicate the cells zoomed in the far right image presented. **f-g.** Fetal HDFs transfected with Wt. LMNB1 and K417A-LMNB1 plasmids were processed for electron microscopy. Cells transfected with Wt. LMNB1 plasmid showed intact peripheral heterochromatin while K417A-LMNB1 transfected cells showed loss of heterochromatin with nuclear envelope breaks. (Scale bar: 1µm). Arrows indicate the zoomed area presented in the insert below. **h.** qRT-PCR to validate expression of EZH2 in UT, shEHMT1 and shEHMT2 transduced HDFs. One sample t-test (two-tailed) (n=2). UT vs. shEHMT1 (*p=0.0496), UT vs. shEHMT2 (*p=0.0449). **i.** Immunostaining for H3K27me3 mark and HP1 protein in fetal HDFs transduced with shCnt, shEHMT1 and shEHMT2. Knockdown of EHMT1 and EHMT2 leads to reduction in H3K27me3 mark, which corroborates with decreased Ezh2 expression while HP1 expression was reduced only in shEHMT1 cells. (Scale bar: 20µm)

Figure 5. Depletion of EHMT1, EHMT2 and LMNB1 in an age dependent manner. a. Western blot analysis for indicated proteins in HDF cell lysates derived from various age groups. **b.** Quantification of EHMT1 and EHMT2 protein expression in HDFs of various age groups. Kruskal-Wallis test (post-hoc: Dunn's multiple comparison test) (n=3). For EHMT1: Fetal vs. 58Y (*p=0.0257), For EHMT2: Fetal vs. 58Y (*p=0.0144)). **c-d.** Immunostaining for EHMT1, EHMT2, H3K9me2 and PanH3 in fibroblasts from indicated age groups (Scale bar: 20µm). **e.** Western blot analysis for H3K9me2 mark in indicated age groups. **f.** Representative

TEM images for nuclei of 18Y, 31Y, 40Y and 58Y HDFs. Arrows indicate peripheral heterochromatin staining. Inset is the zoomed version of the same images. (Scale bar: 1µm)**. g.** Relative expression of EHMT1 and EHMT2 at the mRNA level in fetal, 18Y and 58Y old HDFs. **h.** Western blot for EHMT1 and EHMT2 in 18Y and 58Y old HDFs treated with or without proteosomal degradation inhibitor MG132 (10µM for 6h). **i.** Quantification of EHMT1 and EHMT2 protein levels in 18Y old HDFs treated with or without MG132 treatment. One sample t-test (two-tailed) (n=3). 18Y EHMT2: UT vs. MG132 (**p=0.0154). **j.** Western blot analysis for LMNB1, LMNB2 and LMNA/C in various age groups HDFs. GAPDH was used as an internal control. **k.** Reduced levels of methylated LMNB1 during physiological aging. Nuclear extracts from indicated age groups were subjected to IP using LMNB1 antibody. IPed material was immunoblotted for methyl LMNB1 and LMNB1 using anti anti-Methyl-K and LMNB1 antibodies respectively. 80 µg of fetal HDFs derived nuclear lysate was used as input control.

Figure 6. Overexpression of EHMT1 and EHMT2 with mutant LMNB1 does not restore of peripheral heterochromatin organization in aged cells. a-b. Immunostaining for LMNB1 and H3K9me2 in 58Y HDFs transduced with V5-EHMT1 and Flag-EHMT2 over expression constructs. (Scale bar: 20µm) Arrows indicate the cells zoomed in the far right image presented. **c-e.** Old HDFs over expressing EHMT1 and EHMT2 were processed for electron microscopy. Over expression of EHMT1 and EHMT2 causes restoration of peripheral heterochromatin in old cells compared with control cells (Scale bar: 1µm). Arrows indicate the area zoomed and presented in the insert format.

Figure 7. EHMT1 and EHMT2 knockdown leads to reduced cell proliferation and drives cells towards senescence. a-b. Knockdown of EHMT1 and EHMT2

reduces cell proliferation. Equal number of HDFs were seeded and transduced with shCnt, shEHMT1 and shEHMT2 virus. Fourty eight hours post transduction, number of cells in the culture was counted over a period of four days as indicated. Two-way ANOVA (post-hoc: Tukey's multiple comparison test) (n=3). Day3: shCnt vs. shEHMT1 (**p=0.0015), Day4: shCnt vs. shEHMT1 (***p<0.0001), Day1: shCnt vs. shEHMT2 (***p=0.0002), Day2: shCnt vs. shEHMT2 (***p<0.0001), Day3: shCnt vs. shEHMT2 (***p<0.0001), Day4: shCnt vs. shEHMT2 (***p<0.0001). **c.** Quantification of cell cycle analysis. Increase in sub-G1 population an indication of cell apoptosis upon EHMT2 knockdown. Two-way ANOVA (post-hoc: Tukey's multiple comparison test) (n=3). SubG1: shCnt vs. shEHMT2 (**p=0.0011) **d-e.** Equal number of HDFs were seeded and transduced with shCnt, shEHMT1 and shEHMT2 virus. β-Galactosidase (senescence) assay was performed to monitor the cellular senescence in cultures. Percentage of cells undergoing senescence was quantitated. **f-g.** TRAP assay to detect telomerase activity in indicated age groups as well as in shCnt, shEHMT1 and shEHMT2 transduced cells. Fetal, 18Y and shCnt fibroblast lysates were heat inactivated (HI) as a negative control for the assay. Reduced telomerase activity upon knockdown of EHMT1 and EHMT2 as well as during physiological aging from fetal to 58Y old cells.

Figure 8. Replicative stress leads to molecular defects that correlate with EHMT1 and EHMT2 loss. a. Equal number of cells from various age groups (two different passages) was seeded and number of cells was counted at 24, 48 and 72 h. Two way ANOVA (post-hoc: Tukey's multiple comparison test) (n=4). 72 h: P20 18Y vs. P15 58Y (**p=0.0003), 72 h: P20 31Y vs. P15 58Y (**p=0.0012). **b.** Immunostaining for LMNB1 in HDFs derived from 18Y, 31Y and 58Y (two different passages) was visualized by confocal microscopy. (Scale bar: 20μm) **c.** Quantification

of fibroblasts showing nuclear distortion upon replicative senescence in aging HDFs. Kruskal-Wallis test (post-hoc: Dunn's multiple comparison test) (n=2). P5 18Y vs. P5 58Y (**p=0.0165), P20 31Y vs. P15 58Y (*p=0.0259), P20 18Y vs. P15 58Y (*p=0.0462). **d.** Western blot analysis showing up regulation of senescent marker p16 from P5 to P20. GAPDH was used as an internal control. **e.** Quantitation of p16 expression in aging HDFs (two different passages). Up regulation of p16 expression was observed upon replicative senescence in aging HDFs. **f.** Model depicting EHMT1 and EHMT2 maintaining peripheral heterochromatin in young cells that falls apart upon EHMT1and EHMT2 knockdown or aging.

References

1. Bian, Q. *et al.* (2013) 'β-Globin cis-elements determine differential nuclear targeting through epigenetic modifications', *J Cell Biol*, 203, pp. 767-783. doi: 10.1083/jcb.201305027.
2. Black, J. C. and Whetstine, J. R. (2011) 'Chromatin landscape: methylation beyond transcription.', *Epigenetics : official journal of the DNA Methylation Society*, 6(1), pp. 9–15. doi: 10.4161/epi.6.1.13331.
3. Bodnar, A. G. *et al.* (1998) 'Extension of Life-Span by Introduction of Telomerase into Normal Human Cells', *Science*, 279(5349), pp. 349-352.
4. Bolger, A. M., Lohse, M. and Usadel, B. (2014) 'Trimmomatic: a flexible trimmer for Illumina sequence data', *Bioinformatics*. Oxford University Press, 30(15), pp. 2114–2120. doi: 10.1093/bioinformatics/btu170.
5. Brand, M. *et al.* (2008) 'Analysis of epigenetic modifications of chromatin at specific gene loci by native chromatin immunoprecipitation of nucleosomes isolated using hydroxyapatite chromatography', *Nat. Protocols*. Nature Publishing Group, 3(3), pp. 398–409. Available at: http://dx.doi.org/10.1038/nprot.2008.8.
6. Burke, B. and Stewart, C. L. (2013) 'The nuclear lamins: flexibility in function', *Nat Rev Mol Cell Biol*. Nature Publishing Group, 14(1), pp. 13–24. doi: 10.1038/nrm3488.
7. Camps, J., Erdos, M. R. and Ried, T. (2015) 'The role of lamin B1 for the maintenance of nuclear structure and function', *Nucleus*. 6(1), pp. 8–14. doi: 10.1080/19491034.2014.1003510.
8. Choi, D. *et al.* (2001) 'Telomerase expression prevents replicative senescence

but does not fully reset mRNA expression patterns in Werner syndrome cell strains', *The FASEB Journal* , 15(6), pp. 1014–1020. doi: 10.1096/fj.00-0104com.

9. Coutinho, H. D. M. *et al.* (2009) 'Molecular ageing in progeroid syndromes: Hutchinson-Gilford progeria syndrome as a model', *Immunity & Ageing : I & A*, 6, pp. 4. doi: 10.1186/1742-4933-6-4.
10. Dechat, T. *et al.* (2008) 'Nuclear lamins: major factors in the structural organization and function of the nucleus and chromatin', *Genes & Development*. Cold Spring Harbor Laboratory Press, 22(7), pp. 832–853. doi: 10.1101/gad.1652708.
11. Dixon, J. R. *et al.* (2012) 'Topological domains in mammalian genomes identified by analysis of chromatin interactions', *Nature*. Nature Publishing Group, a division of Macmillan Publishers Limited. All Rights Reserved., 485(7398), pp. 376–380. Available at: http://dx.doi.org/10.1038/nature11082.
12. Dreesen, O. *et al.* (2013) 'Lamin B1 fluctuations have differential effects on cellular proliferation and senescence', *The Journal of Cell Biology*. The Rockefeller University Press, 200(5), pp. 605–617. doi: 10.1083/jcb.201206121.
13. Egorova, K. S., Olenkina, O. M. and Olenina, L. V (2010) 'Lysine methylation of nonhistone proteins is a way to regulate their stability and function', *Biochemistry (Moscow)*, 75(5), pp. 535–548. doi: 10.1134/S0006297910050019.
14. Fan, Y. *et al.* (2005) 'Histone H1 depletion in mammals alters global chromatin structure but causes specific changes in gene regulation', *Cell*, 123(7), pp. 1199–1212. doi: 10.1016/j.cell.2005.10.028.

15. Foisner, R. (2001) 'Inner nuclear membrane proteins and the nuclear lamina', *Journal of Cell Science*, 114(21), pp. 3791-3792. Available at: http://jcs.biologists.org/content/114/21/3791.
16. Freund, A. *et al.* (2012) 'Lamin B1 loss is a senescence-associated biomarker', *Molecular Biology of the Cell*. Edited by T. M. Magin. The American Society for Cell Biology, 23(11), pp. 2066–2075. doi: 10.1091/mbc.E11-10-0884.
17. Gaubatz, J. W. and Cutler, R. G. (1990) 'Mouse satellite DNA is transcribed in senescent cardiac muscle.', *Journal of Biological Chemistry* , 265(29), pp. 17753–17758. Available at: http://www.jbc.org/content/265/29/17753.
18. Goldberg, M., Nili, E. and Cojocaru, G. (1999) 'Functional organization of the nuclear lamina', *Gene Ther Mol Biol*, 4(December), p. 143.
19. Goldman, R. D. *et al.* (2002) 'Nuclear lamins : building blocks of nuclear architecture Nuclear lamins : building blocks of nuclear architecture', pp. 533–547. doi: 10.1101/gad.960502.
20. Guelen, L. *et al.* (2008) 'Domain organization of human chromosomes revealed by mapping of nuclear lamina interactions', *Nature*. Nature Publishing Group, 453(7197), pp. 948–951. Available at: http://dx.doi.org/10.1038/nature06947.
21. Harr, J. C. *et al.* (2015) 'Directed targeting of chromatin to the nuclear lamina is mediated by chromatin state and A-type lamins', *J Cell Biol*, 208, pp.33-52. doi: 10.1083/jcb.201405110
22. Hock, R. *et al.* (2007) 'HMG chromosomal proteins in development and disease', *Trends in cell biology*, 17(2), pp. 72–79. doi: 10.1016/j.tcb.2006.12.001.
23. 'Initial sequencing and analysis of the human genome' (2001) *Nature*.

Macmillian Magazines Ltd., 409(6822), pp. 860–921. Available at: http://dx.doi.org/10.1038/35057062.

24. Kind, J. *et al.* (2013) 'Single-cell dynamics of genome-nuclear lamina interactions', *Cell*, 153, pp. 178-192. doi: 10.1016/j.cell.2013.02.028.
25. Kourtis, N. and Tavernarakis, N. (2011) 'Cellular stress response pathways and ageing: intricate molecular relationships', *The EMBO Journal*. Nature Publishing Group, 30(13), pp. 2520–2531. doi: 10.1038/emboj.2011.162.
26. Kramer, J. M. (2015) 'Regulation of cell differentiation and function by the euchromatin histone methyltranserfases G9a and GLP', *Biochemistry and Cell Biology*. NRC Research Press, 94(1), pp. 26–32. doi: 10.1139/bcb-2015-0017.
27. Langmead, B. and Salzberg, S. L. (2012) 'Fast gapped-read alignment with Bowtie 2', *Nat Meth*. Nature Publishing Group, a division of Macmillan Publishers Limited. All Rights Reserved., 9(4), pp. 357–359. Available at: http://dx.doi.org/10.1038/nmeth.1923.
28. Lanouette, S. *et al.* (2014) 'The functional diversity of protein lysine methylation', *Molecular Systems Biology*. European Molecular Biology Organization, 10(4), p. 724. doi: 10.1002/msb.134974.
29. López-Otín, C. *et al.* (2017) 'The Hallmarks of Aging', *Cell*. Elsevier, 153(6), pp. 1194–1217. doi: 10.1016/j.cell.2013.05.039.
30. Medvedeva, Y. A. *et al.* (2015) 'EpiFactors: a comprehensive database of human epigenetic factors and complexes', *Database: The Journal of Biological Databases and Curation*. Oxford University Press, 2015, p. bav067. doi: 10.1093/database/bav067.
31. Montes de Oca, R., Andreassen, P. R. and Wilson, K. L. (2014) 'Barrier-to-Autointegration Factor influences specific histone modifications', *Nucleus*,

2(6), pp. 580–590. doi: 10.4161/nucl.2.6.17960.

32. Mozzetta, C. *et al.* (2015) 'Sound of silence: the properties and functions of repressive Lys methyltransferases', *Nat Rev Mol Cell Biol*. Nature Publishing Group, a division of Macmillan Publishers Limited. All Rights Reserved., 16(8), pp. 499–513. Available at: http://dx.doi.org/10.1038/nrm4029.
33. Murga, M. *et al.* (2007) 'Global chromatin compaction limits the strength of the DNA damage response', *The Journal of Cell Biology*. The Rockefeller University Press, 178(7), pp. 1101–1108. doi: 10.1083/jcb.200704140.
34. Oberdoerffer, P. *et al.* (2008) 'SIRT1 Redistribution on Chromatin Promotes Genomic Stability but Alters Gene Expression during Aging', *Cell*. Elsevier Inc., 135(5), pp. 907–918. doi: 10.1016/j.cell.2008.10.025.
35. Osmanagic-Myers, S., Dechat, T. and Foisner, R. (2015) 'Lamins at the crossroads of mechanosignaling', *Genes & Development* , 29(3), pp. 225–237. doi: 10.1101/gad.255968.114.
36. Pegoraro, G. *et al.* (2009) 'Aging-related chromatin defects via loss of the NURD complex', *Nature cell biology*, 11(10), pp. 1261–1267. doi: 10.1038/ncb1971.
37. Rathert, P. *et al.* (2008) 'Protein lysine methyltransferase G9a acts on non-histone targets', *Nature chemical biology*, 4(6), pp. 344–346. doi: 10.1038/nchembio.88.
38. Razafsky, D. *et al.* (2016) 'Lamin B1 and lamin B2 are long-lived proteins with distinct functions in retinal development', *Molecular Biology of the Cell*. Edited by T. Misteli. The American Society for Cell Biology, 27(12), pp. 1928–1937. doi: 10.1091/mbc.E16-03-0143.
39. Roopra, A., Qazi, R., Schoenike, B., Daley, T. J. & Morrison, J. F. (2004)

Localized domains of G9a-mediated histone methylation are required for silencing of neuronal genes. *Mol. Cell*, 14**,** pp. 727–738. doi: 10.1016/j.molcel.2004.05.026

40. Scaffidi, P. and Misteli, T. (2006) 'Lamin A-Dependent Nuclear Defects in Human Aging', *Science (New York, N.Y.)*, 312(5776), pp. 1059–1063. doi: 10.1126/science.1127168.
41. Shevelyov, Y. Y. and Nurminsky, D. I. (2012) 'The nuclear lamina as a gene-silencing hub', *Current Issues in Molecular Biology*, 14(1), pp. 27–38. doi: v14/27 [pii].
42. Shimi, T. *et al.* (2011) 'The role of nuclear lamin B1 in cell proliferation and senescence', *Genes & Development*. Cold Spring Harbor Laboratory Press, 25(24), pp. 2579–2593. doi: 10.1101/gad.179515.111.
43. Shinkai, Y. and Tachibana, M. (2011) 'H3K9 methyltransferase G9a and the related molecule GLP', *Genes & Development*. Cold Spring Harbor Laboratory Press, 25(8), pp. 781–788. doi: 10.1101/gad.2027411.
44. Shumaker, D. K. *et al.* (2006) 'Mutant nuclear lamin A leads to progressive alterations of epigenetic control in premature aging', *Proceedings of the National Academy of Sciences of the United States of America*. National Academy of Sciences, 103(23), pp. 8703–8708. doi: 10.1073/pnas.0602569103.
45. Simon, D. N. and Wilson, K. L. (2013) 'Partners and post-translational modifications of nuclear lamins', *Chromosoma*, 122(0), pp. 13–31. doi: 10.1007/s00412-013-0399-8.
46. Singh Nanda, J., Kumar, R. and Raghava, G. P. S. (2016) 'dbEM: A database of epigenetic modifiers curated from cancerous and normal genomes'. The

Author(s), 6, p. 19340. Available at: http://dx.doi.org/10.1038/srep19340.

47. Snider, N. T. and Omary, M. B. (2014) 'Post-translational modifications of intermediate filament proteins: mechanisms and functions', *Nature reviews. Molecular cell biology*, 15(3), pp. 163–177. doi: 10.1038/nrm3753.
48. Solovei, I. *et al.* (2013) 'LBR and lamin A/C sequentially tether peripheral heterochromatin and inversely regulate differentiation', *Cell*, 152.
49. Subramanian, A. *et al.* (2005) 'Gene set enrichment analysis: A knowledge-based approach for interpreting genome-wide expression profiles', *Proceedings of the National Academy of Sciences* , 102(43), pp. 15545–15550. doi: 10.1073/pnas.0506580102.
50. Tachibana, M. et al. (2002) G9a histone methyltransferase plays a dominant role in euchromatic histone H3 lysine 9 methylation and is essential for early embryogenesis. Genes Dev, 16, pp. 1779–1791. doi:10.1101/gad.989402
51. Tachibana, M. *et al.* (2005) Histone methyltransferases G9a and GLP form heteromeric complexes and are both crucial for methylation of euchromatin at H3-K9. *Genes Dev*, 19**,** pp. 815–826. doi: 10.1101/gad.1284005.
52. Tacutu, R. *et al.* (2013) 'Human Ageing Genomic Resources: Integrated databases and tools for the biology and genetics of ageing', *Nucleic Acids Research*. Oxford University Press, 41(Database issue), pp. D1027–D1033. doi: 10.1093/nar/gks1155.
53. Towbin, B. D. *et al.* (2012) 'Step-wise methylation of histone H3K9 positions heterochromatin at the nuclear periphery', *Cell*, 150(5), pp. 934–947. doi: 10.1016/j.cell.2012.06.051.
54. Trapnell, C. *et al.* (2012) 'Differential gene and transcript expression analysis of RNA-seq experiments with TopHat and Cufflinks', *Nature Protocols*, 7(3),

pp. 562–578. doi: 10.1038/nprot.2012.016.

55. Trapnell, C. *et al.* (2013) 'Differential analysis of gene regulation at transcript resolution with RNA-seq', *Nature biotechnology*, 31(1), p. 10.1038/nbt.2450. doi: 10.1038/nbt.2450.
56. Trapnell, C., Pachter, L. and Salzberg, S. L. (2009) 'TopHat: discovering splice junctions with RNA-Seq', *Bioinformatics*, 25. doi: 10.1093/bioinformatics/btp120.
57. Trojer, P. and Reinberg, D. (2008) 'A gateway to study protein lysine methylation', *Nat Chem Biol*. Nature Publishing Group, 4(6), pp. 332–334. Available at: http://dx.doi.org/10.1038/nchembio0608-332.
58. Zhang, X., Wen, H. and Shi, X. (2012) 'Lysine methylation : beyond histones Modifying Enzymes for Lysine Methylation', *Acta Biochim Biophys Sin*, 44, pp. 14–27. doi: 10.1093/abbs/gmr100.Review.
59. Zhang, Y. *et al.* (2008) 'Model-based Analysis of ChIP-Seq (MACS)', *Genome Biology*, 9(9), p. R137. doi: 10.1186/gb-2008-9-9-r137.
60. R Development Core Team (2011), R: A Language and Environment for Statistical Computing. Vienna, Austria : the R Foundation for Statistical Computing. ISBN: 3-900051-07-0.

Euchromatic histone methyltransferases regulate peripheral heterochromatin tethering via histone and non-histone protein methylations

Alhad Ashok Ketkar[1ξ], Radhika Arasala Rao[1,3ξ], Neelam Kedia[1], Febina Ravindran[1], Vairavan Lakshmanan[2,3], Pankaj Kumar[1], Abhishek Mohanty[1], Shilpa Dilip Kumar[2], Sufi O Raja[2], Akash Gulyani[2], ChandraPrakash Chaturvedi[5], Marjorie Brand[4], Dasaradhi Palakodeti[2], Shravanti Rampalli[1*]

Supplementary Figure Legends

Supplementary Figure 1. EHMT1 interacts with LMNB1 domain and co-regulate a subset of genes a. EHMT1 interacts with EHMT2, LMNB1 and HP1. Whole cell lysates from fetal HDFs were subjected for IP reaction using EHMT1 or LMNB1 antibody. Subsequently western blot was performed using IPed material to detect EHMT1, EHMT2, LMNB1 and HP1. ASH2L did not show any interaction with EHMT1 and LMNB1 thus acted as a negative control. **b.** EHMT1 interacts with LMNB1 and EHMT2 via SET domain. HEK293 cells were transfected with pEGFP-Ankyrin (pEGFP-ANK) or pEGFP-SET domains of EHMT1 to determine domain specific association with LMNB1. Cell extracts were subjected to IP using GFP-antibody and the bound complexes were then analyzed by immunoblotting using LMNB1, EHMT2 and GFP antibodies. HEK-293 whole cell extract represents 1% input**.** pEGFPC1 empty vector transfected HEK293 or untransfected HEK293 cells were used as control reactions. Arrows indicate specific band. **c.** Coomassie stained SDS-PAGE gel showing 6X His EHMT1-SET purified protein used for methyltransferase assays. **d-f.** Gene Ontology (GO) analysis of EHMT1 and LMNB1

bound genes. Representative figure showing enriched GO terms for EHMT1 **(d)**, LMNB1 **(e)** and EHMT1 and LMNB1 **(f)** co-bound genes. The length of the bar (y-axis) denotes total genes falling within GO term. **g.** Circos plot showing genome wide peak density of EHMT1 (green) and LMNB1 (red).

Supplementary Figure 2. Mutation in LMNB1 causes distortion of the nuclear architecture. a. Coomassie stained SDS-PAGE gel showing 6X His LMNB1-CT purified protein used for methyltransferase assays. **b.** Increasing concentrations of LMNB1-GST showed greater degree of methylation by EHMT1-SET. Methyltransferase assay was performed using a fixed concentration of recombinant 6X His EHMT1-SET as enzyme source, and SAM as a methyl group donor. Recombinant GST-LMNB1 (4.5 ng and 9 ng) and Histone H3 peptide (10 ng) were used as substrates in the assay. Histone H3 peptide was used as a positive control. The mean relative fluorescence unit (RFU) values represented in the graph were obtained after subtracting the values obtained for controls EHMT1-SET only, SAM only, LMNB1-GST (4.5 ng) with those of the LMNB1-GST (4.5 ng and 9 ng) and Histone H3 (10 ng). **c.** Immunostaining for LMNB1 in fetal HDFs transduced with K417A-LMNB1 mutant construct. (Scale bar: 20µm). Arrows indicate the cells zoomed in the far right image presented. **d.** Immunostaining for LMNA/C in fetal HDFs transduced with Wt. LMNB1 and K417A-LMNB1 mutant construct. (Scale bar: 20µm). Arrows indicate the cells zoomed in the far right image presented.

Supplementary Figure 3. EHMT1 and EHMT2 knock-down causes nuclear distortion. a. Western blot analysis for EHMT1 and EHMT2 in fetal HDFs upon knock down of EHMT1 and EHMT2. GAPDH was used as a loading control. **b-c.** Relative protein levels of EHMT1 and EHMT2 upon knockdown. **d.** Percentage of

distorted nuclei increase in human fibroblasts transduced with shEHMT1 and shEHMT2 virus compared to UT or shCnt.

Supplementary Figure 4. Knock-down of EHMT1 and EHMT2 reduce H3K9me2 marks. a. Western blot analysis for H3K9me2 and H3K9me3 in UT, shCnt, shEHMT1 and shEHMT2 transduced HDFs. Pan H3 was used as loading control. **b.** Quantification of H3K9me2 upon EHMT1 and EHMT2 knockdown. **c.** Immunostaining for H3K9me2 co-stained for nuclear lamina using LMNB1 antibody in fetal HDFs transduced with shCnt, shEHMT1 and shEHMT2 virus. (Scale bar: 20µm). Inserts are zoomed images of cells in the merge. **d.** H3K9me2 immunostaining in fetal HDFs transduced with shEHMT1.1 (lentivirus) and shEHMT2.1 (retrovirus) was visualized by confocal microscopy. (Scale bar: 20µm). **e.** Mean Fluorescence Intensity (MFI) profile (Centre to periphery) with standard deviation for all the measured nuclei of shCnt, shEHMT1 and shEHMT2. **f.** Immunostaining for H3K9me2 in fetal HDFs treated with or without Bix-01294 (1µM) for 48h. (Scale bar: 20µm) **g.** MFI plot for H3K9me2 staining in fetal HDFs treated with or without Bix-01294 (1µM) for 48h. ($p<0.0001$, Mann-Whitney test, two tailed) **h.** Western blot for LMNB1 and H3K9me2 on cells treated with Bix-01294 or vehicle control. Bix-01294 treatment resulted in reduction of H3K9me2 levels without altering LMNB1 expression. **i.** TEM image for fetal HDFs treated with Bix-01294. Bix-01294 treatment did not affect the peripheral heterochromatin distribution. **j**. in vitro methylation assays were performed using recombinant LaminB1 protein (c-Term) and EHMT1 set domain in presence or absence on EHMT1/2 inhibitor BIX-01294. H3 peptide was used as positive control.

Supplementary Figure. 5 Transcriptome analysis of EHMT depleted cells a-b. Heat map for differential expression of **(a)** all genes and **(b)** chromatin modifiers

obtained from RNA-seq analysis of shEHMT1 or shEHMT2 compared to shCnt tranduced HDFs. Representative genes that were altered similarly or distinctly in EHMT1 vs EHMT2 are indicated from few clusters.

Supplementary Figure 6. Depletion of EHMTs alters the expression of longevity-associated genes. a Heat map demonstrating differential expression of age related genes in EHMT1 and EHMT2 depleted fibroblasts. Representative genes that were altered similarly or distinctly in EHMT1 vs EHMT2 are indicated from few clusters. **b.** Validation for differential expression of candidate genes obtained from RNA-Seq analysis by semiquantitative PCR. **c.** Validation for differential expression of candidate genes obtained from RNA-Seq analysis by qRT-PCR. One sample t-test (two-tailed) (n=2). UT vs FGFR1 (*p=0.0156), UT vs CDKN2B (***p=0.0007), UT vs FOXM1 (**p=0.0099).**d.** Immunostaining for H3K9me3, H3K27me3 and HP1 in fetal, 18Y old and 58Y old HDFs followed by confocal imaging. (Scale bar: 20µm) **e.** Western blot analysis for H3K9me3 and H3K27me3 in fetal, 18Y and 58Y old HDFs. **f-g.** Western blot analysis for EHMT1, EHMT2 and H3K9me2 in various age groups HDFs. GAPDH and pan H3 were used as internal controls.

Supplementary Figure 7. Interaction of EHMTs with LMNB1 during aging. a-c. MFI (Centre to periphery) with standard deviation for H3K9me2 staining in all the measured nuclei of fetal, 18Y and 58Y old HDFs. **d.** MFI for H3K9me2 staining in fetal, 18Y and 58Y old HDFs. MFI has been represented as center vs periphery of nuclei. $p<0.001$, Kruskal-Wallis test (Dunn's multiple comparison post hoc test) **e-f.** Cell lysates prepared from human fibroblasts of indicated age groups were subjected for IP using EHMT1/EHMT2 antibody. IPed material was analyzed by immunoblotting using LMNB1 and LMNA/C antibodies. 30 µg of fetal cell lysate was used as input control.

Supplementary Figure 8. Co-expression of mutant LMNB1 with EHMTs aggregates H3K9me2 in the nucleoplasm. a-b. Quantitation of LMNB1 expression in aged HDFs upon overexpression of EHMT1 and EHMT2. Overexpression of EHMT1 significantly increased the LMNB1 expression while EHMT2 transfected cells did not show any change compared to untransfected cells. For V5-EHMT1 and Flag-EHMT2 quantitation, $p<0.05$, Mann-Whitney test, two tailed (n=14 nuclei of untransfected control for EHMT1-OE, n=22 nuclei for V5-EHMT1 OE, n=17 nuclei of untransfected control for EHMT2-OE, n=7 nuclei for Flag-EHMT2 OE). **c-e.** Old HDFs expressing Wt. LMNB1 + V5-EHMT1, K417A-LMNB1 + V5-EHMT1 and K417A-LMNB1 + Flag-EHMT2 were stained with H3K9me2 antibody. Mutation at lysine 417 position of LMNB1 affects the overall distribution H3K9me2 and morphology (Scale bar: 20μm). Arrows indicate the cells zoomed in the far right image presented.

Supplemantary Figure 9. Physiological aging results in cell cycle arrest. **a-c.** Cell cycle analysis for shCnt, shEHMT1 and shEHMT2 transduced fetal HDFs. **d.** Cell cycle distribution showing percentage of cells in G0/G1, S and G2/M phase in the aging HDFs after 48 and 72 h of culture. Two-way ANOVA (post-hoc: Tukey's multiple comparison test) (n=3). 18Y: 48h G0/G1 vs 72h G0/G1 (***$p<0.0001$), 31Y: 48h G0/G1 vs 72h G0/G1 (**$p=0.0084$). **e.** Percent senescent positive cells in 18Y, 31Y and 58Y old HDFs. Senescence assay did not show significant increase in percentage of β-Galactosidase positive cells during aging.

Ketkar and Rao et al Figure 1

a

Protein	% Coverage	Peptide Score
Lamin B1	36	27.65
Histone 1.2	23.1	43.89
Histone 2B	7.1	8.55

c

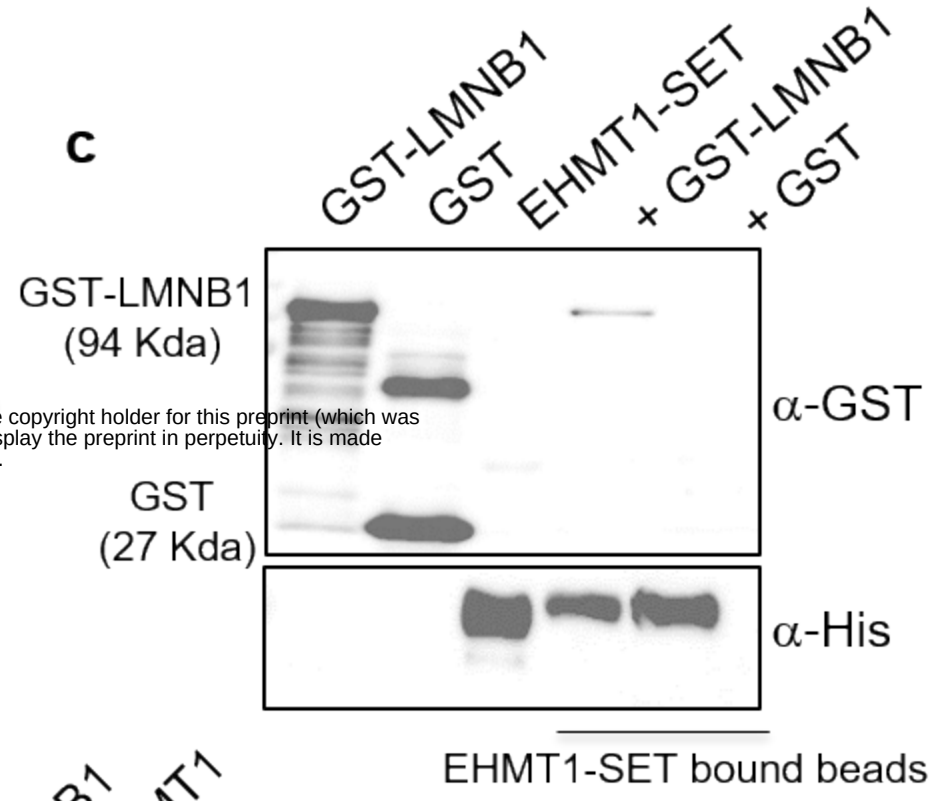

b

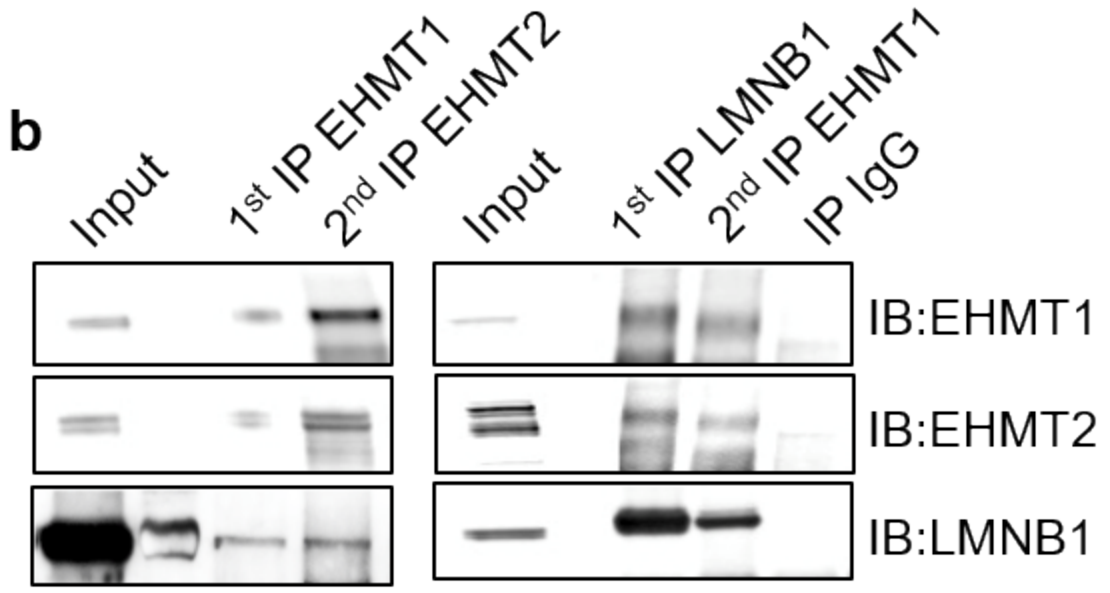

d

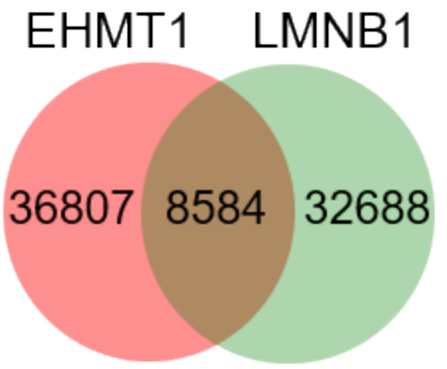

e

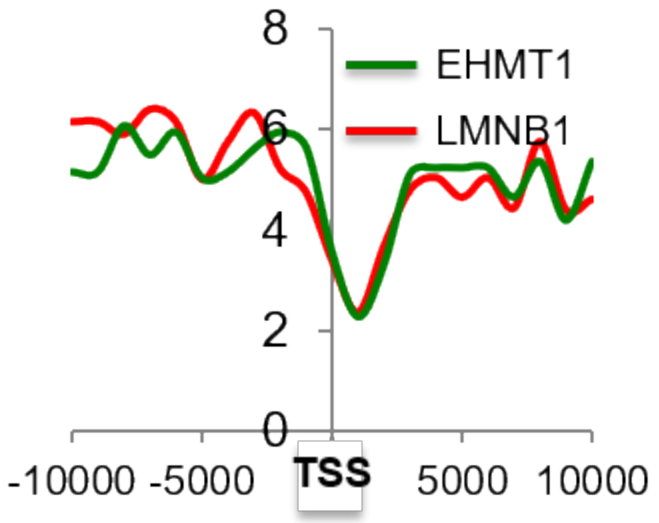

f

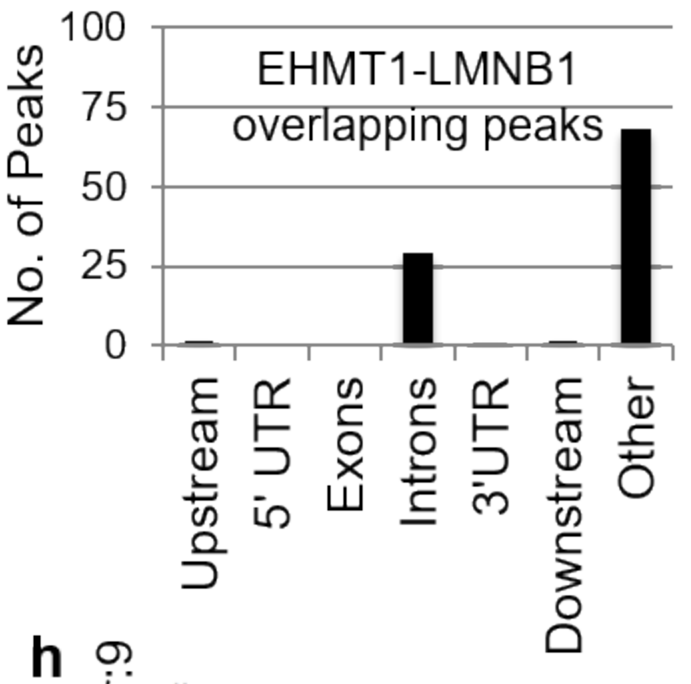

g

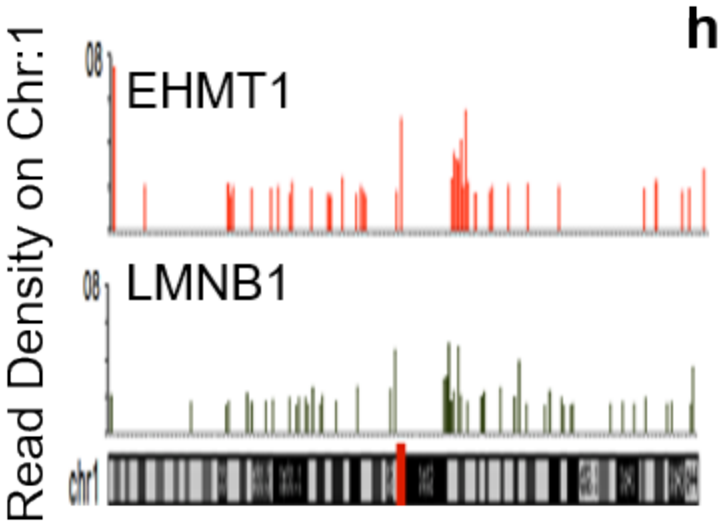

h

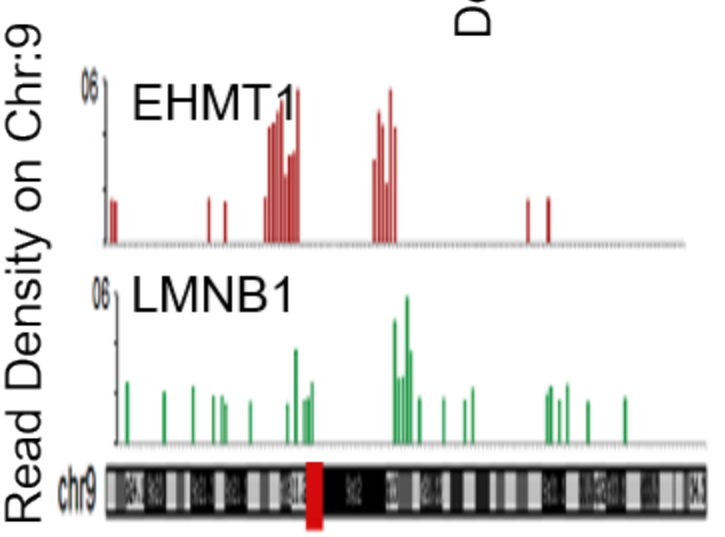

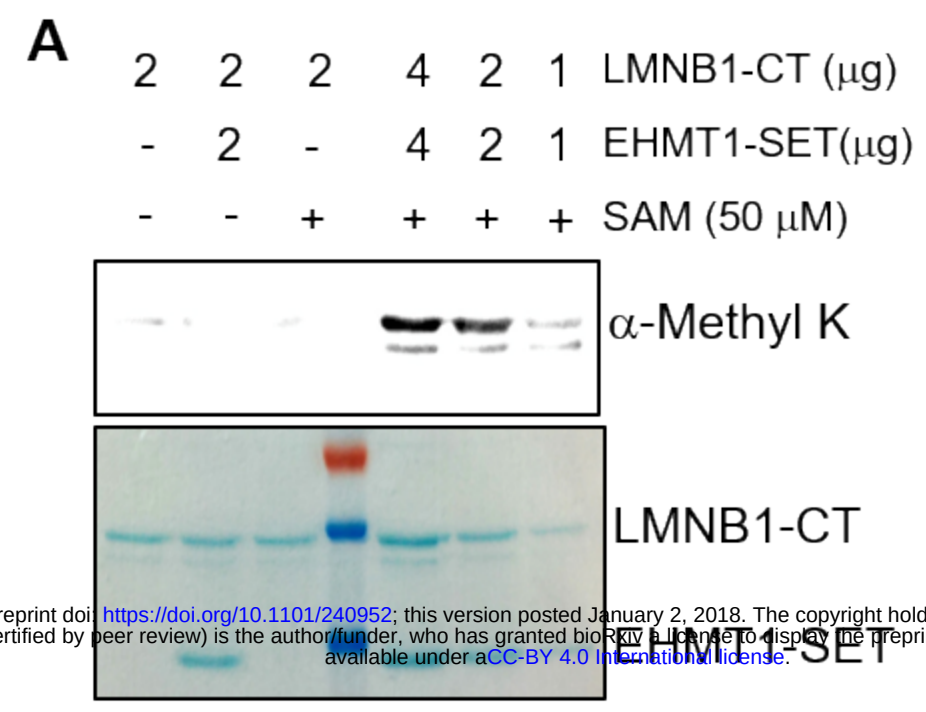

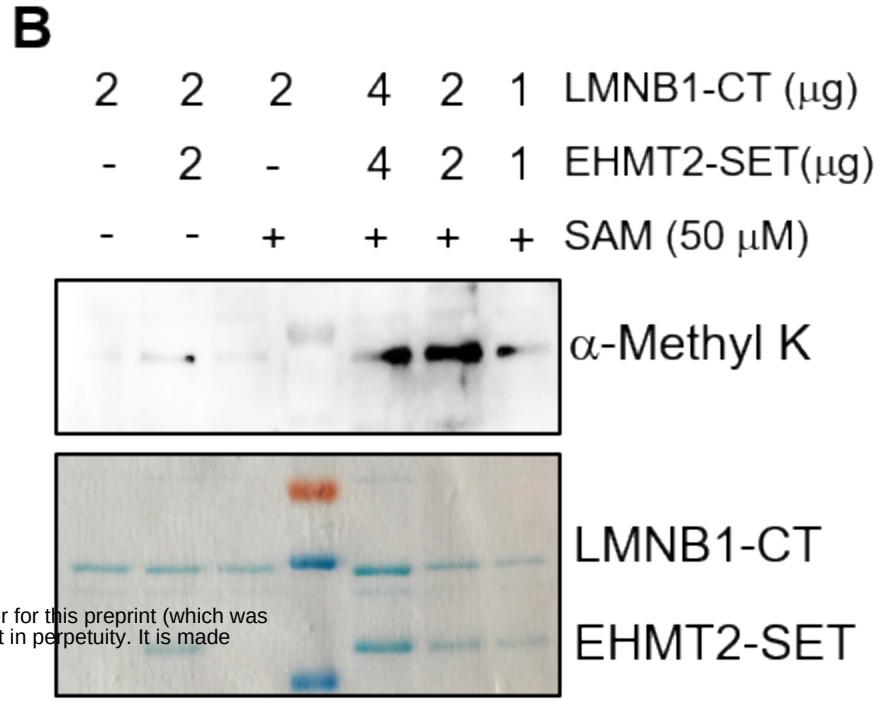

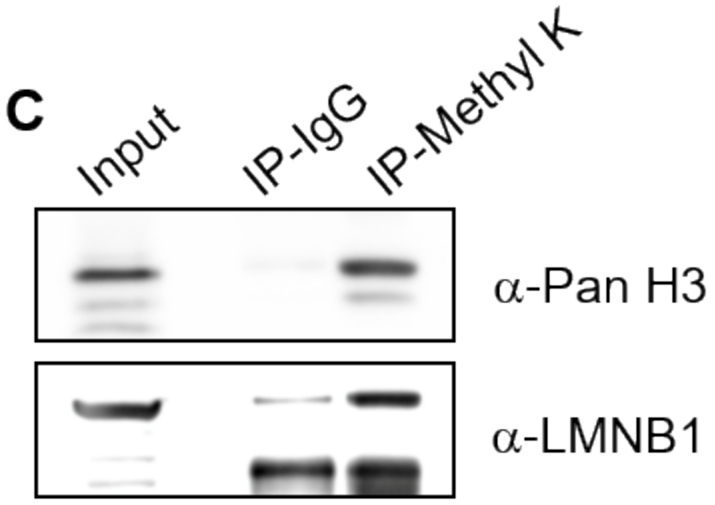

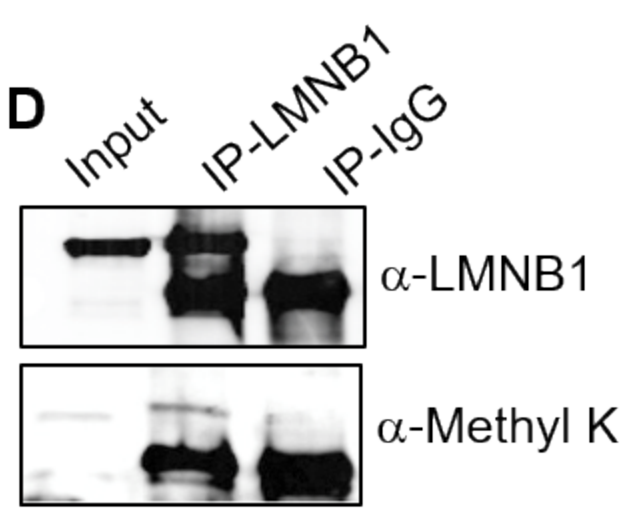

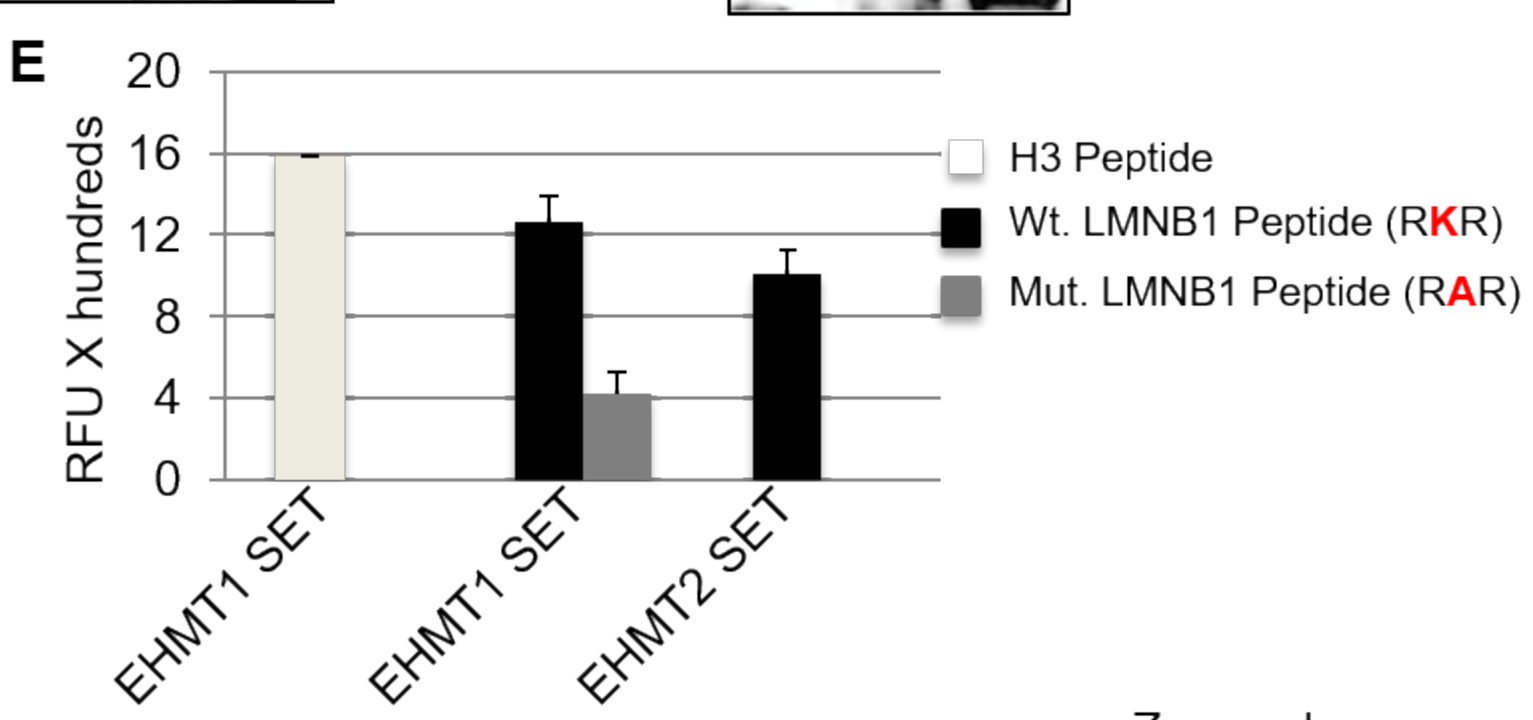

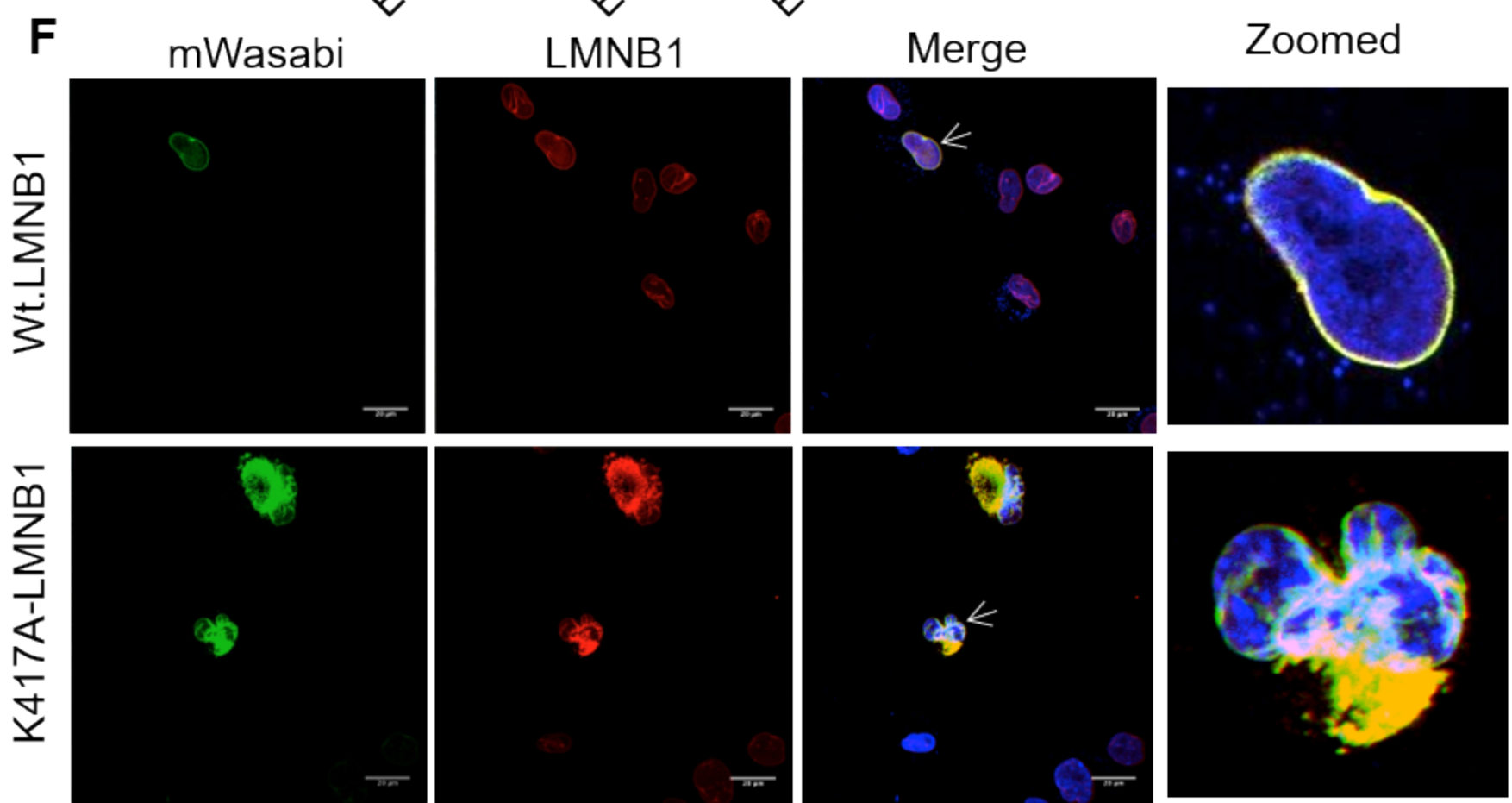

Ketkar and Rao et al Figure 3

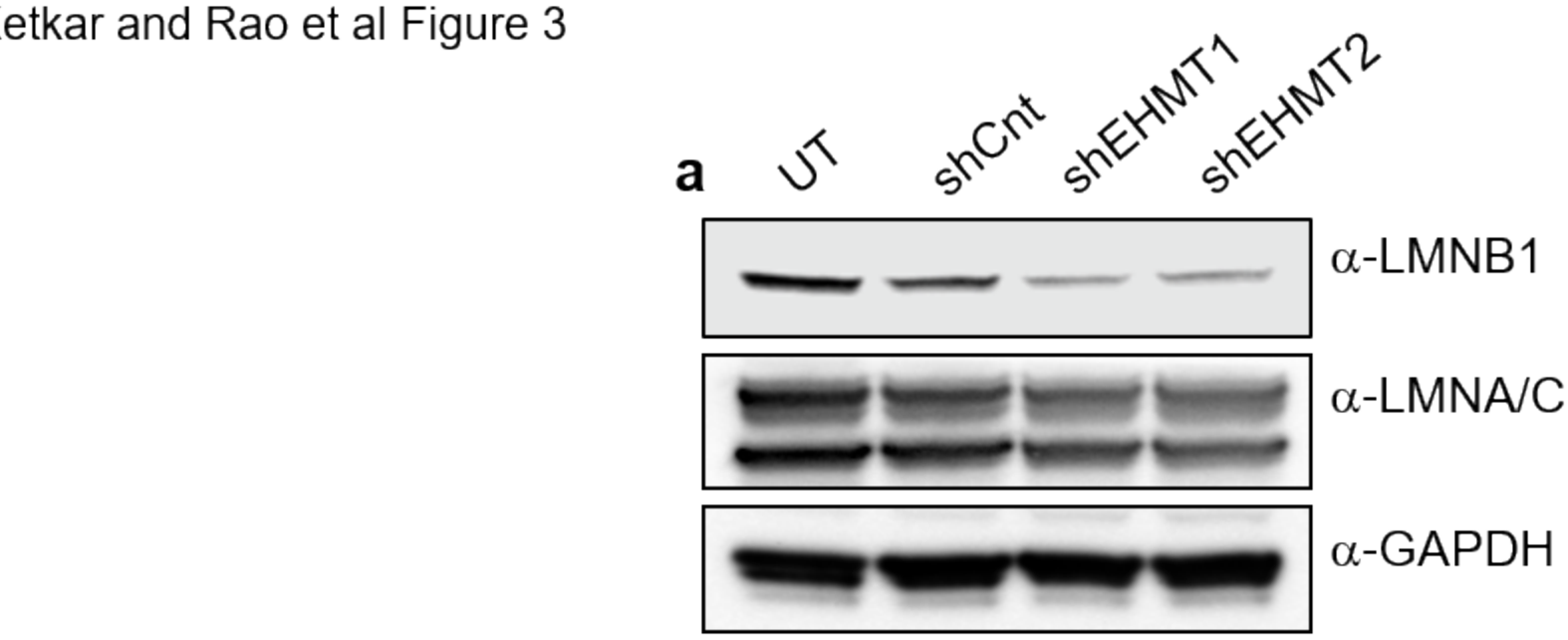

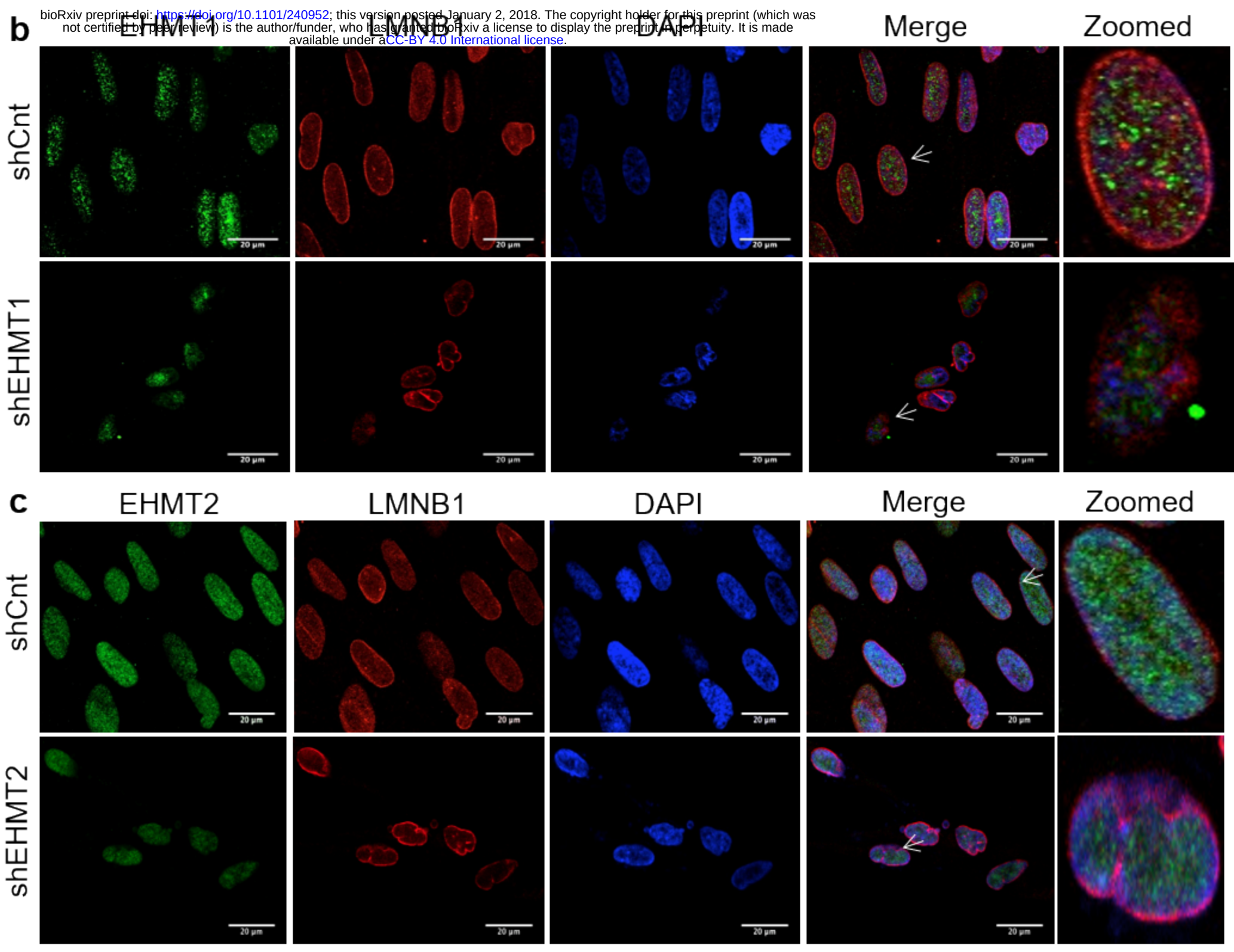

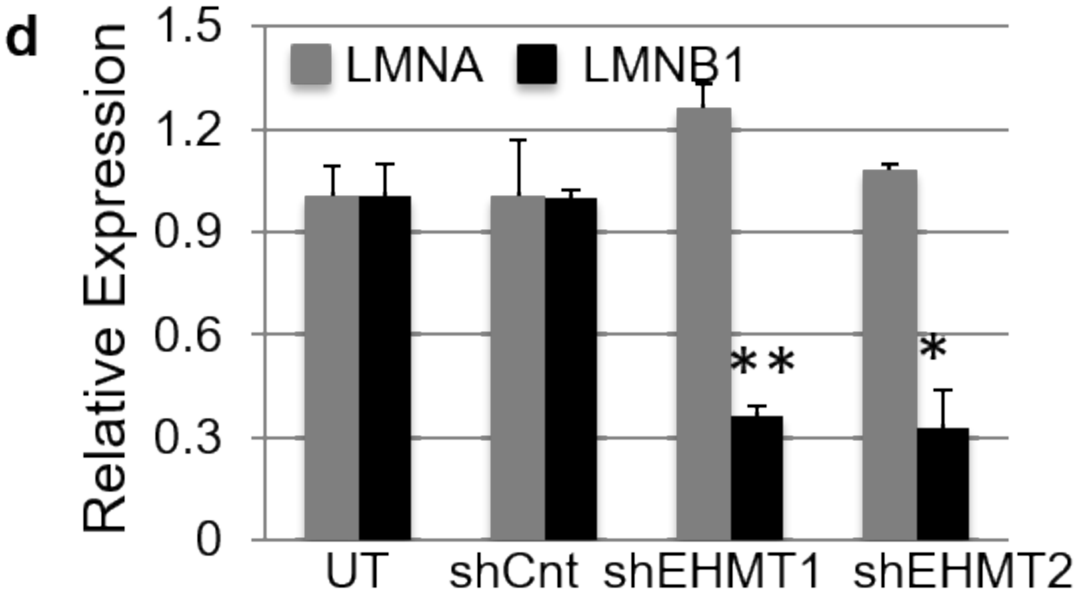

Ketkar and Rao et al Figure 4

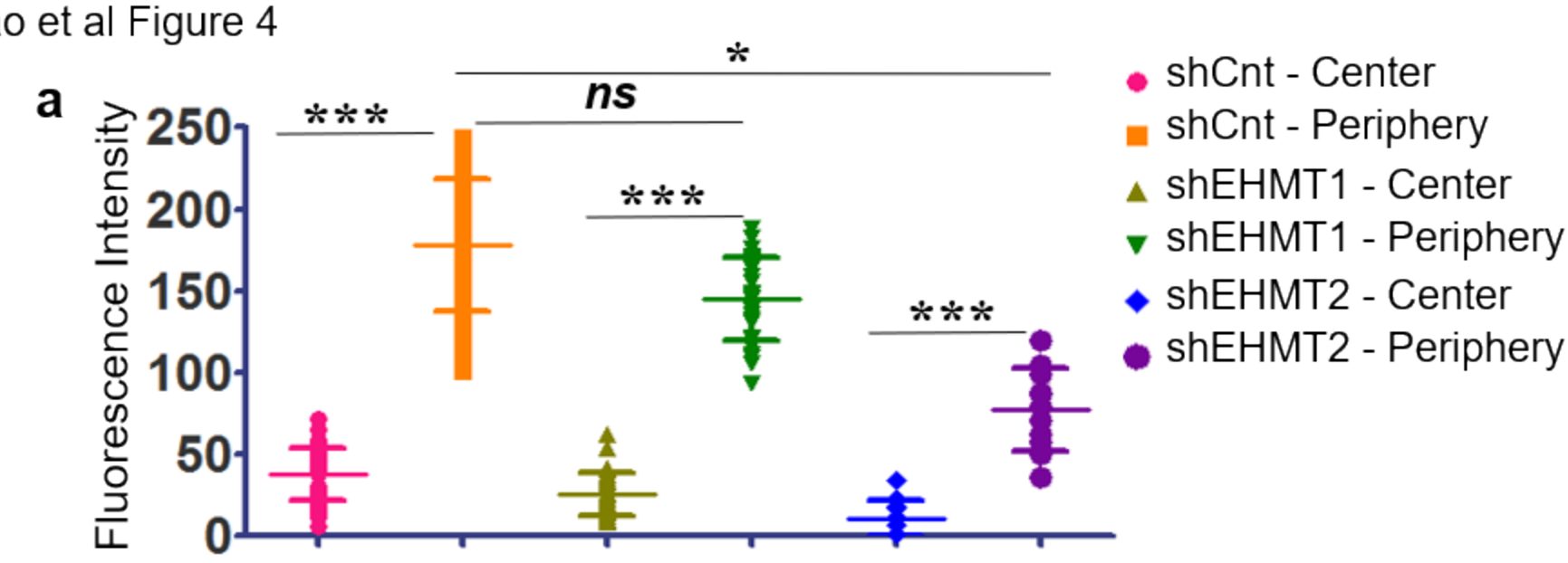

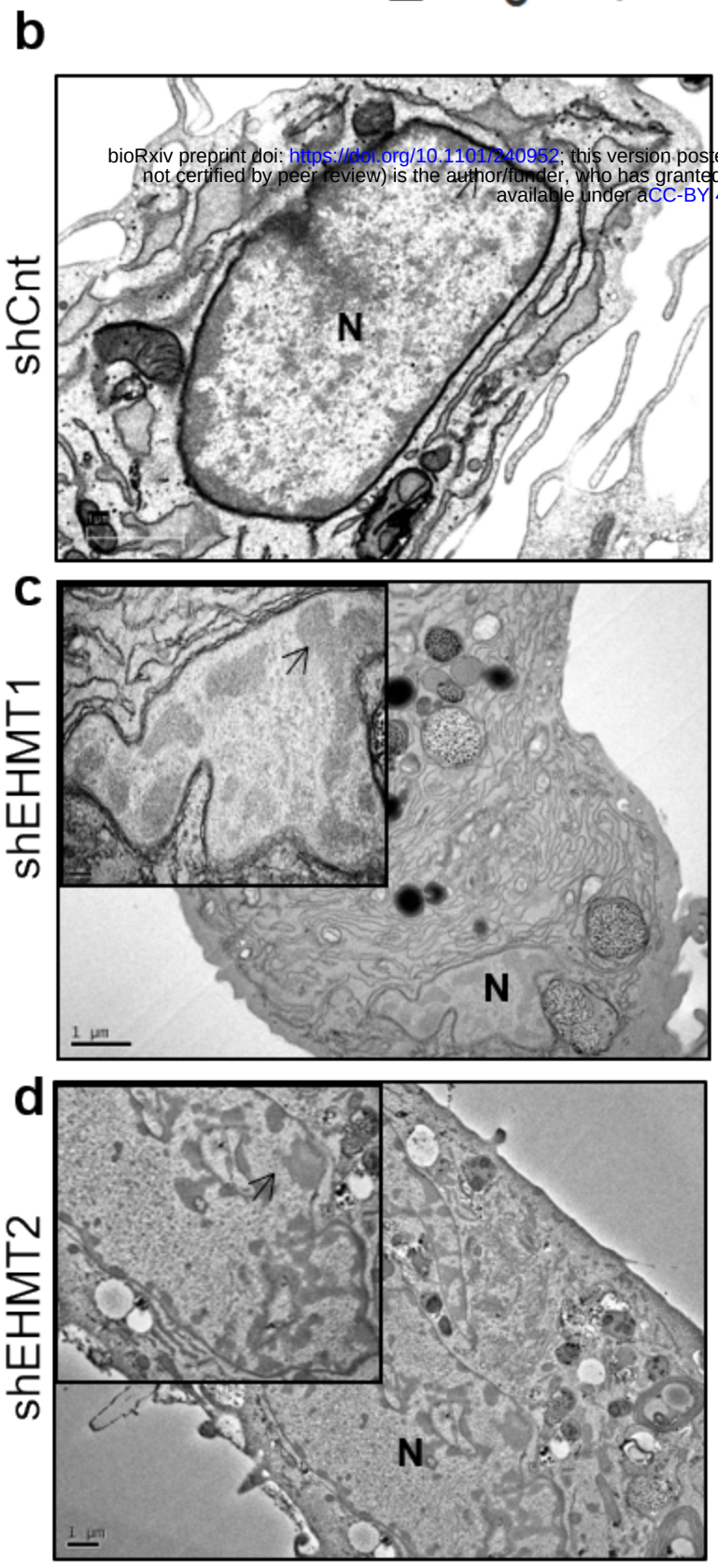

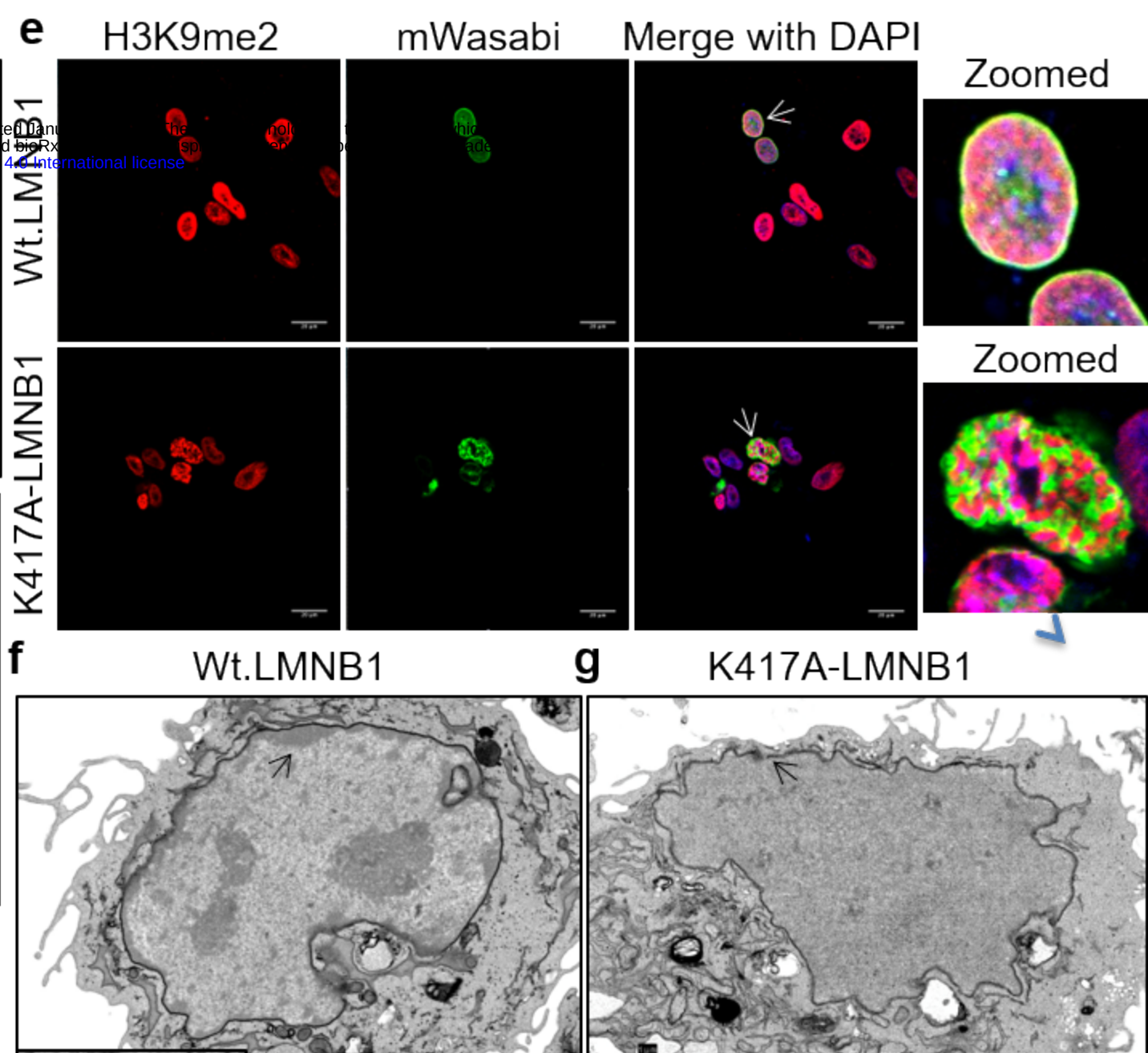

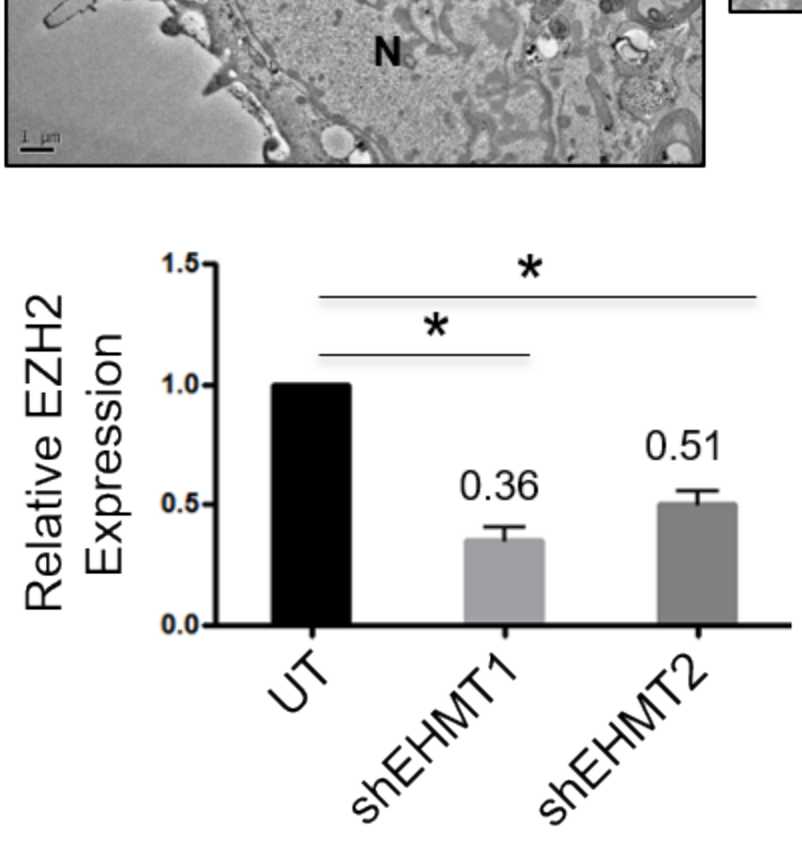

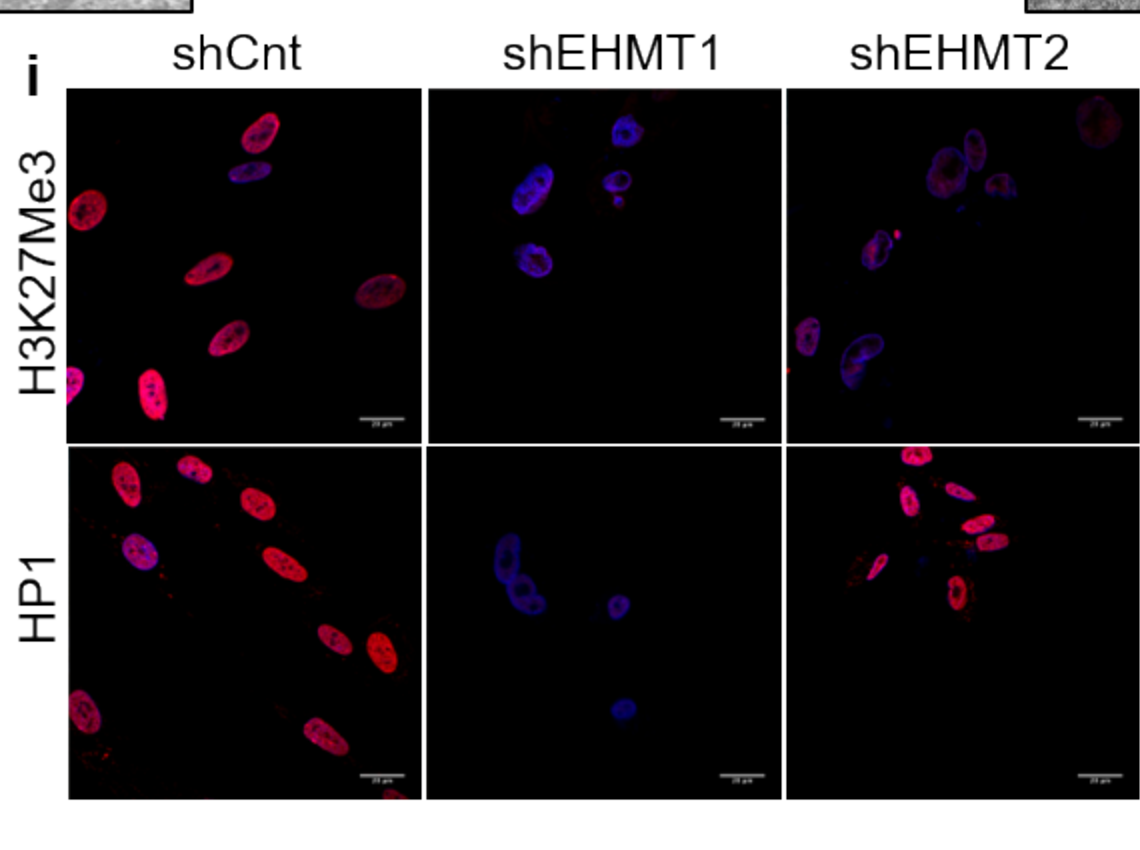

Ketkar and Rao et al Figure 5

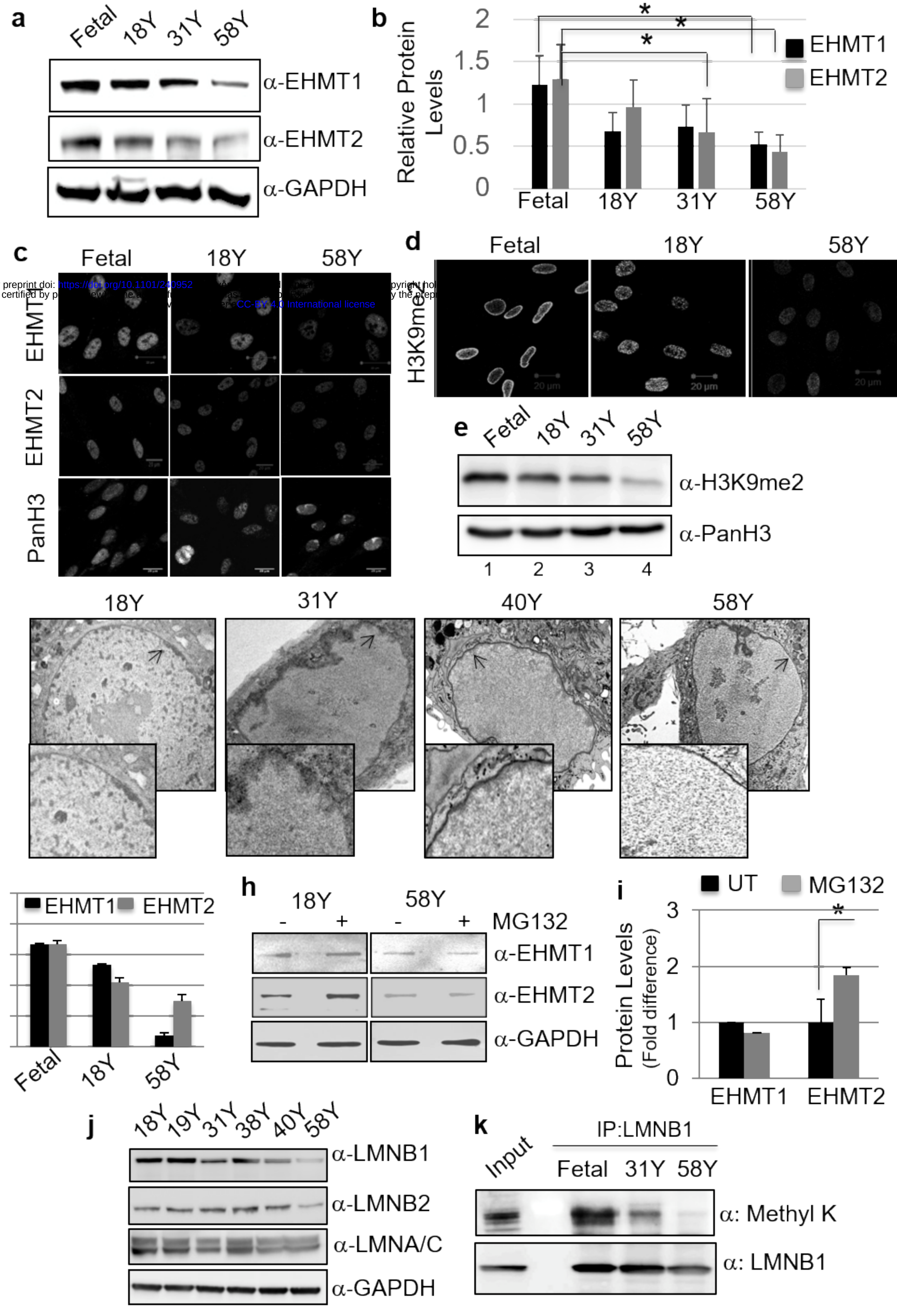

Ketkar and Rao et al Figure 6

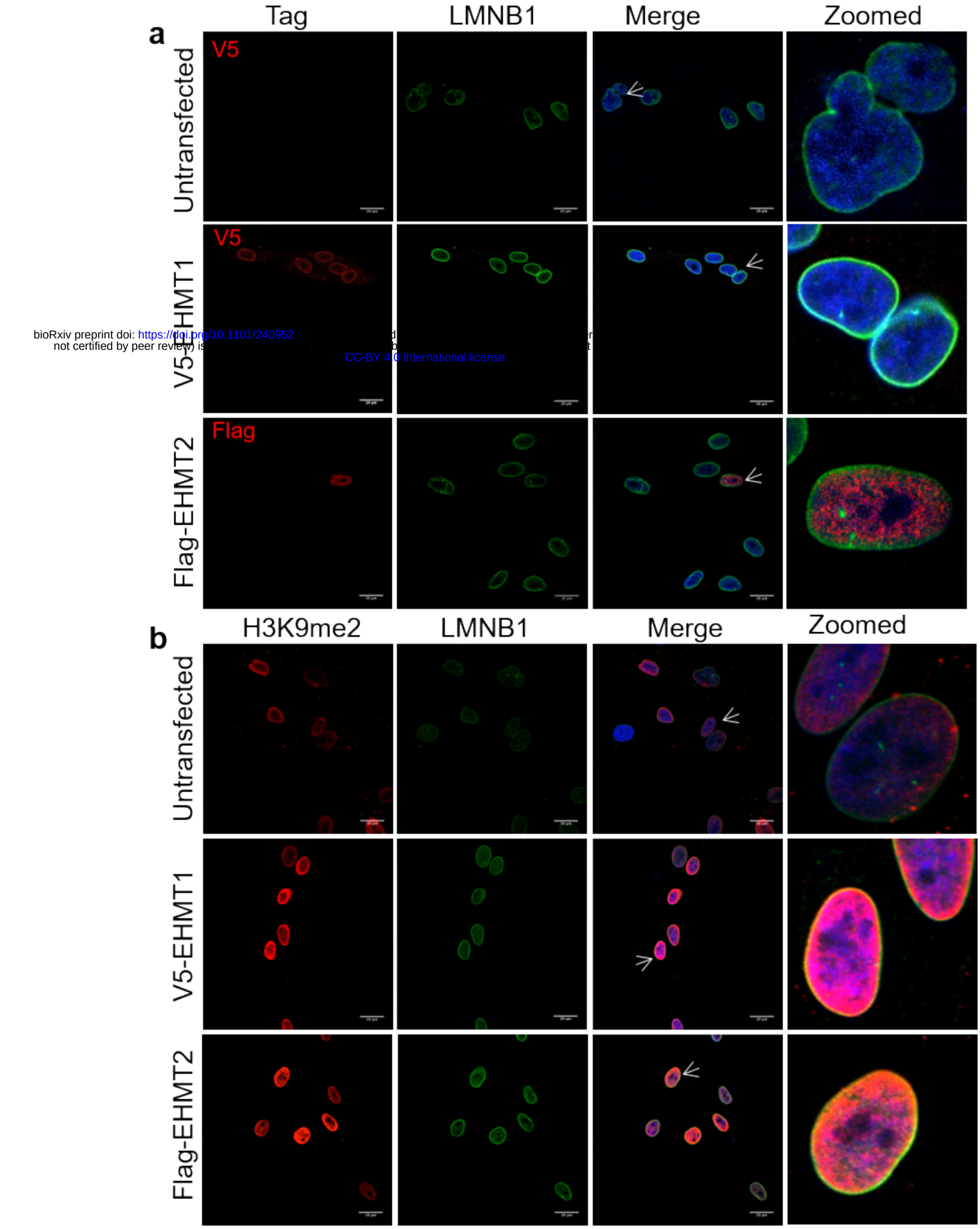

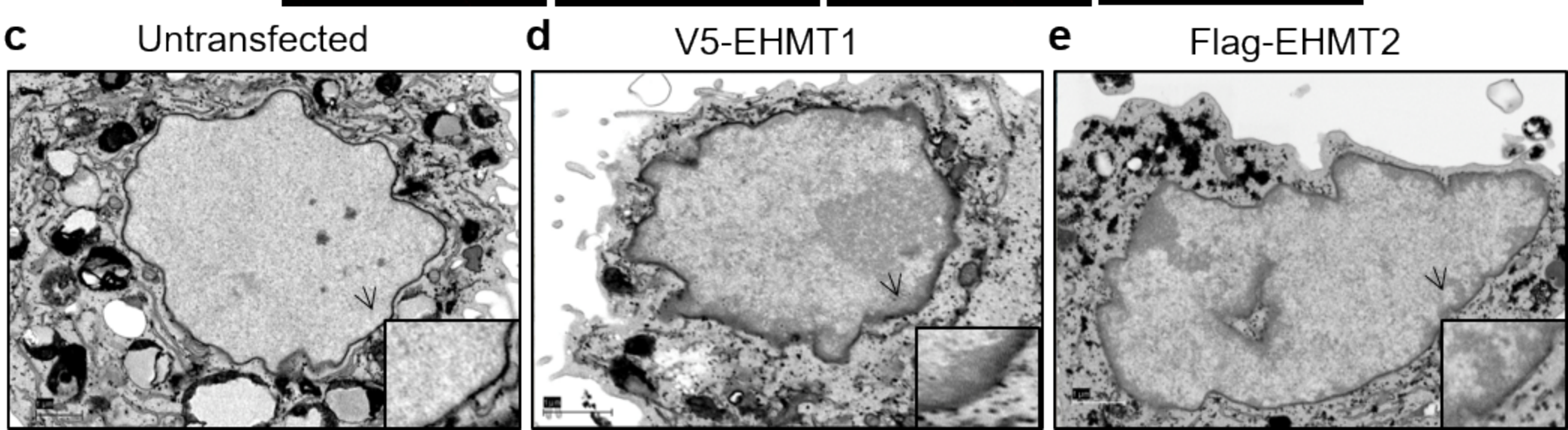

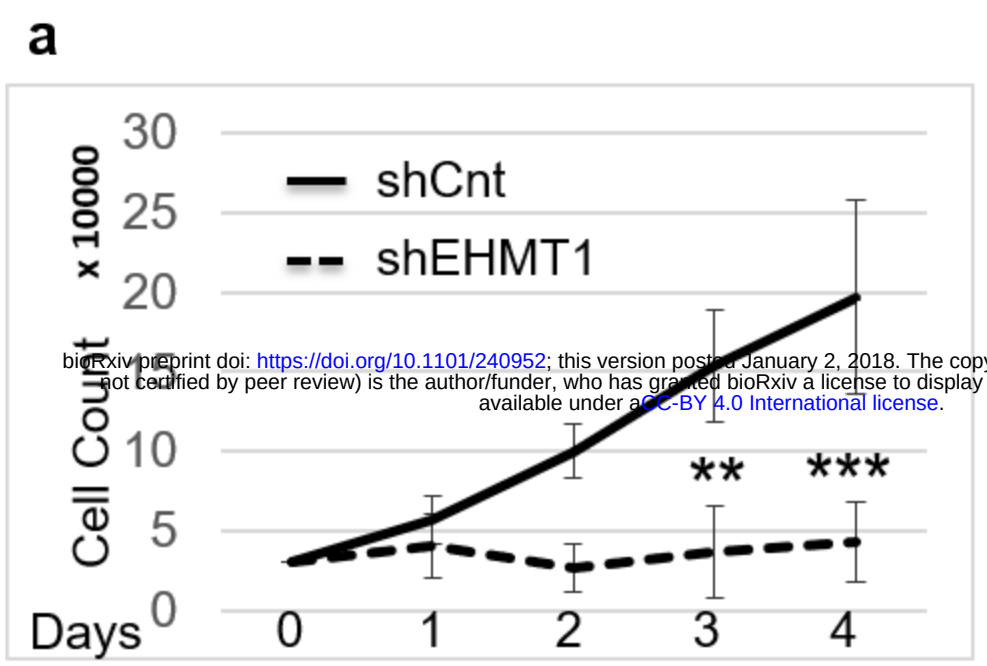

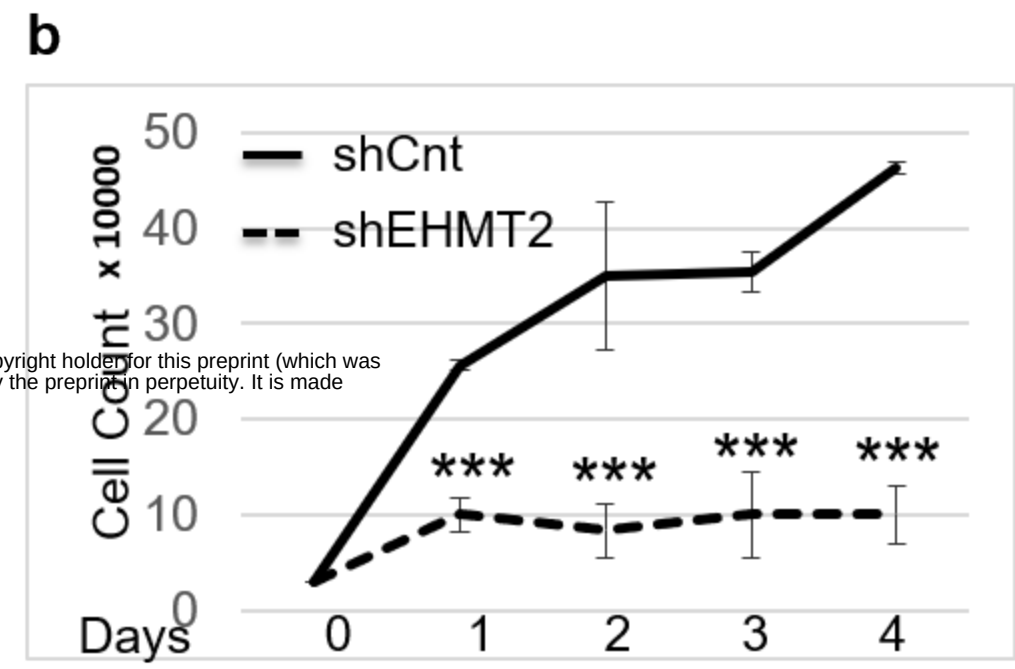

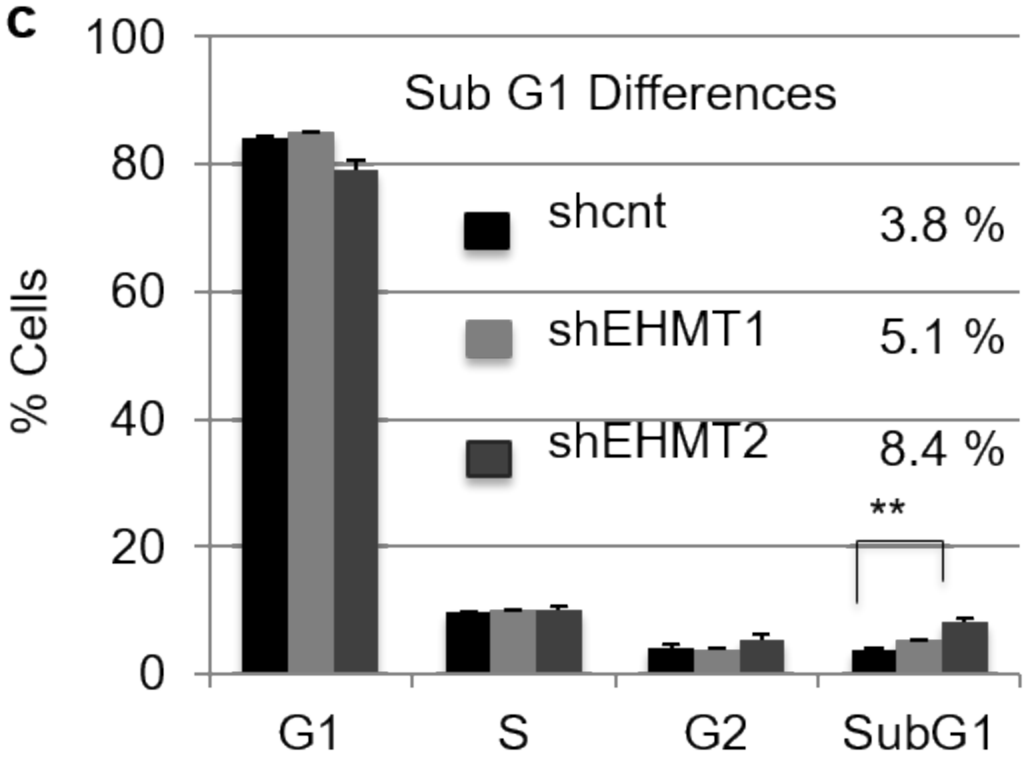

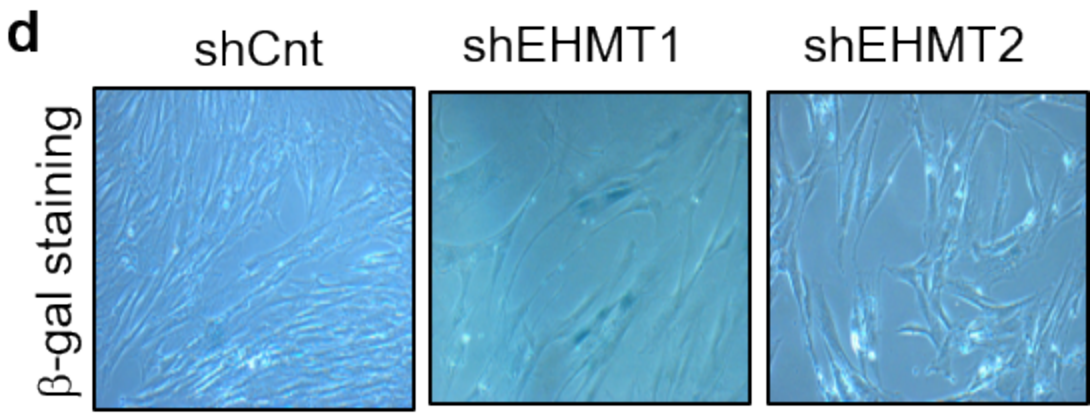

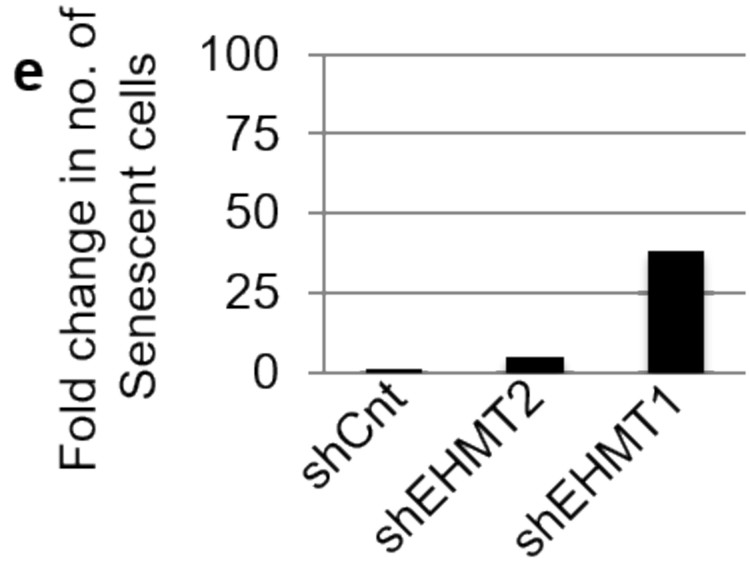

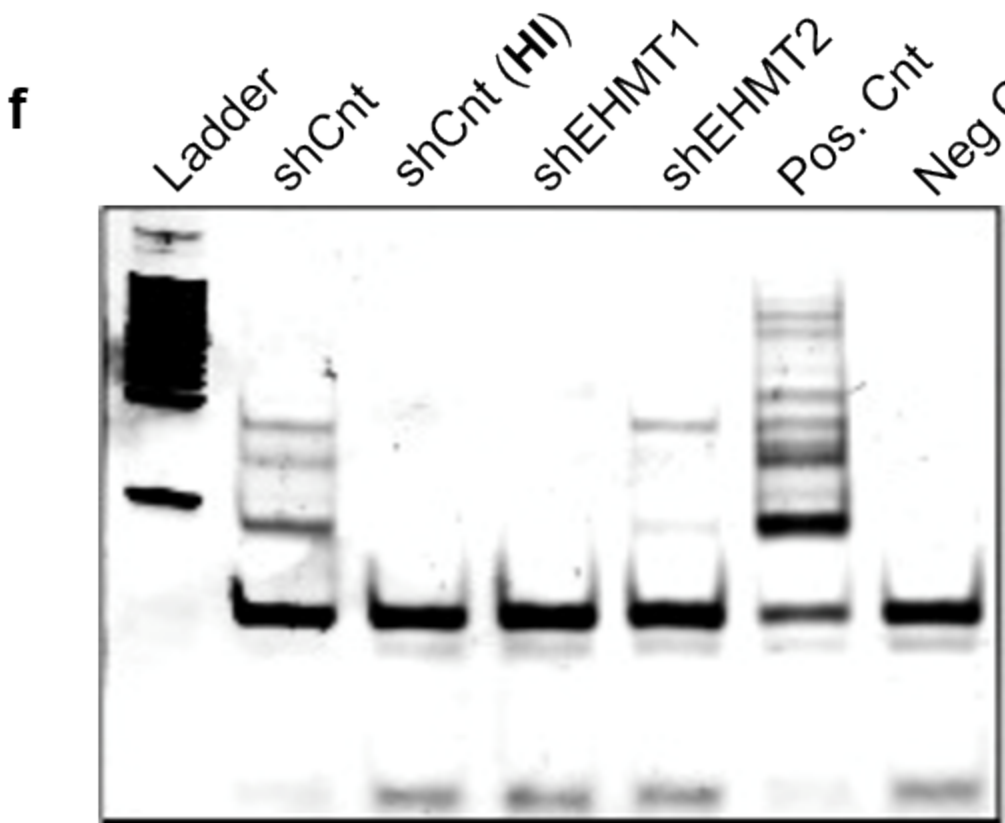

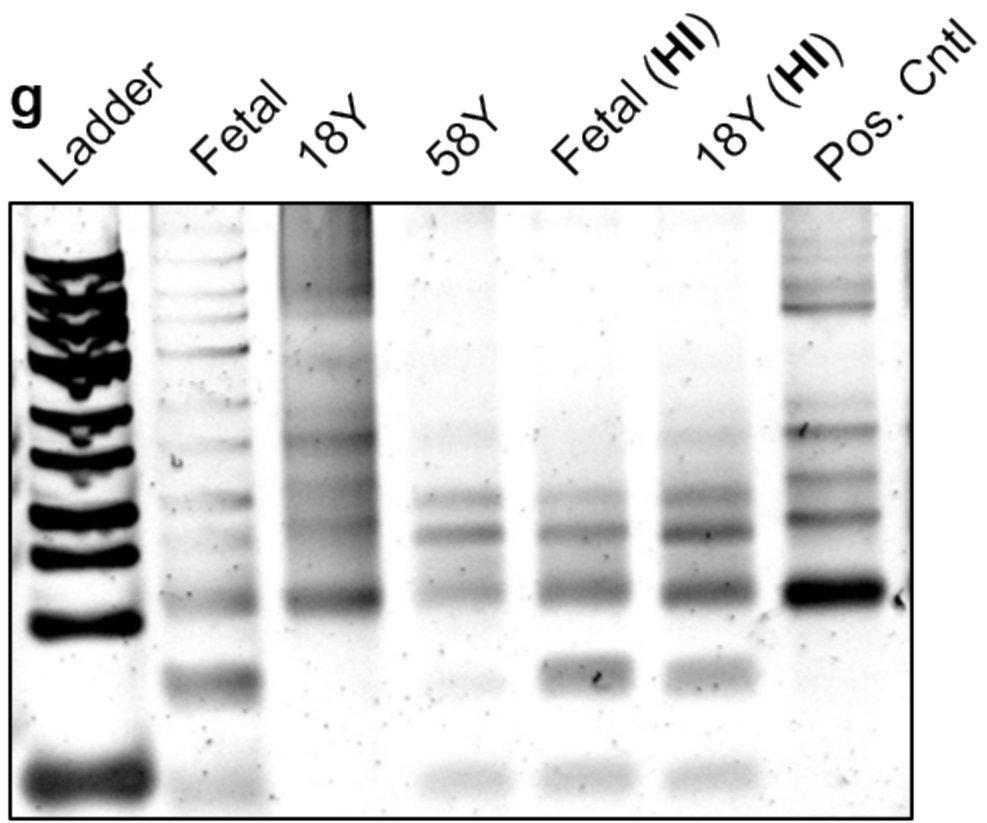

Ketkar and Rao et al Figure 8

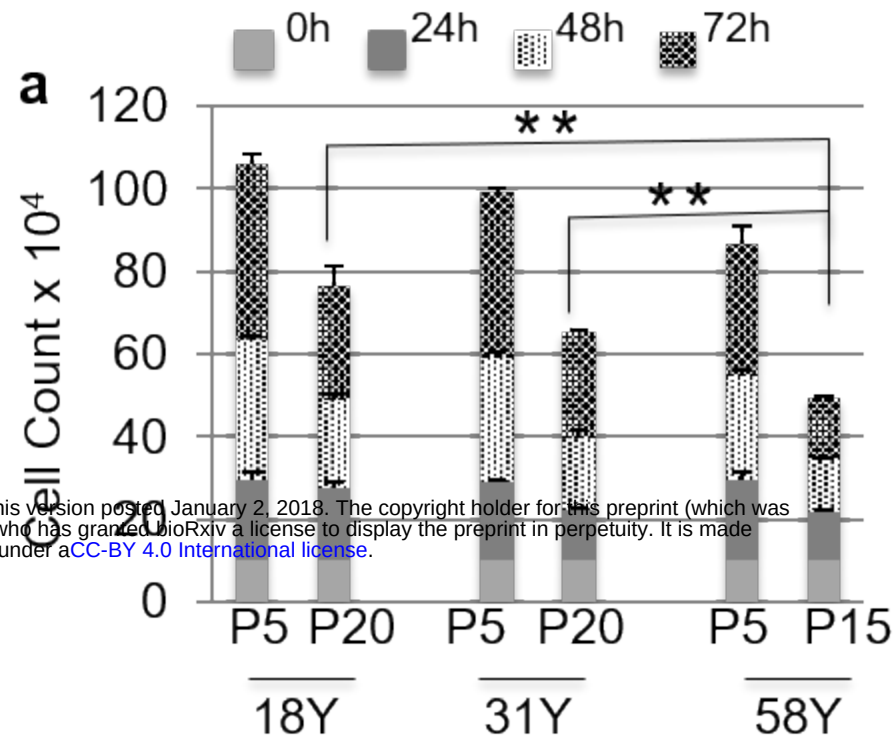

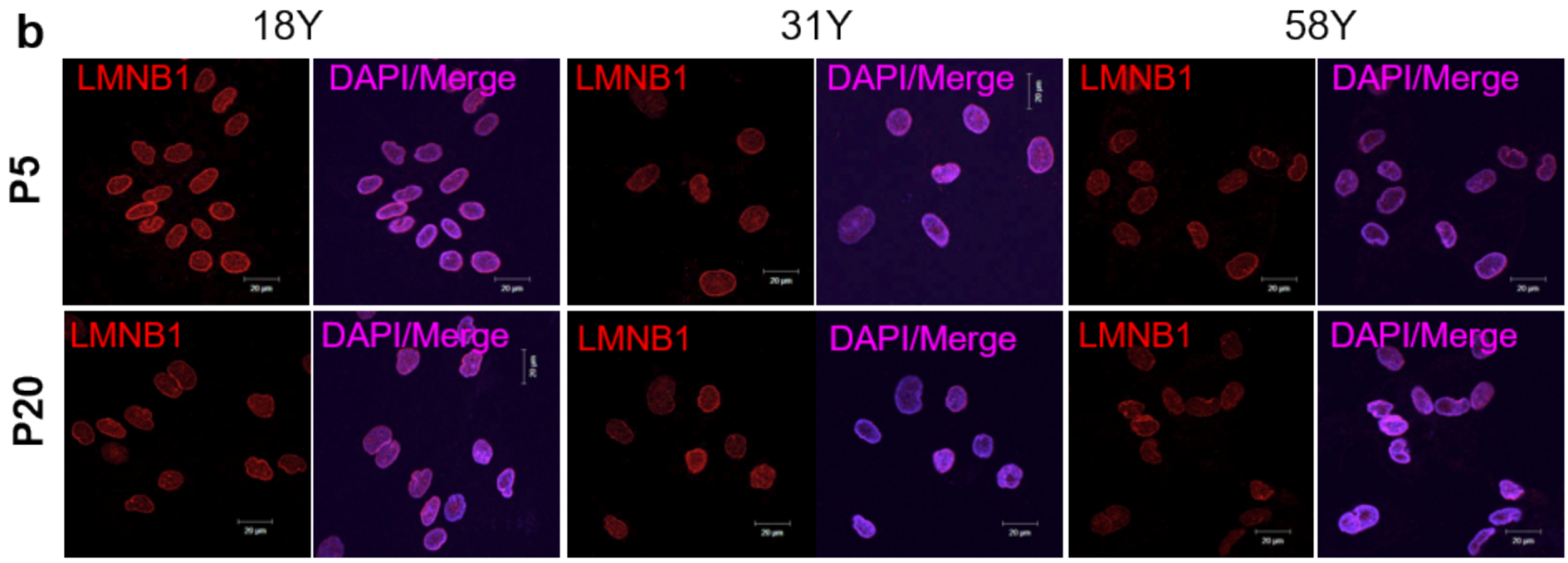

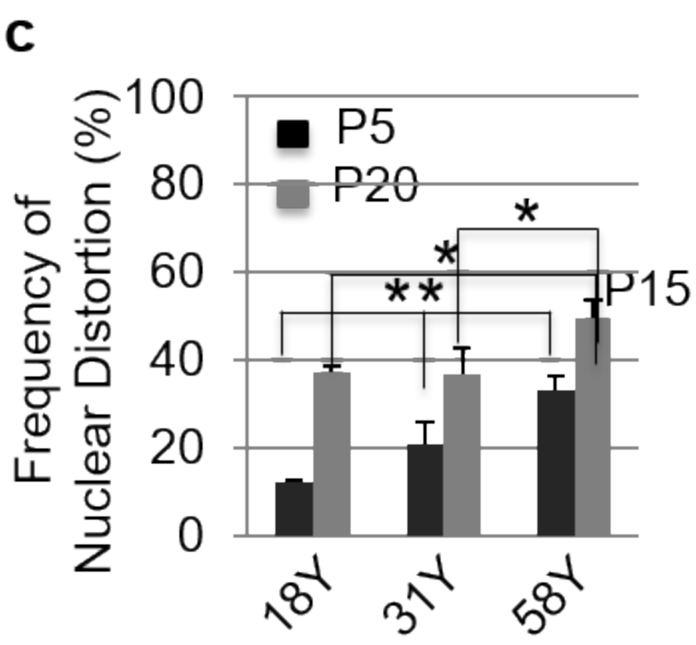

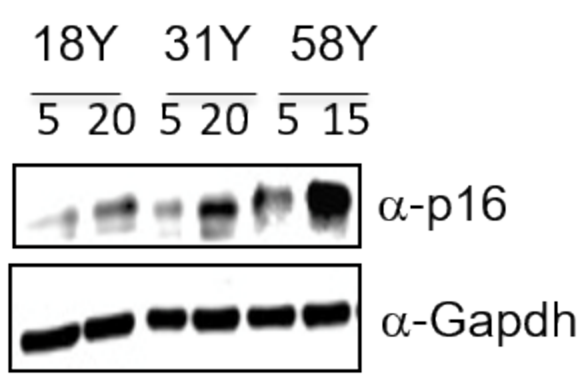

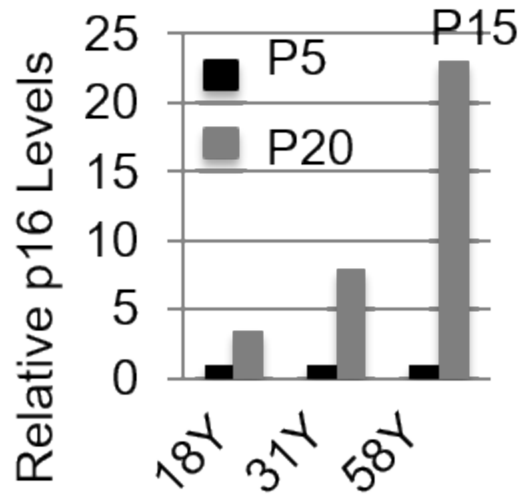

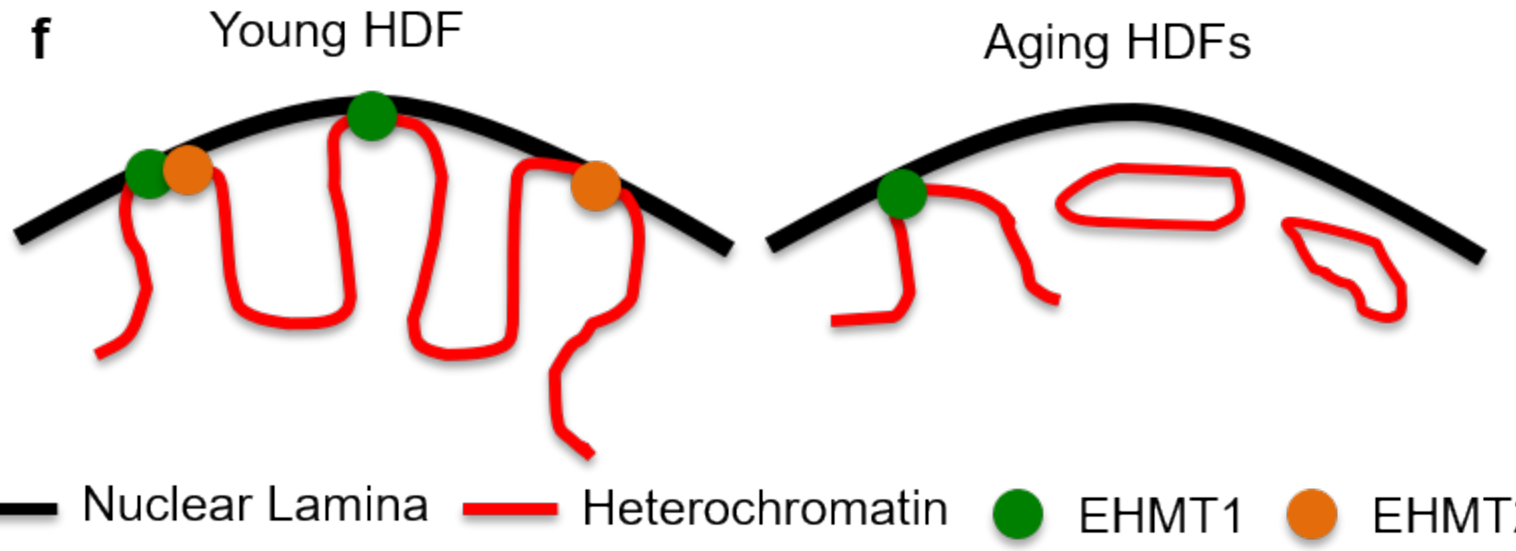

Ketkar and Rao et al Supplementary Figure 1

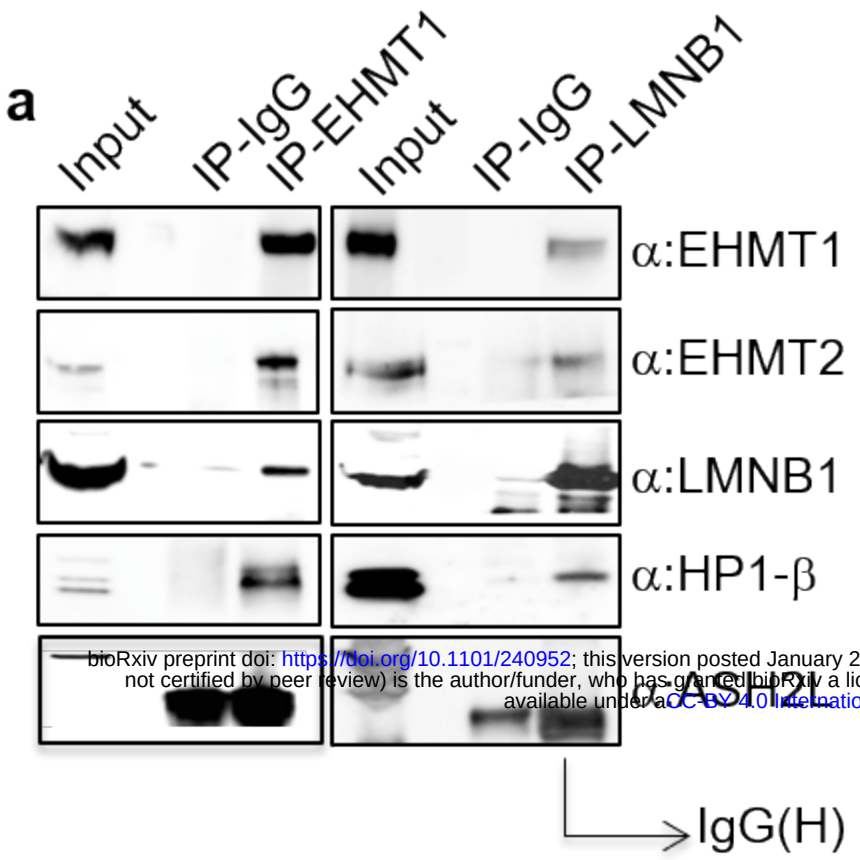

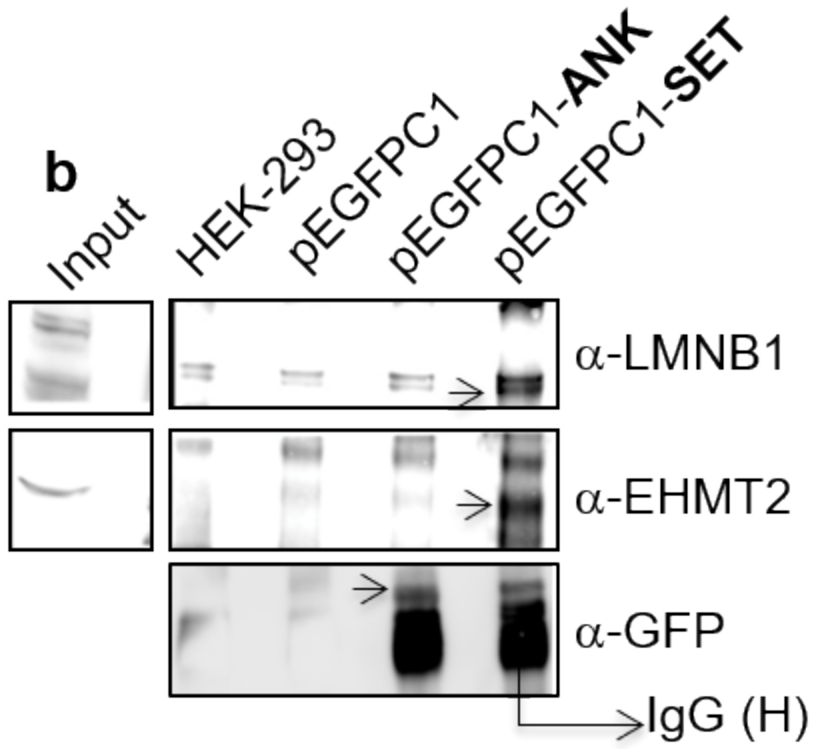

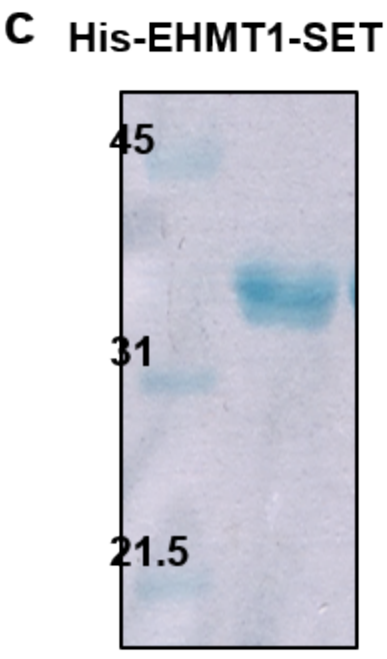

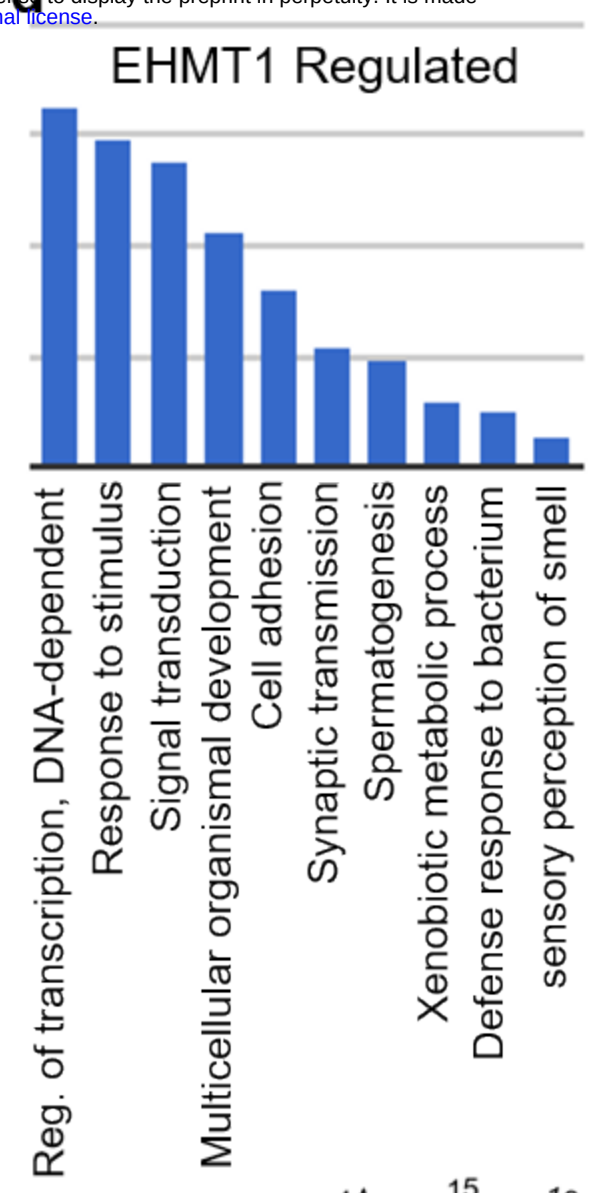

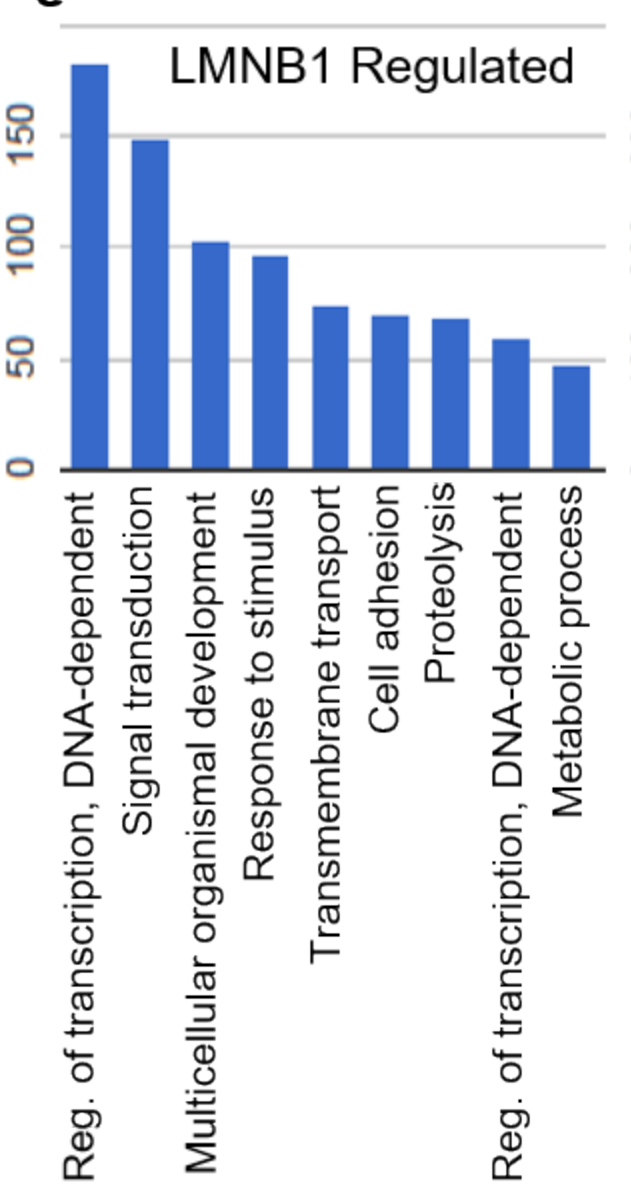

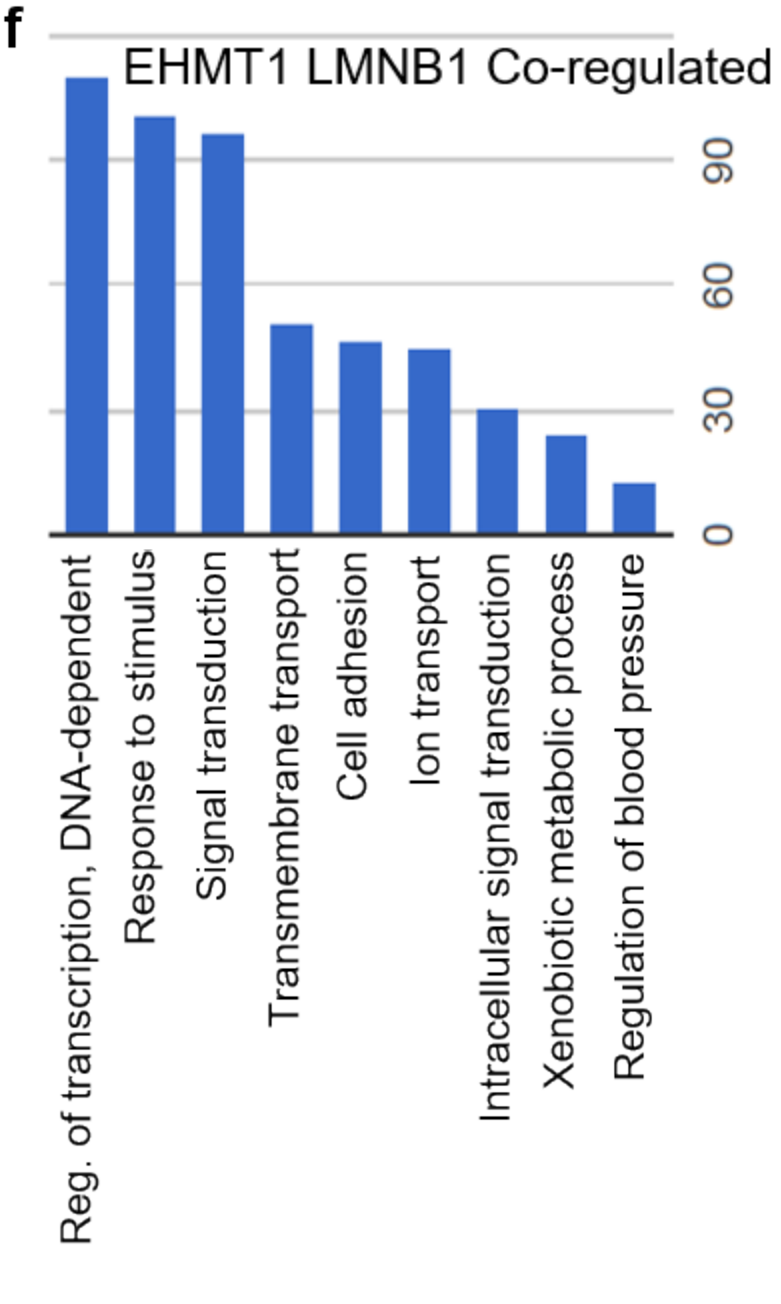

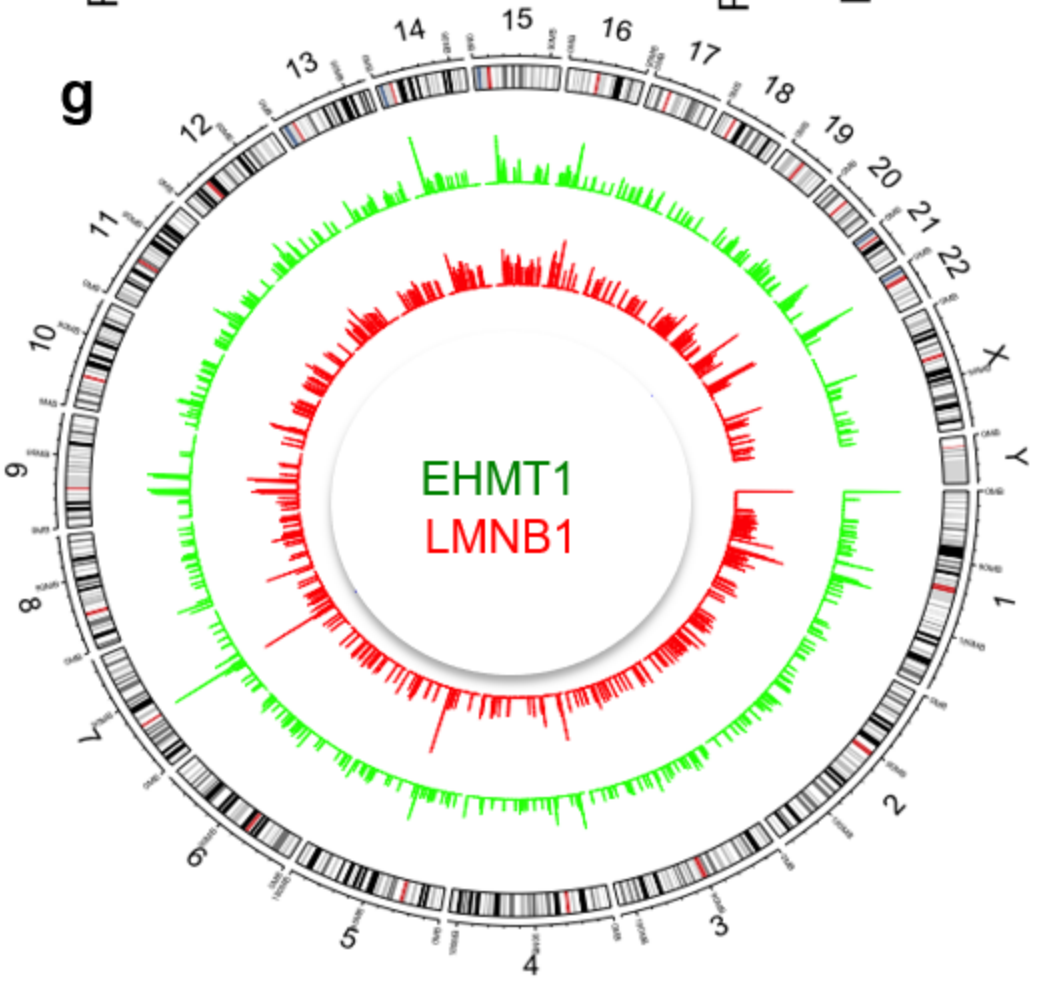

Ketkar and Rao et al Supplementary Figure 2

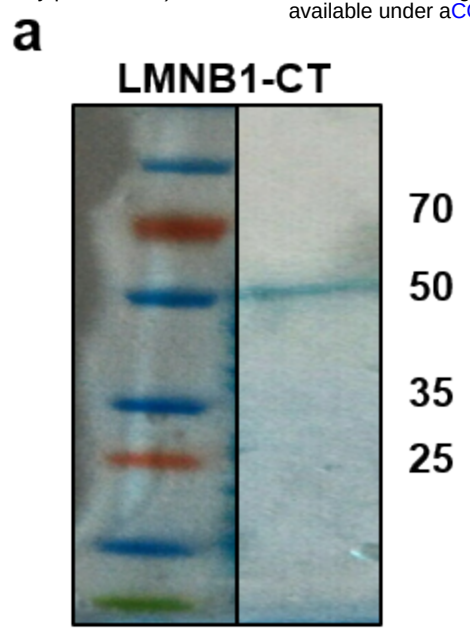

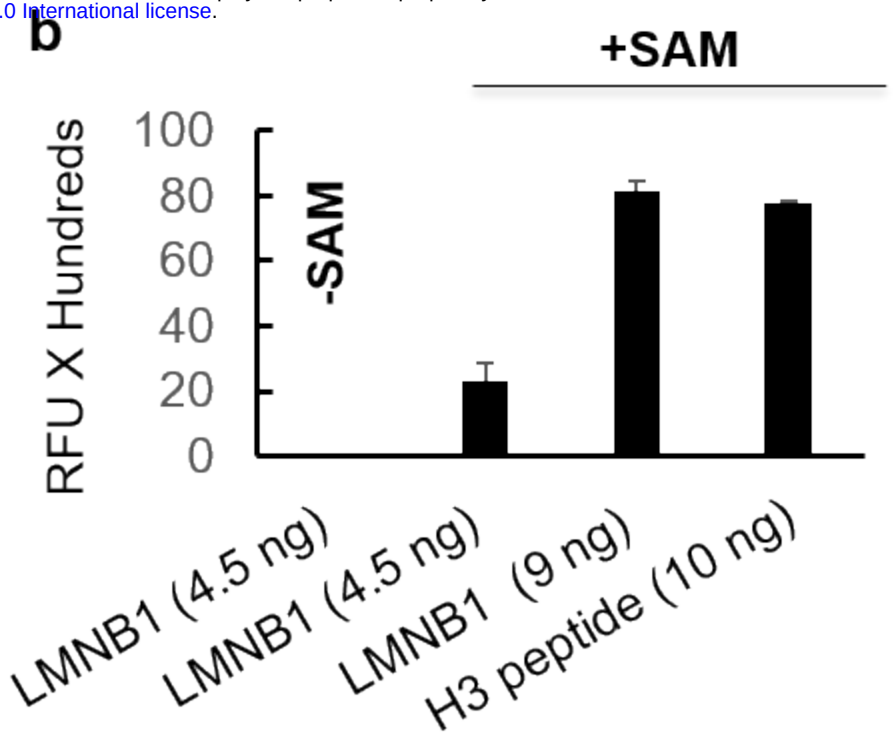

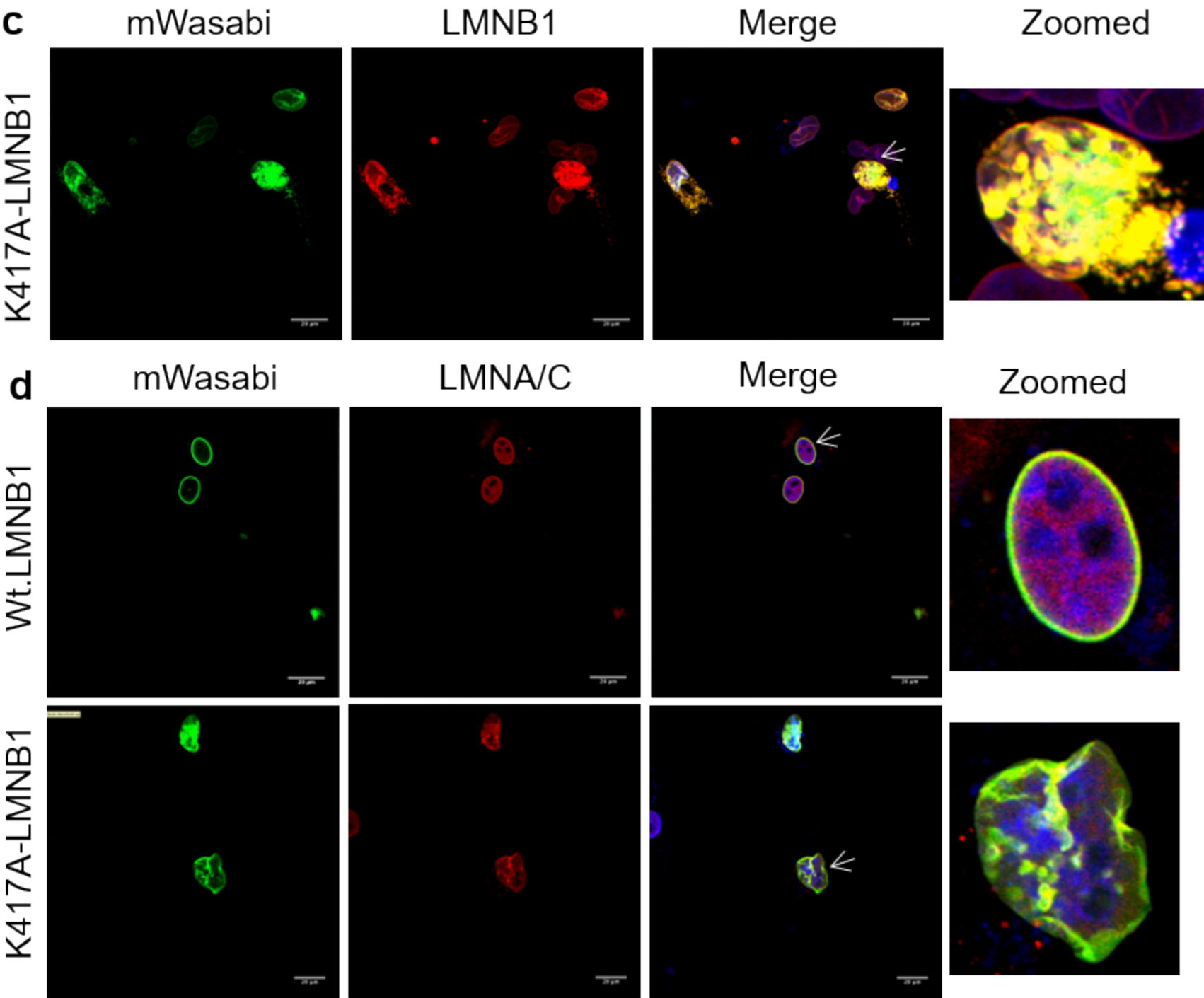

Ketkar and Rao et al Supplementary Figure 3

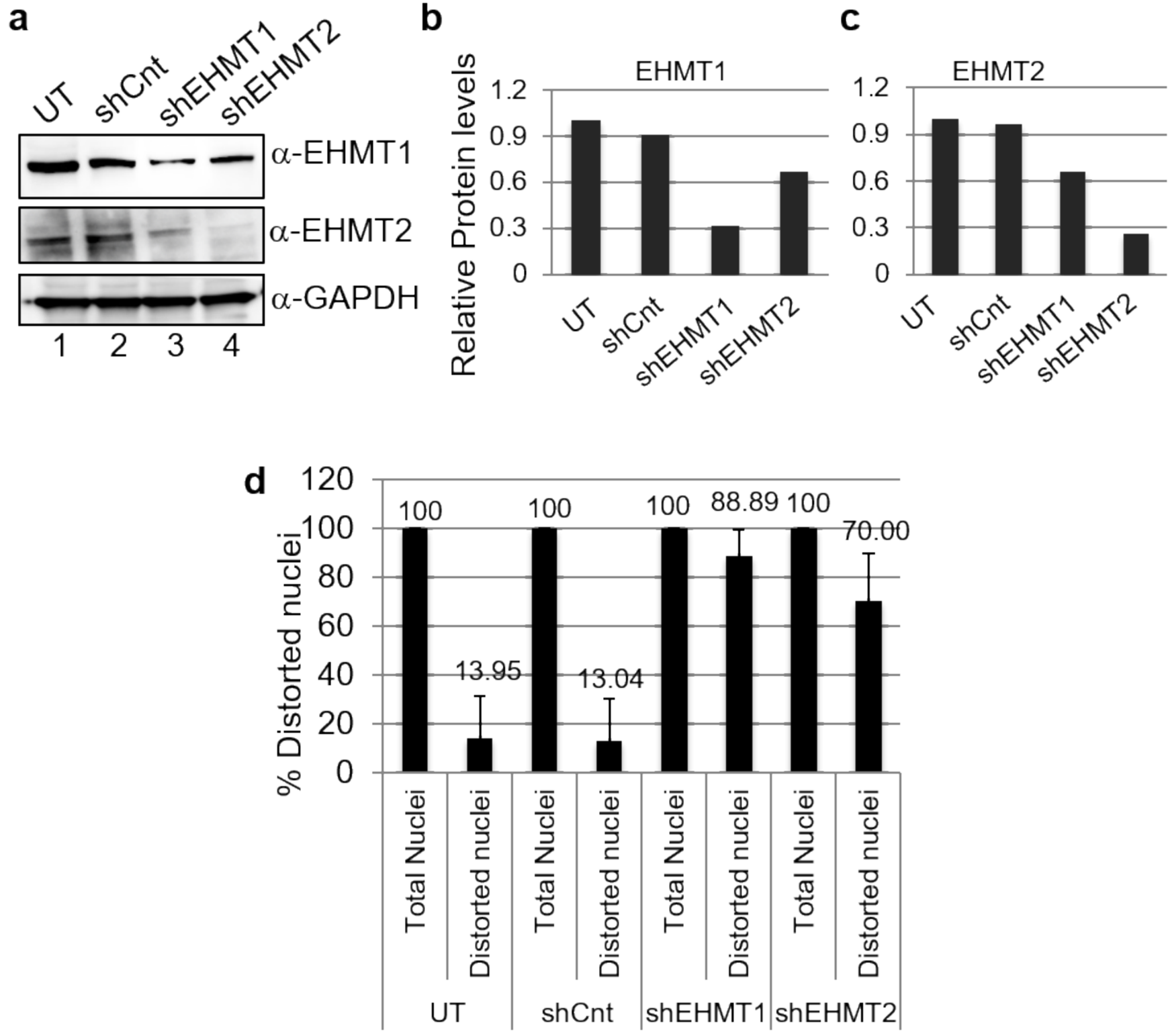

Ketkar and Rao et al Supplementary Figure 4

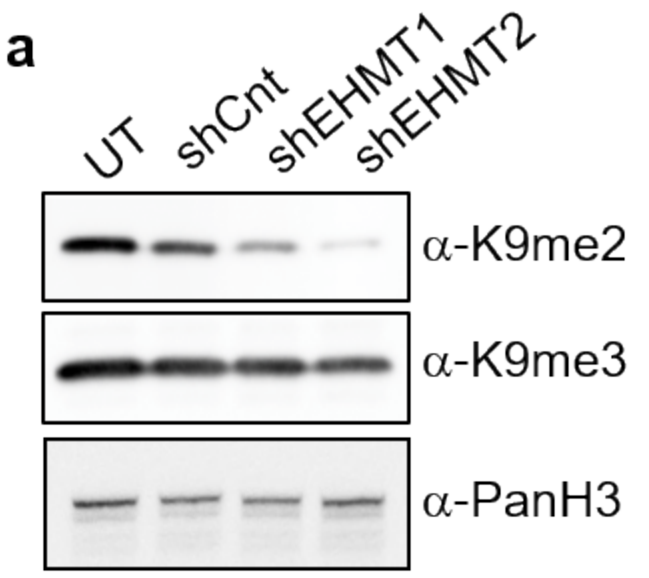

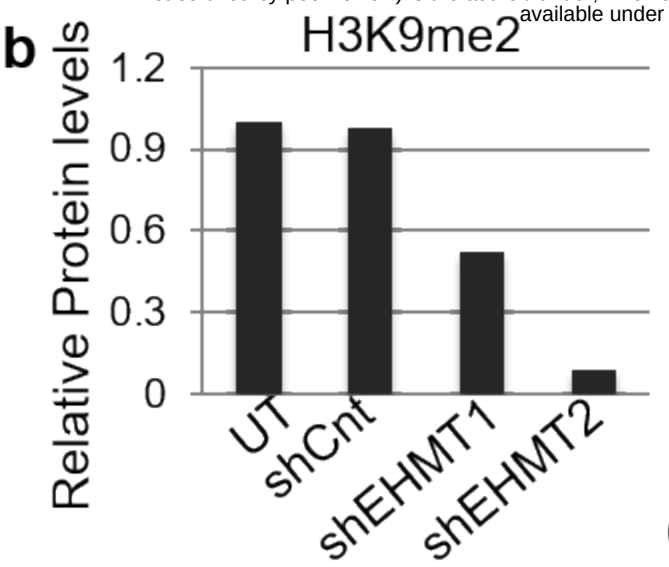

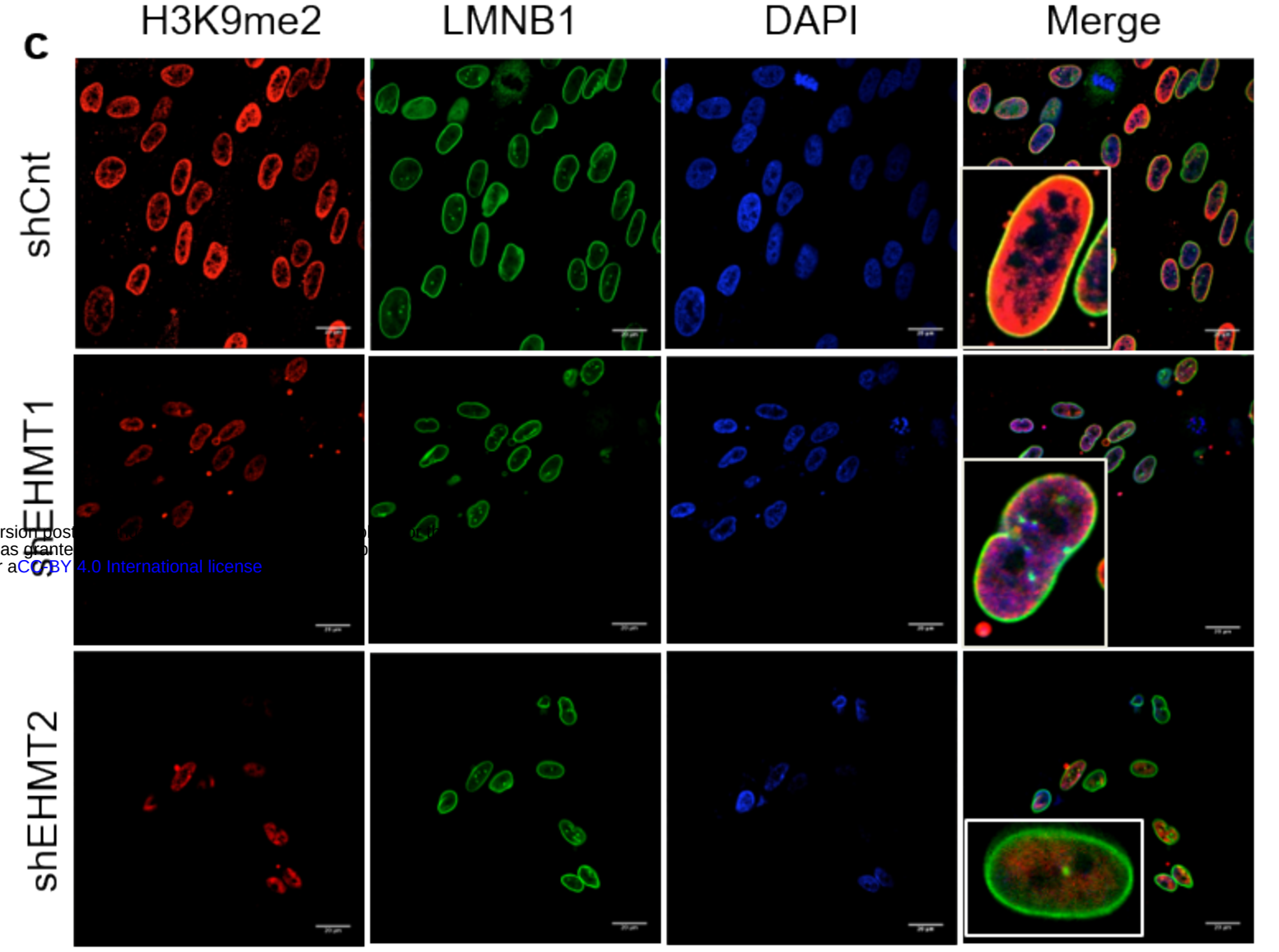

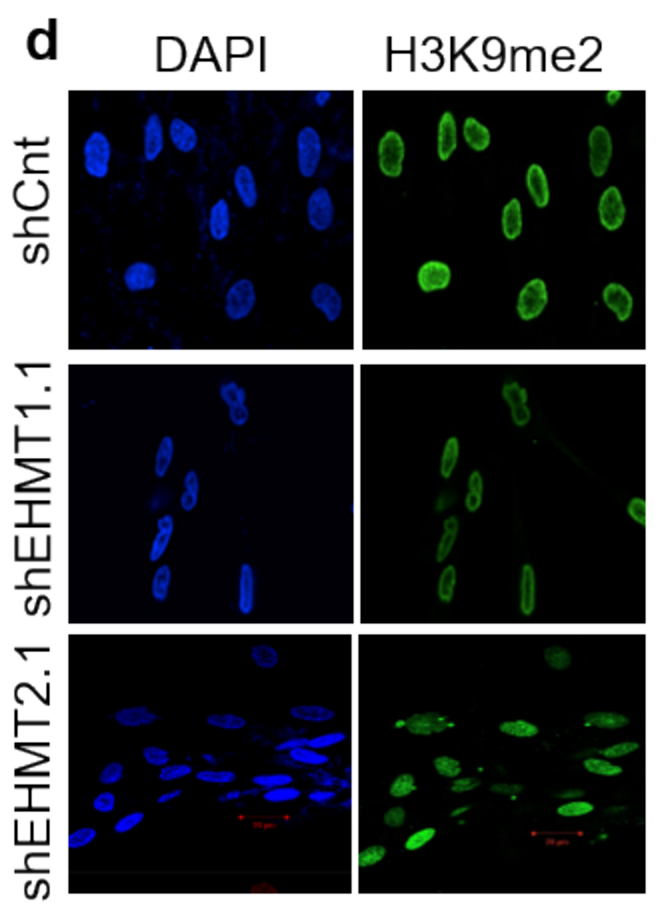

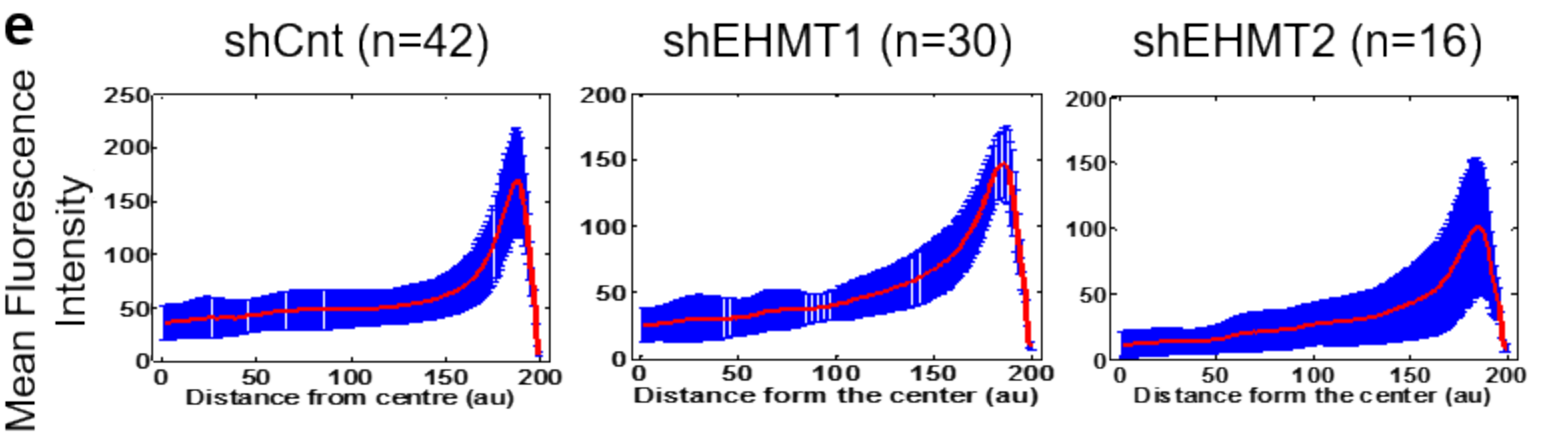

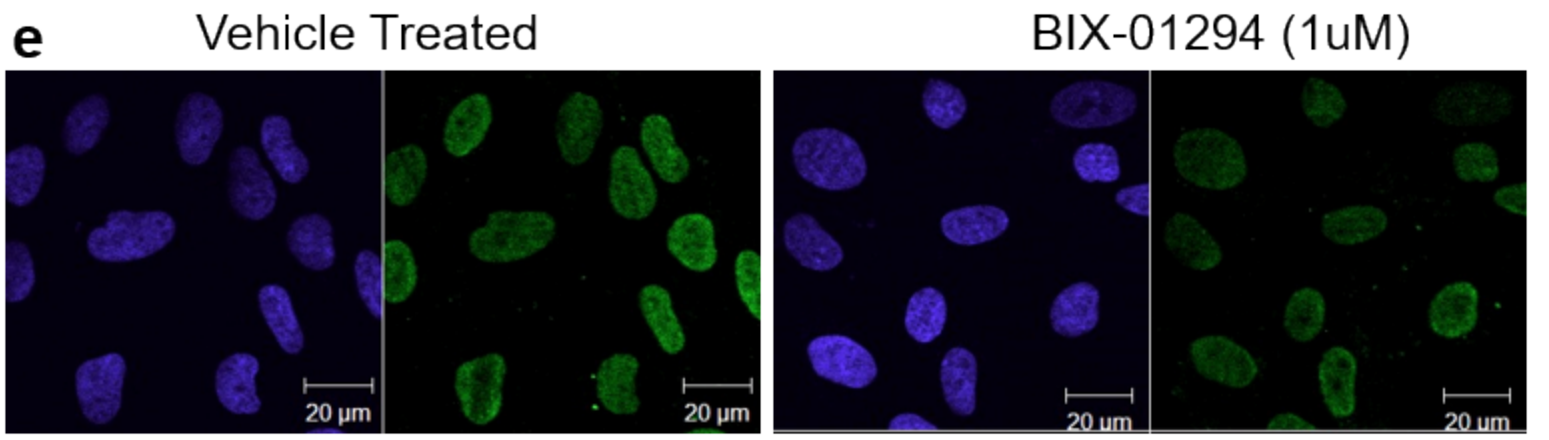

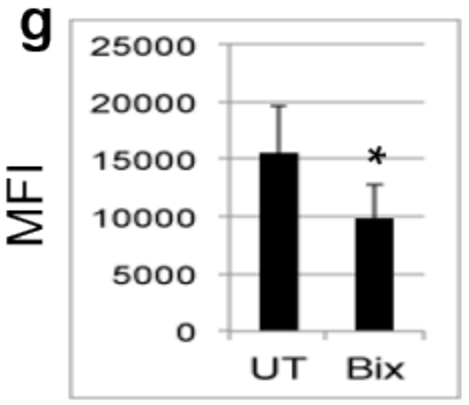

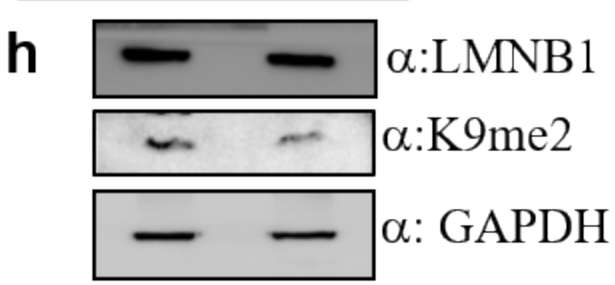

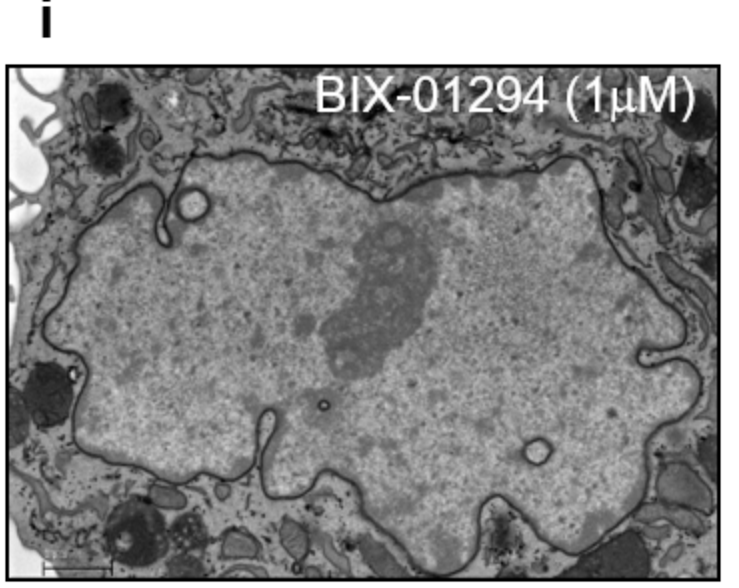

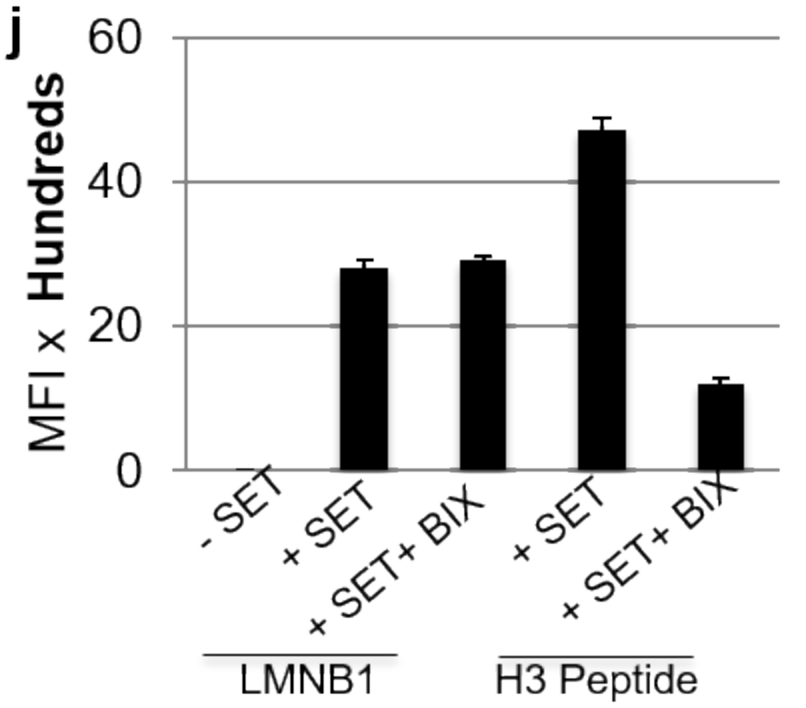

Ketkar and Rao et al Supplementary Figure 5

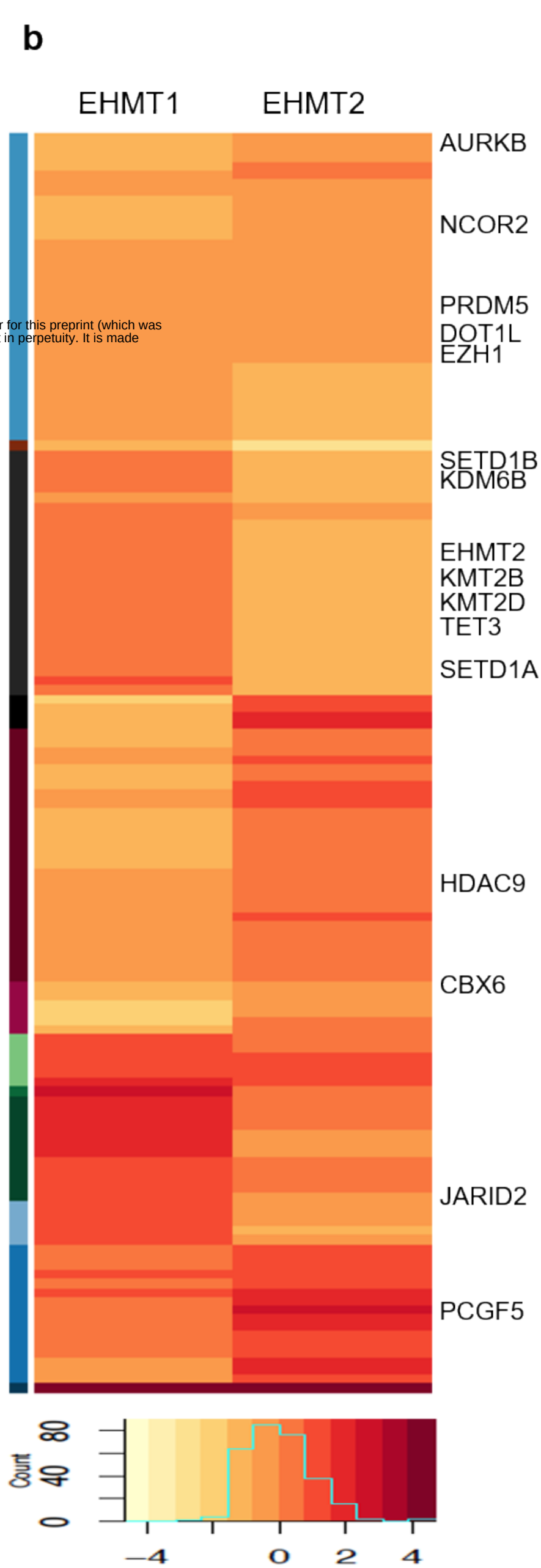

Ketkar and Rao et al Supplementary Figure 6

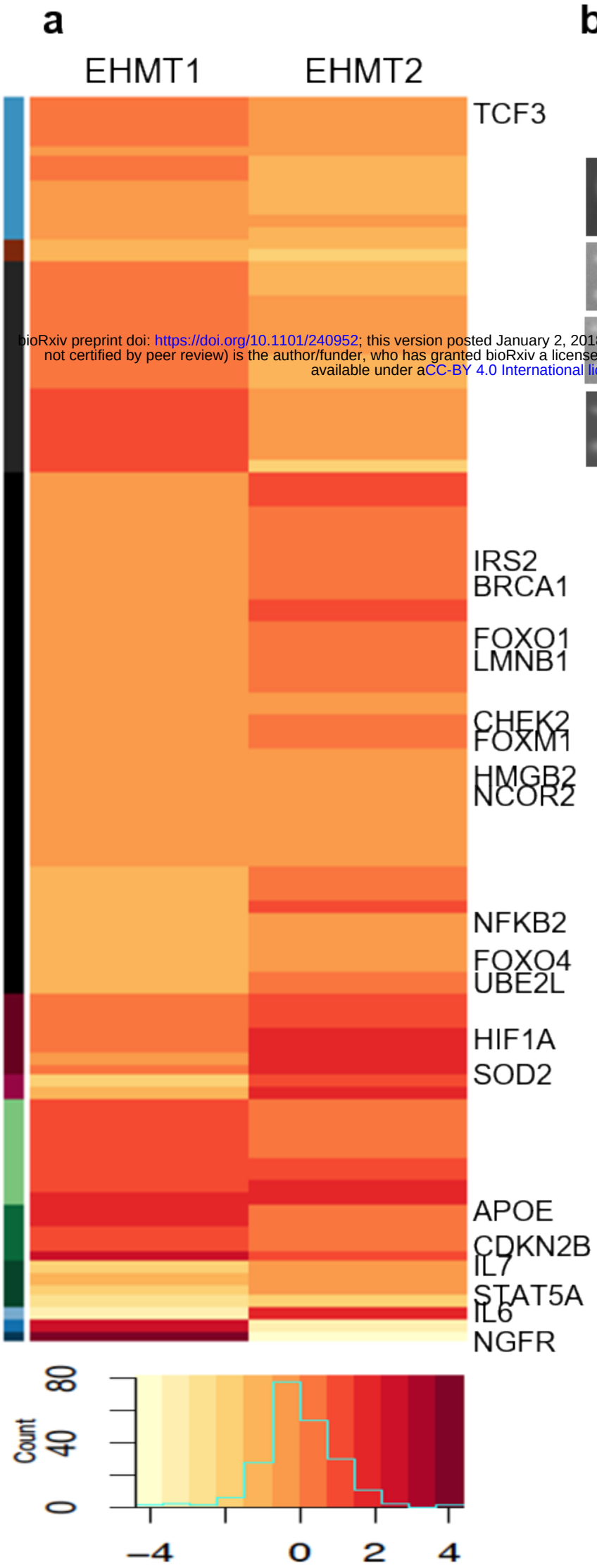

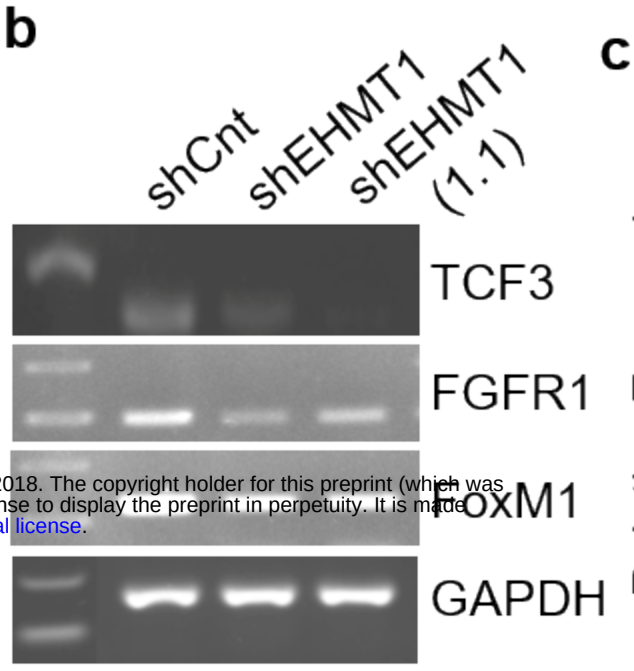

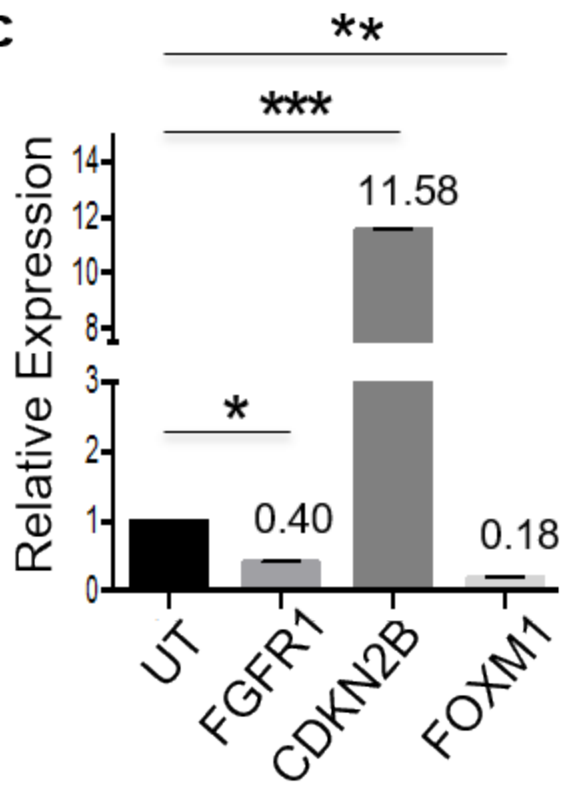

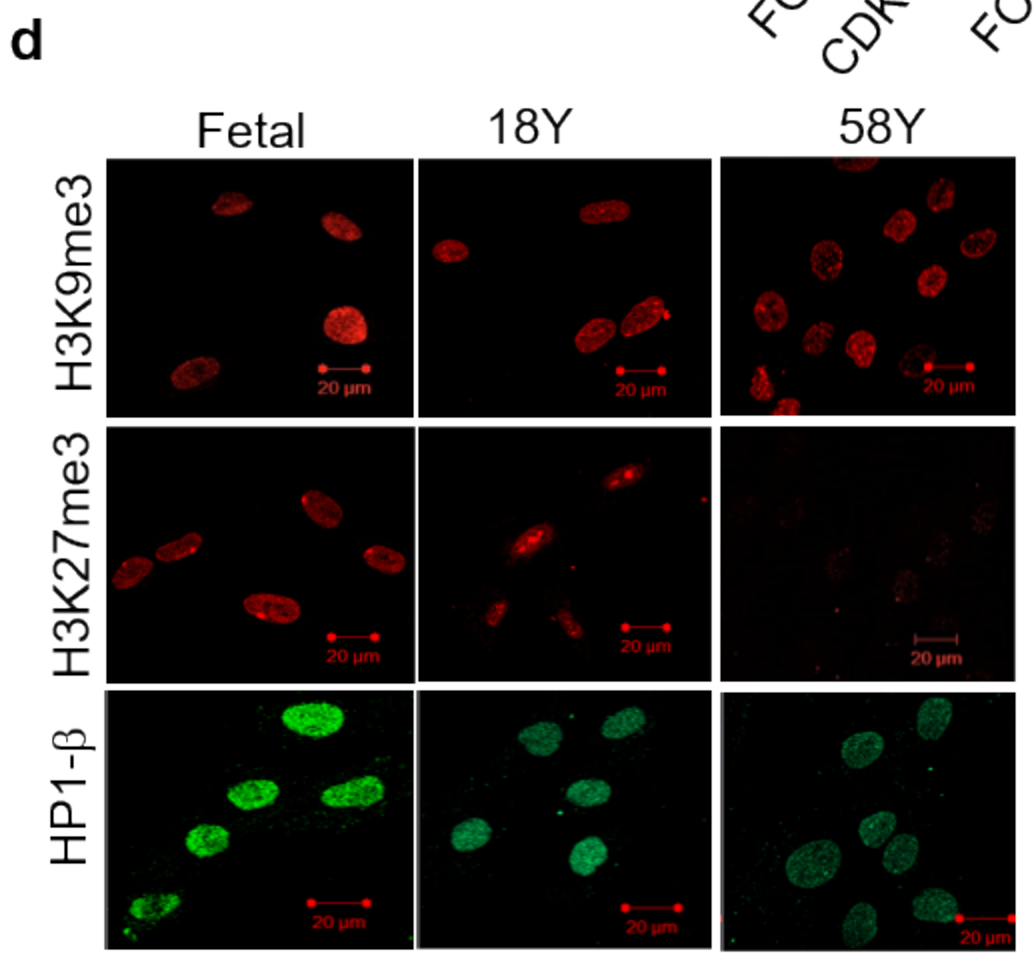

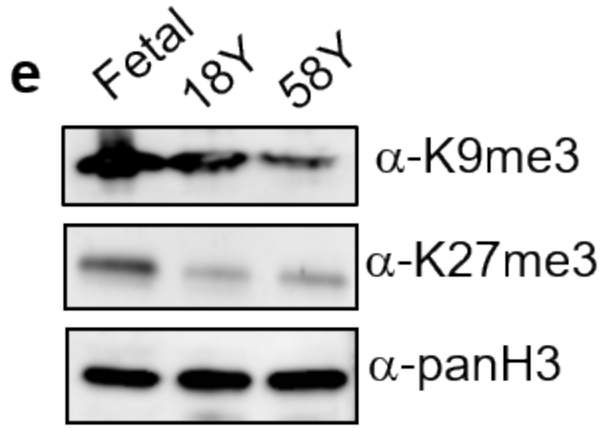

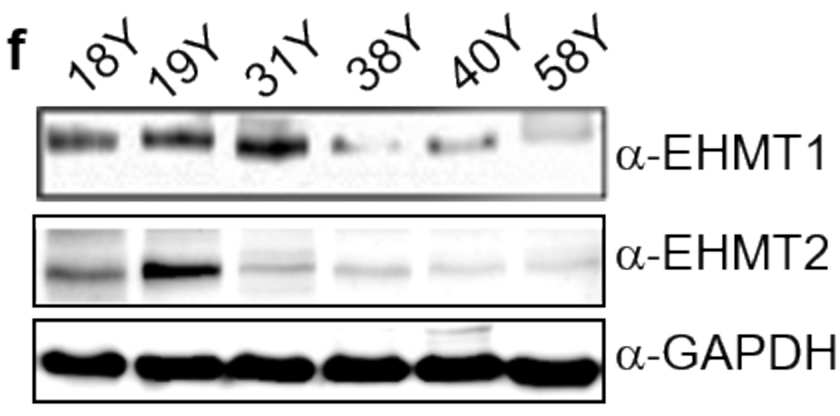

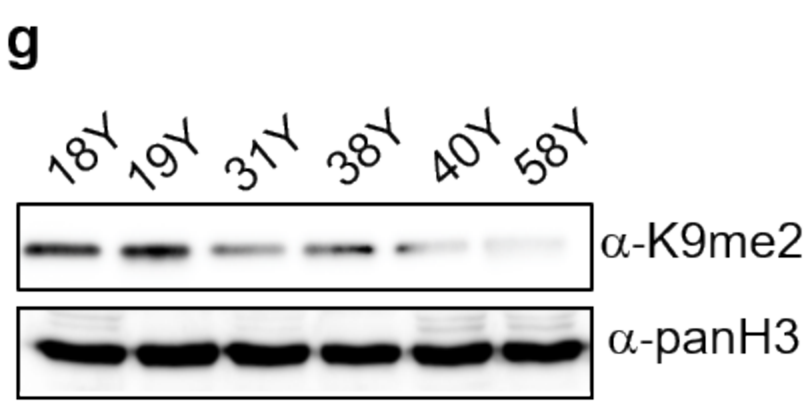

Ketkar and Rao et al Supplementary Figure 7

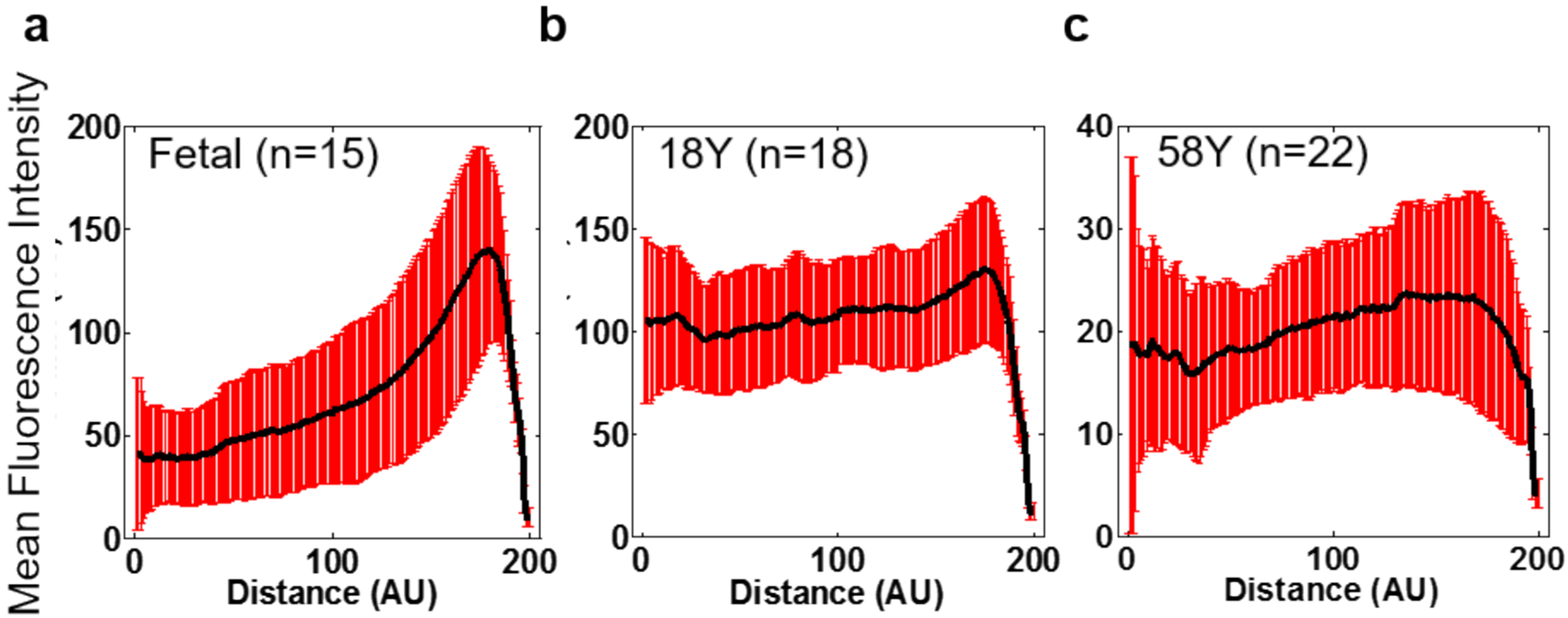

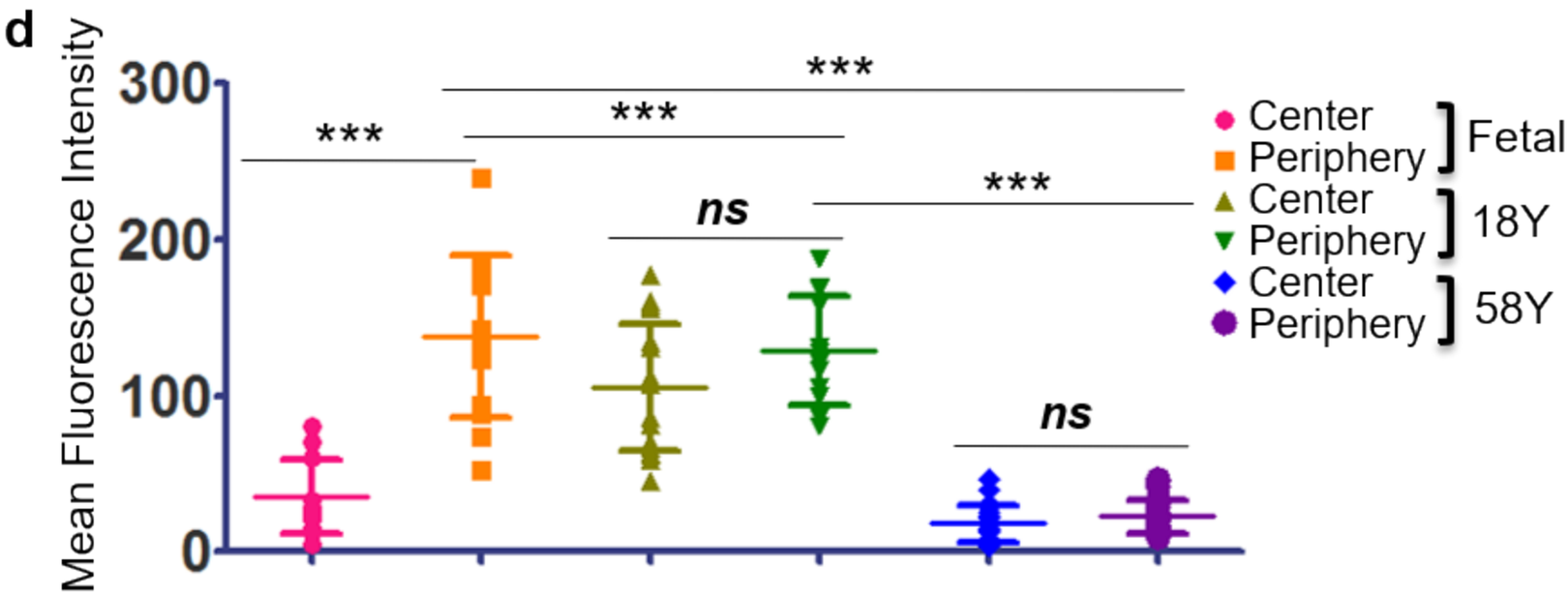

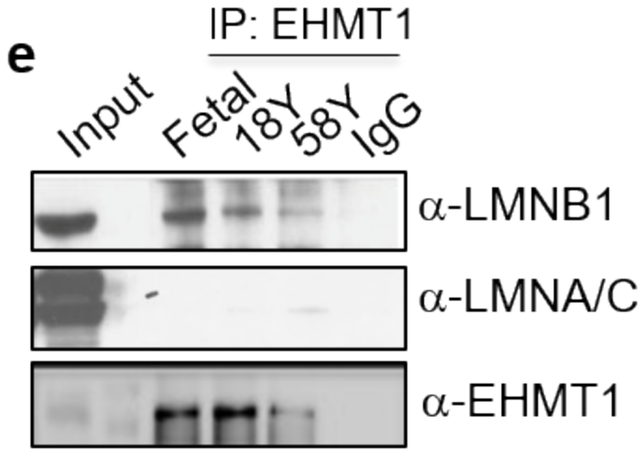

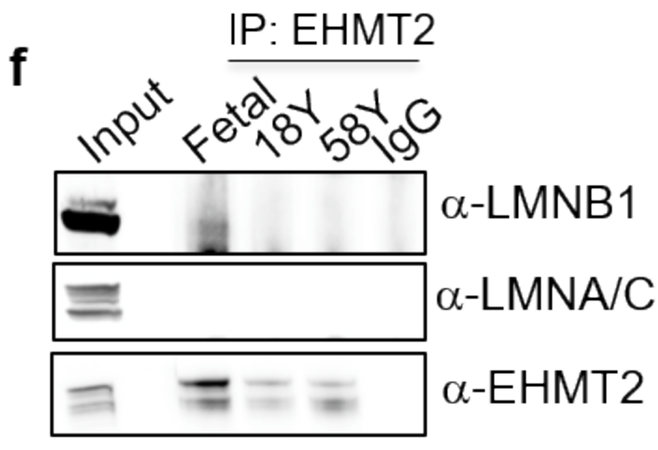

Ketkar and Rao et al Supplementary Figure 8

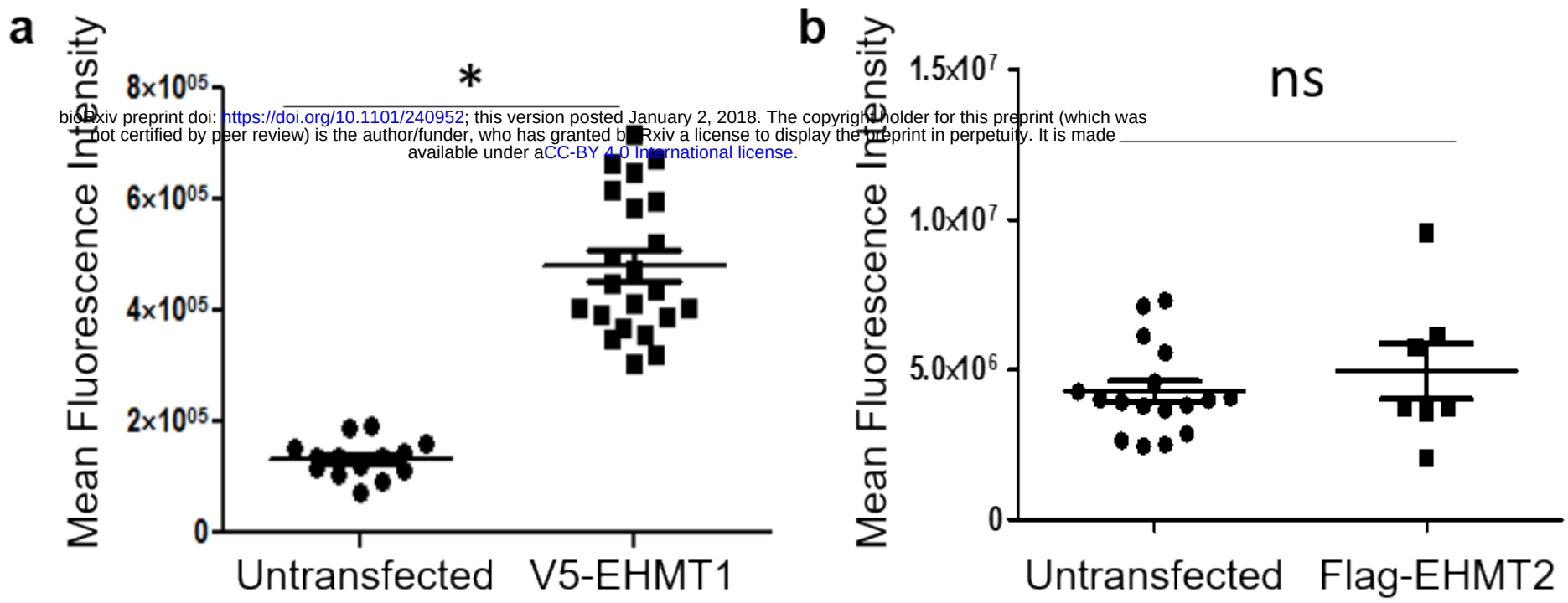

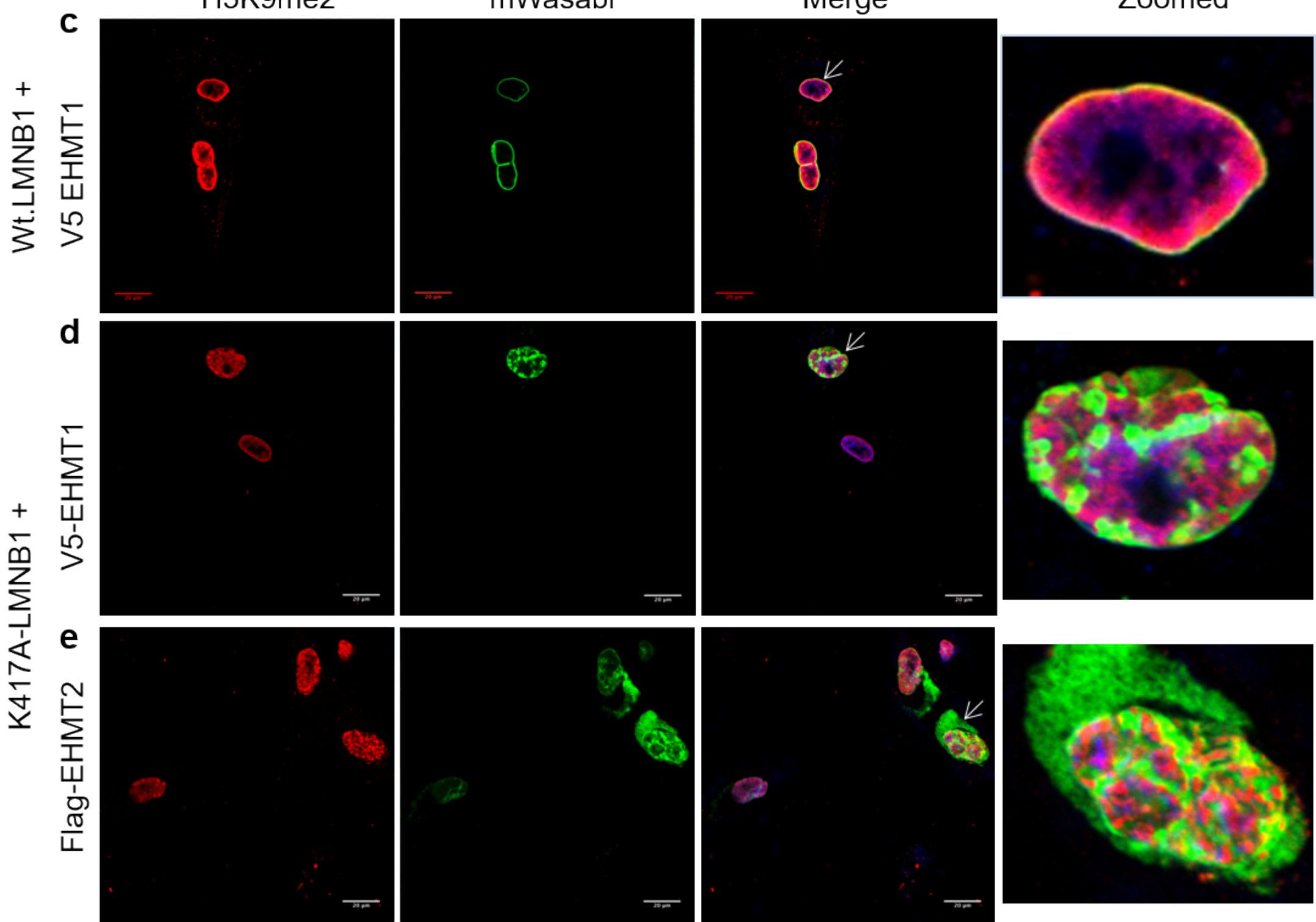

Ketkar and Rao et al Supplementary Figure 9